



FACULTY OF SCIENCE AND TECHNOLOGY
MASTER THESIS

Study programme / specialisation: Marine
and Offshore Technology.

The spring semester, 2022

Open / ~~Confidential~~

Author: Marius Thorstad Hansen.

(signature author)

Course coordinator: Professor Yihan Xing.

Supervisor(s): Associate Professor Lin Li and Ph.D. Xinying Zhu.

Thesis title: Numerical study on splash zone crossing with GRP protection cover.

Credits (ECTS): 30 ECTS

Keywords:

- Offshore lifting operation
- GRP Protection cover
- Sensitivity study
- Time-domain simulation
- Diffraction analysis
- Allowable sea state assessment

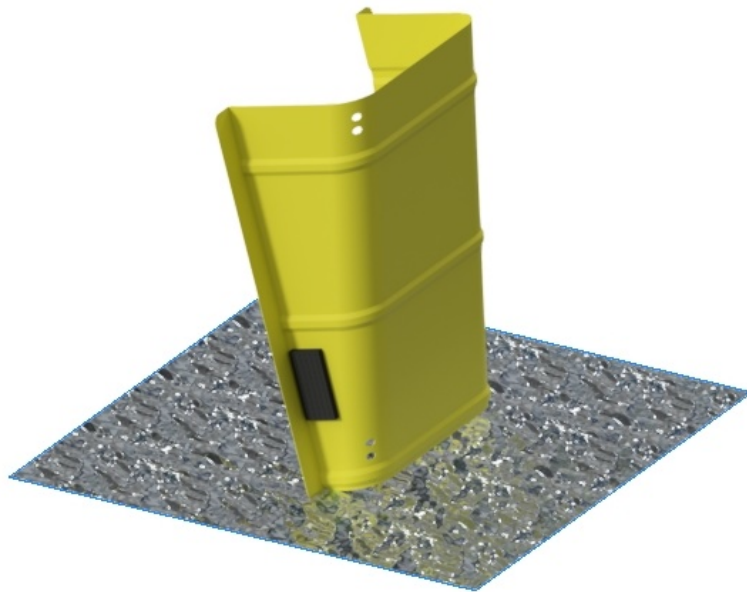
Pages: 116

+ appendix: 121

Stavanger, 15/07-2022

date/year

NUMERICAL STUDY ON SPLASH ZONE CROSSING WITH GRP PROTECTION COVER



Author : Marius Thorstad Hansen

Supervisor : Associate Prof. Lin Li

External supervisor : Ph.D. Xinying Zhu

University of Stavanger

Faculty of Science and Technology

Department of Mechanical and Structural Engineering and Material Science

Master of Science Thesis, Spring 2022

Abstract

For oil and gas fields moving further offshore, it has been more common to use a subsea production system or a combination of rig and subsea structures. These subsea structures must be overtrawlable if they are not marked with a buoy or vessel. One solution for overtrawlable subsea structures is to use a protection cover. This study focuses on GRP pipeline protection covers, which are highly weather-sensitive due to their low weight and large surface area. Installation of subsea protective covers typically involves overboard, lowering through the splash zone, and lowering to the seabed. This study will focus on the lowering through the splash zone, which is usually considered one of the most critical phases of a deployment operation. The hydrodynamic property for the cover is calculated based on DNV-RP-H103 simplified methods [1].

The vessel's properties are collected with a diffraction analysis program that calculates the responses and loading for wet bodies using potential flow theory. Hence, body results are generated for: damping, added mass, displacement RAOs, and load RAOs. In addition, the calculated pressure in the fluid will yield the sea state RAOs for the fluid pressure. The vessel was then implemented into the numerical time-domain program with the cover.

For the numerical methods, two sensitivity studies are conducted to evaluate the number of wave seeds and vessel motion to be applied to assess sea states. First, the numbers of seeds selected were based on the extreme values for the sling tension. Then, analyzing the extreme values with a statistical method and the cumulative average for minimum and maximum tension. The extracted results indicated that 30 seeds were enough to yield reliable predictions of the sea states. The same procedure was applied for the vessel motion as for the number of wave seeds. In addition, the simulation demo file was closely investigated to observe any differences between the motions. From the extracted extreme values, the difference between the motion where slightly more conservative for the coupled motion. However, the uncoupled vessel motion was selected to assess the allowable sea states. The uncoupled motion would better represent the real-life, where for the coupled vessel it was observed large yaw motions for longer wave periods

In the assessment of the sea states, three simulation cases were selected to investigate the hydrodynamic forces during the splash zone crossing. Firstly, the different lifting angles of the cover made it possible to adjust the waterplane area. Secondly, evaluate the vessel position for wave directions of 165 and 180 degrees. Lastly, use the vessel to disrupt the incoming waves generating a shielding effect for the cover. Concerning the operational criteria, the extreme values were fitted to a Gumbel probability paper to assess the allowable sea states.

The results indicated that the shielding effect on the cover would yield the best applicable sea states for all tested methods. For the different tested lifting angles of the cover. The cover with the lowest waterplane area resulted in the highest sea states due to lower hydrodynamic forces on the cover. Lastly, for the two tested wave directions. The vessel for head waves yielded slightly better allowable sea states. The increased roll motion for the wave direction at 165 degrees resulted in larger slamming loads and lower sling tensions for the cover.

Acknowledgements

This Master Thesis concludes my Master of Science in Marine and Offshore Technology at the University of Stavanger. I greatly appreciate my girlfriend leaving everything behind in Bergen and moving with me so that I could pursue a degree in Master of Science.

First, I want to thank my supervisor, Associate Professor Lin Li, for all the support and guidance. She has been very helpful and greatly interested in my work throughout the master period. Her enthusiasm has motivated me to execute and produce a master thesis to the best of my ability.

I would also like to thank Ph.D. Xinying Zhu, for all the guidance and help she provided with the modeling in OrcaFlex.

Lastly, I would like to thank my family. They have always been there for me, providing me with great advice and support.

This Master Thesis is dedicated to my grandfather Hans Birger Hansen, for all the help he has provided me throughout the years of my studies.

Marius Thorstad Hansen

Stavanger, June 2022

Abbreviations

GRP	Glass Fiber Reinforced Plastic
DNV	Det Norske Veritas
GL	Germanischer Lloyd
NORSOK	The Norwegian Shelf's Competitive Position
WLL	Working Load Limit
JONSWAP	Joint North Sea Wave Project
RAO	Response Amplitude Operator
ROV	Remote Operated Vehicle
QTF	Quadratic Transfer Function
COG	Center of Gravity
CAD	Computer Aided Design
DOF	Degrees of Freedom
CFD	Computational Fluid Dynamics
PDF	Probability Density Function

Table of Contents

- Abstract i
- Acknowledgements iii
- Abbreviations iv
- Table of Contents v
- List of Figures viii
- List of Tables..... xi
- 1 Introduction..... 1**
 - 1.1 Background and Motivation 1
 - 1.2 State of the Art..... 5
 - 1.3 Aim and Scope..... 7
 - 1.4 Outline 9
- 2 Theory 10**
 - 2.1 Waves 10
 - 2.1.1 Potential Flow Theory 10
 - 2.1.2 Regular Waves 12
 - 2.1.3 Irregular Waves 13
 - 2.2 Rigid Body Motions in Waves 16
 - 2.2.1 Rigid Body Dynamics 16
 - 2.3 Wave Force on Slender Elements..... 18
 - 2.3.1 Added Mass Coefficient 18
 - 2.3.2 Drag Coefficient 19
 - 2.3.3 Slam Force 19
 - 2.4 Probability Model..... 20
 - 2.4.1 Extreme Value Distribution 20

3	Hydrodynamic Analysis of Wavefields and Installation Vessel	22
3.1	Overview	22
3.2	Vessel Setup	24
3.3	Hydrodynamic Analysis Results	28
3.3.1	RAOs for Heave, Pitch, and Roll	28
3.3.2	Shielding Results	31
4	Numerical Model for Time Domain Simulation	34
4.1	Overview	34
4.2	Vessel Setup	36
4.3	GRP Protection Cover	36
4.4	Analysis of Hydrodynamic Forces	41
4.4.1	Added Mass and Damping	41
4.4.2	Drag Coefficients and Inertia	46
4.4.3	Slamming Force	47
4.5	Lifting Setup	50
4.6	Environmental Conditions	53
4.7	Simulation Setup	54
5	Sensitivity Study on Numerical Methods.....	55
5.1	Overview	55
5.2	Numbers of Wave Seeds.....	55
5.2.1	Seeds	55
5.2.2	Simulation	56
5.2.3	Maxima Sling Tension	57
5.2.4	Minima Sling Tension	64
5.2.5	Discussion of the Numbers of Seeds	70
5.3	Coupled and Uncoupled Motion.....	71
5.3.1	Simulation	71
5.3.2	Shackle Position	73

5.3.3 Maxima Sling Tension	75
5.3.4 Minima Sling Tension	78
5.3.5 Comparison of Different Seeds	81
5.3.6 Discussion of Coupled and Uncoupled Motion	90
6 Assessment of Allowable Sea States	91
6.1 Operational Criteria	91
6.2 GRP Cover Lifting Angle.....	92
6.2.1 Operational Limits	92
6.2.2 Allowable Sea States	95
6.2.3 Discussion of Lifting Angles	97
6.3 Assessment of Allowable Sea States	98
6.3.1 Operational Limit	98
6.3.2 Allowable Sea States	100
6.3.3 Shielding Effect on Allowable Sea States	106
6.3.4 Discussion of Assessment of Allowable Sea States	109
7 Conclusion and Future Work	110
7.1 Conclusion	110
7.2 Recommendations for Future Work	113
References	114
Appendix A	A
Appendix B	D
Appendix C	E

List of Figures

Figure 1 - 1 Analog tide predicting computer [4]. 1

Figure 1 - 2 Splash zone crossing of a subsea template [7]. 3

Figure 1 - 3 GRP pipeline cover modeled in Autodesk Inventor..... 4

Figure 1 - 4 General scope of the thesis. 8

Figure 2 - 1 Wave spectrum [7].....15

Figure 3 - 1 Vessel mesh in Orcawave.....24

Figure 3 - 2 Vessel mesh with given wave headings 25

Figure 3 - 3 Vessel with field points for the calculation of sea state RAOs 27

Figure 3 - 4 Heave RAO for wave direction 90°, 165°, 180°, and added mass. 29

Figure 3 - 5 RAO for pitch and roll for wave direction 90°, 165°, and 180°..... 30

Figure 3 - 6 Shielding effect T = 6 s for wave direction 165° and 180° 31

Figure 3 - 7 Shielding effect T = 8 s for wave direction 165° and 180..... 31

Figure 3 - 8 Shielding effect T = 10 s for wave direction 165° and 180..... 32

Figure 3 - 9 Shielding effect T = 12 s for wave direction 165° and 180..... 32

Figure 4 - 1 GRP deployment vessel in OrcaFlex.....34

Figure 4 - 2 GRP Cover modeled in OrcaFlex and Autodesk Inventor. 36

Figure 4 - 3 Dimensions for GRP cover, (A) view from the front, (B) view from the back, (C) view from above..... 37

Figure 4 - 4 GRP model from OrcaFlex..... 38

Figure 4 - 5 Lifting angles for GRP cover. 39

Figure 4 - 6 Center of mass from Autodesk Inventor. 40

Figure 4 - 7 added mass for A11, A22, and A33, with the projected area marked in grey..... 42

Figure 4 - 8 GRP cover with trapped water from Autodesk Inventor..... 42

Figure 4 - 9 Ramping of slam force for lumped buoys [24]. 47

Figure 4 - 10 Slam area for GRP cover at different angles..... 48

Figure 4 - 11 Lifting arrangement in OrcaFlex. 50

Figure 4 - 12 Sling position from Autodesk Inventor. 52

Figure 5 - 1 Average maxima tension for sling 1..... 57

Figure 5 - 2 Average maxima tension for sling 2..... 58

Figure 5 - 3 Gumbel plot for maxima tension sling 1 (30, 50, and 100 seeds)..... 60

Figure 5 - 4 Gumbel plot for maxima tension sling 2 (30, 50, and 100 seeds)..... 61

Figure 5 - 1 Average maxima tension for sling 1.....	57
Figure 5 - 2 Average maxima tension for sling 2.....	58
Figure 5 - 3 Gumbel plot for maxima tension sling 1 (30, 50, and 100 seeds).....	60
Figure 5 - 4 Gumbel plot for maxima tension sling 2 (30, 50, and 100 seeds).....	61
Figure 5 - 5 Tail fitted Gumbel plot.	62
Figure 5 - 6 Weibull plot for maxima tension sling 1 (30, 50, and 100 wave seeds).....	63
Figure 5 - 7 Average minima tension for sling 1.	64
Figure 5 - 8 Average minima tension for sling 2.	65
Figure 5 - 9 Gumbel plot for minima tension sling 1 (30, 50, and 100 seeds).....	66
Figure 5 - 10 Gumbel plot for minima tension sling 2 (30, 50, and 100 seeds).....	67
Figure 5 - 11 Weibull plot for minima tension sling 1 (30, 50, and 100 wave seeds).	69
Figure 5 - 12 Average maxima and minima for shackle position.	73
Figure 5 - 13 Cumulative average maximum for coupled and uncoupled motion.....	75
Figure 5 - 14 Maximum tension for individual seeds.	76
Figure 5 - 15 Gumbel plot for maxima tension, coupled and uncoupled motion.	77
Figure 5 - 16 Cumulative average minima tension for coupled and uncoupled motion.	78
Figure 5 - 17 Minimum tension for individual seeds.	79
Figure 5 - 18 Gumbel plot for minima tension, coupled and uncoupled motion.	80
Figure 5 - 19 Sling 1 tension for seeds 18 and 19.	81
Figure 5 - 20 Sling 2 tension for seeds 18 and 19.	82
Figure 5 - 21 Slam force for seeds 18 and 19.....	83
Figure 5 - 22 Heave motion for seeds 18 and 19.	84
Figure 5 - 23 Shackle position for seeds 18 and 19.	85
Figure 5 - 24 Seed 19 yaw cover rotation for uncoupled and coupled motion.	86
Figure 5 - 25 Example of pendulum motion from OrcaFlex.....	87
Figure 5 - 27 Shackle force in Y-direction.....	88
Figure 5 - 26 Pendulum motion for shackle.....	88
Figure 5 - 28 Roll motion for seed 19.	89
Figure 5 - 29 Example of different events co-occurring for seed 19	89
Figure 6 - 1 Gumbel plot for maxima and minima for grp cover at 75°.....	92
Figure 6 - 2 Gumbel plot for minima clearance.	93
Figure 6 - 3 Gumbel plot for minimum tension for lifting angles 65°, 70°, and 75°.....	94
Figure 6 - 4 Allowable Sea state for different lifting angles.....	95

Figure 6 - 5 Example of slam forces at different lifting angles..... 96

Figure 6 - 6 Example of tension in sling 1 for splash zone crossing at different lifting angles.
..... 97

Figure 6 - 7 Gumbel plot for wave direction 165° and 180° for $Tp = 5$ s..... 98

Figure 6 - 8 Gumbel plot for wave direction 165° and 180° for $Tp = 9$ s..... 99

Figure 6 - 9 Example of slam forces for $Tp = 9$ s at different wave directions. 100

Figure 6 - 10 Example of sling tension for $Tp = 9$ s at different wave directions. 101

Figure 6 - 11 Example of slam forces for $Tp = 5$ s at different wave directions. 102

Figure 6 - 12 Example of sling tension for $Tp = 5$ s at different wave directions. 103

Figure 6 - 13 Gumbel plot for $Tp = 5$ s with and without shielding..... 106

Figure 6 - 14 Example of slam with and without shielding. 107

List of Tables

Table 1 - 1 Standard	5
Table 3 - 1 data inputted for the environment.....	25
Table 3 - 2 Vessel properties.....	26
Table 4 - 1 Data extracted from Autodesk Inventor.....	37
Table 4 - 2 Model dimensions in OrcaFlex.....	40
Table 4 - 3 Model COG and mass moment of inertia in OrcaFlex.....	40
Table 4 - 4 Added mass for a rectangular plate Table 2-A DNV [1].....	41
Table 4 - 5 Parameters for added mass	43
Table 4 - 6 Comparison between added mass	43
Table 4 - 7 Parameters and added mass for lumped buoys.....	44
Table 4 - 8 Linear damping for cover	45
Table 4 - 9 Drag coefficient and drag area for lumped buoys.....	46
Table 4 - 10 Slam coefficient and waterplane area for lumped buoys.....	49
Table 4 - 11 Winch setup in OrcaFlex.....	51
Table 4 - 12 Sling data from Gunnebo (Appendix B).....	51
Table 4 - 13 Sling connection to the GRP cover in OrcaFlex.....	52
Table 4 - 14 Time-domain simulation.....	54
Table 5 - 1 Sea state description for the sensitivity study for seeds.....	56
Table 5 - 2 Sea state description for coupled and uncoupled.....	72
Table 5 - 3 Shackle position for the mean value of 50 seeds.....	74
Table 6 - 1 Allowable sea states for wave direction 180°.....	104
Table 6 - 2 Allowable sea states for wave direction 165°.....	105
Table 6 - 3 Allowable sea states for different wave directions with shielding.....	108

Chapter 1

Introduction

1.1 Background and Motivation

In the 1860s, Lord Kelvin put his full scientific effort into measuring and predicting the tides. At that time, tide gauges used a buoy to recode the height of the sea onto a roll of paper. Kelvin set out to determine how sine waves with frequencies identified by Laplace could add together to produce the observed tidal curve [2]. The key to this was to apply the work of French mathematician Joseph Fourier, who had shown how to decompose any function into a sum of sine waves. Applying Fourier's analysis to tidal curves is straightforward, but the computation required was enormous. The solution for Kelvin was to make one of the first analog computers that could automate the tedious task of predicting future tides [3].



Figure 1 - 1 Analog tide predicting computer [4].

The same principles for predicting future events are still used today for marine operations. However, with more considerable computing power due to the invention of the digital computer. Digital computer software for predicting and analyzing different marine operations has been created. The software used is based on a more extensive set of mathematical formulas used to

For oil and gas fields moving further offshore, it has been more common to use a subsea production system or a combination of rig and subsea structures. These subsea production systems may consist of:

- Subsea templates.
- Wellhead and Xmas tree systems.
- Flowline systems with pipelines and risers.
- Subsea Manifolds.
- Control systems.

All these systems must be placed at their required destination at the sea bottom, which involves different methods depending on the object. For pipelines, this is done with S-lay, J-lay or Reel lay, depending on the pipe dimension and depth to the sea bottom [5]. Deployment of a subsea template or similar systems depends on an offshore lifting operation, usually executed with a crane vessel. The crane vessel is selected based on operational criteria, such as maximum lifting capacity.

Installation of subsea systems involves high risks due to the uncertainty and harsh nature of the marine environment. Analytical engineering work is required to validate and handle the risk and uncertainties related to the offshore lifting operation [6]. Numerical models are usually implemented to analyze various phases to determine the operational limits with the desired level of confidence that an accident is avoided [6]. Execution of any offshore lifting operations can be divided into different phases:

- **Stage 1 - Lift-off**
- **Stage 2 - In air**
- **Stage 3 - Crossing the splash zone**
- **Stage 4 - Deeply submerged**
- **Stage 5 – Landing**

The five stages mentioned are subjected to analytic engineering before executing the offshore lifting operation. This is done to ensure the safe and successful completion of the offshore lifting operation. This thesis focuses on analyzing stage 3, crossing the splash zone. For the splash zone crossing, the hydrodynamic forces acting on the object must be estimated as accurately as possible. This is to achieve as close to a realistic numerical model as possible, predicting the induced motion experienced on the object and the vessel during the splash zone crossing.



Figure 1 - 2 Splash zone crossing of a subsea template [7].

The installed subsea structures usually attract fish or are located at fishing grounds. In order to continue fishing in these areas, the subsea structures are required to be overtrawlable if they are not marked with a buoy or vessel. In the case of an unfortunate hit, an incidence between a fishing trawler and a subsea structure can cause significant damage to the structure and technical equipment. Overtrawlable protective covers are used to protect equipment, and subsea structures from dropped objects, dragged anchors, or fishing vessels. This can be integrated with a template or have a separate structure for protection. This study focuses on the installation of GRP protection covers. GRP covers are protective covers that are made of glass fiber reinforced plastic and designed to be overtrawlable/fishing friendly. Compared to a steel structure, the lower weight of the GRP protection covers makes them more cost-efficient. This is due to larger selections of vessels that can be used to operate a low-weight cover.

In addition, the covers are stackable, making the transportation/logistic easier, and given the low weight, lessens the impact it may have on soft soil areas. GRP protection covers are primarily used in the oil and gas industry to protect pipelines and wellhead jumpers.

The installation of GRP cover is particularly weather sensitive compared to steel structures. As a result, the hydrodynamic forces can exceed the submerged weight even in low sea states. This is due to the large surface area, and the low weight/density of the plastic reinforced cover. Therefore, the splash zone crossing is considered the most critical phase of the operation for this study.

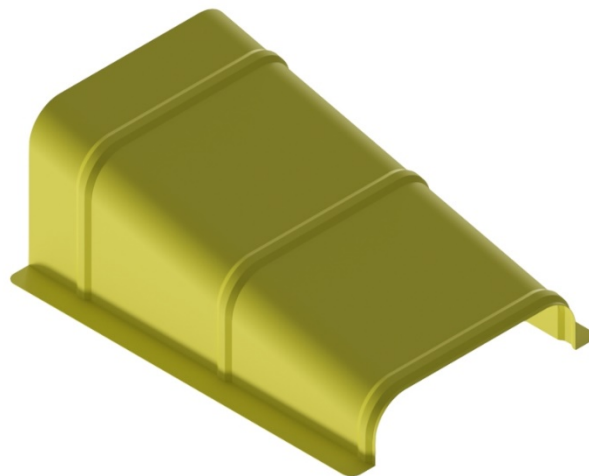


Figure 1 - 3 GRP pipeline cover modeled in Autodesk Inventor.

1.2 State of the Art

Lifting operations are described in various regulations and standards. The main standards used for Norwegian offshore are DNV, GL, and NORSOK. The overall objective of these standards is to ensure that marine operations are performed inside defined and recognized safety limits. Therefore, this study will focus mainly on the standards in Table 1 - 1

Table 1 - 1 Standard

Certifier	Standard	Content
DNV	DNV-RP-H103	Modeling and Analysis of Marine Operations
DNV	DNV-RP-C205	Environmental Conditions and Environmental Loads

DNV-RP-H103 gives guidance on modeling and analysis, particularly for lifting operations. This includes lifting through the splash zone, deeply submerged, and lowering to the seabed [1]. DNV-RP-C205 provides guidance for modeling, analyzing, and predicting environmental conditions and calculating environmental loads acting on structures [8].

Time-domain simulation can be used to predict motions and loads for the given model. Several dynamic analysis programs can be used for time-domain simulations of a marine operation. Examples of programs that can be used for time-domain analysis for a marine operation are OrcaFlex, Ansys AQWA, and SIMO. From frequency domain analysis software, the hydrodynamic properties of the vessel can be obtained. The software which uses potential flow theory is OrcaWave, Ansys AQWA, and WADAM. For this study, the vessel properties are extracted from OrcaWave, of which the time-domain analysis is done in OrcaFlex. OrcaFlex defines the time-domain analysis as fully nonlinear, where mass, stiffness loading, and damping are evaluated at each timestep. This is done by considering the instantaneous time-varying geometry. Two types of time-domain integration schemes are available for OrcaFlex, implicit and explicit [9].

The general theory for the marine operation is based on DNV-RP-H103 Modeling and Analysis of Marine Operations [1]. DNV-RP-H103 is used to apply operational limits and assess the hydrodynamic properties of the GRP cover.

The theory behind the simulation and modeling of the GRP cover is based on a paper written by Frøydis Solaas et al. [10]. In this paper, the GRP cover has been lowered for a significant wave height of three meters and a wave period of eight seconds without the slamming forces included in the simulations. The paper has been used to validate and compare results.

Splash zone crossing for different types of objects has been addressed in several studies, where the effects of shielding during the splash zone crossing can drastically affect the outcome. For example, the effect of shielding during the lowering of an offshore wind turbine monopile has been investigated by Li et al. [11]. The study concluded that if the shielding effects were not accounted for, the responses could be greatly overestimated. Thus, making the weather window more conservative and leading to unnecessary economic consequences. A typical example of this will be the day rate for the vessel and personnel due to waiting on weather. It is also important to notice that in some cases, the allowable sea state can be lower because of shielding. For example, Li et al. investigated splash zone lowering of a sizeable subsea spool piece, where the allowable wave height was reduced with shielding [12]. The conclusion for this result was due to the unbalanced wave kinematics along the spool pieces, which generated more rotations of the spool. However, excluding the shielding effect, the operability would be greatly overestimated.

Operational limits for offshore lifting operations have been conducted for multiple papers. Solaas et al. [10] have conducted a study on the dynamic forces and limiting sea states by installing a GRP protection cover. Methodology for assessment of the operational limits and operability of marine operations by Guachamin-Acero et al. [13] demonstrates a general method for assessment of operational limits. For operations dominated by waves, the operational limits are expressed in terms of allowable sea states. Whom of Li et al. [14] have conducted a case

study for lifting operations to address the uncertainties in the allowable sea state associated with the sea state description. The papers stated above included discussion for the assessment of allowable sea states and some with the effect of shielding.

Other studies for offshore lifting operations, such as a numerical study on splash zone crossing with subsea template and ROV by Hauge [15], have been used as guidance. Published work for analysis and modeling marine operations is plentiful, covering various aspects of an operation. Good knowledge is key to simulating actual events as accurately as possible, with the ability to make and assess reasonable assumptions and simplifications. This thesis aims to increase the knowledge of the effect coupled and uncoupled systems may have on the cover during the splash zone crossing. In addition, the effect of shielding and the responses it may have on the allowable sea states. However, few studies have been conducted on different types of vessel motion. Hauge et al. [16] paper on a numerical study on deploying a subsea template using coupled and uncoupled models has been used as a reference. The paper concluded that the uncoupled system yielded lower predictions when assessing the allowable sea states.

1.3 Aim and Scope

The general scope of this report is to evaluate the allowable sea states with and without the use of shielding. Several different cases will be analyzed using the simulation software OrcaFlex. The numerical model in OrcaFlex will be based on the acquired hydrodynamic properties through DNV-RP-H103 chapter 4 lifting through wave zone – simplified method. The report focuses on one single vessel, where the hydrodynamic properties have been calculated using the frequency domain analysis software OrcaWave. The dynamic responses from the time-domain simulation will be used as the basis for the statistical modeling and then compared with predefined limiting criteria. This study aims to achieve a conclusion based on the comparison of the allowable sea states with and without the use of shielding. In addition, a comparison between different lifting angles and the effects of the waterplane area will also be discussed.

- ❖ Diffraction analysis
 - GRP deployment vessel
 - Generate displacement and load RAO
 - Generate added mass and damping
 - Generate shielding effects based on sea state RAO
- ❖ Time-domain simulation
 - GRP deployment
 - Determine allowable sea state for deployment through splash zone without shielding.
 - Determine allowable sea state for deployment through splash zone with shielding.
 - Determine allowable sea states for different lifting angles.

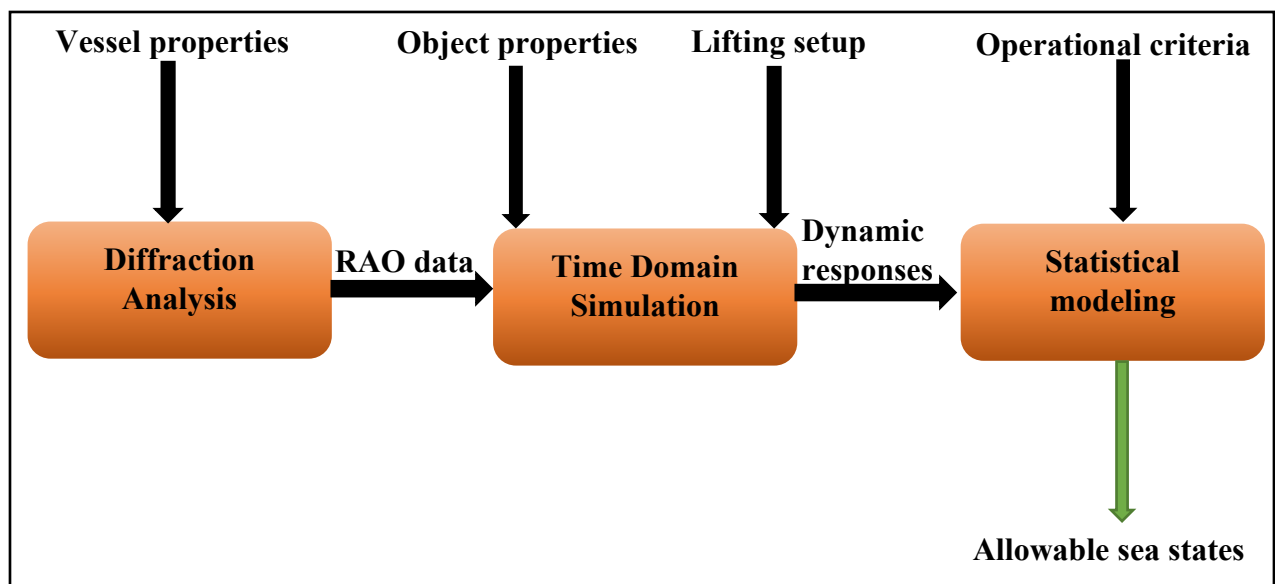


Figure 1 - 4 General scope of the thesis.

1.4 Outline

This report is divided into seven chapters, each containing its separate subchapters. The goal is to create a smooth transition from the introduction to the conclusion.

Chapter 1 introduces the study with a brief background and motivation regarding the tasks. Then, it introduces the object that will be lowered through the splash zone, with challenges related to this operation. It also includes a literature review of previous related work and relevant standards.

Chapter 2 contains an overview of the theory behind the time-domain simulation and analysis method. It provides an explanation of ocean waves, their influence on manufactured structures, and the motions of free-floating bodies in a fluid. The statistical modeling will also be present in this chapter.

Chapter 3 explains the numerical model for OrcaWave with assumptions and simplifications, with obtained results from the diffraction analysis, which ranges from displacement RAOs to sea state RAOs.

Chapter 4 presents the numerical model used for the time-domain simulation. The geometrical and hydrodynamic properties for the lifted object are provided, where the theory behind OrcaFlex is included.

Chapter 5 provides a sensitivity study for the numerical methods. These numerical methods are wave seed and decoupled/coupled systems. Chapter 5 provides the number of seeds needed to assess the allowable sea states. In addition, the effect that coupled or decoupled systems may induce on the assessment of sea states.

Chapter 6 provides the result for allowable sea states from the time-domain simulations. In addition, chapter 6 includes the different lifting angles and the difference in allowable sea states with and without the used shielding effect.

Chapter 7 presents a discussion and conclusion of the study conducted. Again, previous studies/papers will be used to compare and discuss the results acquired for this thesis.

Chapter 2

Theory

2.1 Waves

Ocean waves causes varying loads on all man-made structures in sea. All man-made structures will respond in some way to the wave-induced periodic load. Waves can be generated in different ways as:

- Ship or a floating structure which is moving.
- Interaction from wind on the sea surface
- Astronomical forces such as tides
- Earthquakes or landslides

There is no single solution for problems related different types of waves. Even the simplest cases need approximations to be solved. It is important to know the limitations for the given simplification of the system, especially for nonlinear effects [17].

2.1.1 Potential Flow Theory

Euler flow or potential flow theory assumes that in a region of the flow the net viscous forces are negligible compared to pressure and inertial forces. The water is an ideal, incompressible fluid, where there are no shear forces (no net rotations) between the particles. This approximation is appropriate for regions of flow far away from solid walls and bodies. Since the rotation of the velocity vector is a zero vector, there is two equations to describe velocity [18].

$$\nabla * \vec{U} = 0 \text{ (incompressible approximation)} \quad (1)$$

$$\nabla \times \vec{U} = 0 \text{ (irrotational approximation)} \quad (2)$$

The potential function is a continues function that satisfies the laws of conservation of mass and momentum, where the partial derivation of the potential function gives us the flow velocity in wanted direction [18].

$$\vec{U} = \left. \begin{array}{l} u = \frac{\partial \varphi}{\partial x} \\ v = \frac{\partial \varphi}{\partial y} \\ w = \frac{\partial \varphi}{\partial z} \end{array} \right\} \text{Velocity for } x, y, \text{ and } z \text{ based on the potential function} \quad (3)$$

\vec{U} can be defined as:

$$\vec{U} = \nabla \varphi \quad (4)$$

The velocity must still satisfy the conservation of mass equation, where substitution with the relationship regarding potential and velocity derives the Laplace equation.

$$\nabla * \vec{U} = 0 \quad (5)$$

$$\nabla * \nabla \varphi = 0 \quad (6)$$

$$\nabla^2 \varphi = 0 \quad (7)$$

When solving the Laplace equation boundary conditions must be defined to find a solution.

Usually there are three boundary conditions used to solve the Laplace equation [19]:

- Bottom boundary condition
- Wall boundary condition
- Surface boundary conditions
 - Kinematic free surface boundary condition
 - Dynamic free surface boundary condition

2.1.2 Regular Waves

For the linear wave theory, it is assumed that waves are sinusoidal with constant wave amplitude, length, and period. The sinusoidal wave has the following surface profile [19]:

$$\xi = \xi_0 \sin(\omega t - kx - \theta) \quad (8)$$

ξ_0 is the amplitude.

ω is the wave frequency

t is time

k is the wave number.

x is the position.

This equation is derived from the potential function by using the dynamic boundary condition. When the sea surface is $z = 0$ which yields the sinusoidal wave equation.

$$\varphi(x, z, t) = \frac{\xi_0 g \cosh k(z+d)}{\omega \cosh(kd)} \cos(\omega t - kx - \theta) \quad (9)$$

$$\xi = -\frac{1}{g} \frac{\partial \varphi}{\partial t} \quad (10)$$

$$\xi = -\frac{1}{g} * -\omega \frac{\xi_0 g \cosh k(z+d)}{\omega \cosh(kd)} \sin(\omega t - kx - \theta) \quad (11)$$

$$\xi = \xi_0 \frac{\cosh k(z+d)}{\cosh(kd)} \sin(\omega t - kx - \theta) \quad (12)$$

$$\xi = \xi_0 \sin(\omega t - kx - \theta) \quad (13)$$

2.1.3 Irregular Waves

Irregular waves are more realistic description for representing ocean waves. The basic assumption regarding wave superposition is that it is possible to represent the irregular sea surface using linear superposition of wave components. A superposition with many regular waves yields a more realistic record of the sea surface profile. Characterization of the irregular sea state can be done with the average zero up crossing and the significant wave height out from given available time history [17].

Obtaining the average wave height, measurement for successive wave heights need to be classified with intervals. These number for each group is divided by the total number of wave heights to obtain the probability density function. The PDF function for wave height usually fits a Gaussian distribution or a normal distribution quite well. With the standard deviation for the surface elevation being directly linked to the significant wave height [17].

$$H_{1/3} = 4 * \sigma \quad (14)$$

$$\sigma = \sqrt{\frac{1}{N-1} \sum_{n=1}^N \xi_n^2} \quad (15)$$

Generally, sea and swell satisfy the condition of narrow banded frequency spectrum. In that case for a narrow band Gaussian distribution, then the wave height statics follows a Rayleigh distribution.

$$F_{CG}(c) = 1 - e^{-\frac{1}{2}(\frac{c}{\sigma_E})^2} \quad (16)$$

The given equation above is the cumulative density function for the global maxima. Given a time interval of n-amount global maxima the distribution of the largest maxima will also follow a Rayleigh distribution [20].

$$F_{C_N}(c) = F_{C_{G1}}(c) * F_{C_{G2}}(c) \dots * F_{C_{GN}}(c) = [F_{C_N}(c)]^N \quad (17)$$

As stated earlier that an irregular wave can be the superposition of many sinusoidal waves, it's possible to study the frequency characteristics of such an irregular signal using Fourier series analysis. The wave elevation in a time series can be written as the sum of many regular wave components [20].

$$\xi(t) = \sum_{n=1}^N \xi_n \cos(\omega_n t - \theta_n) \quad (18)$$

θ_n is the phase angle component.

One method for solving this is to introduce the phase angle as a random variable, being uniformly distributed between 0 and 2π . The stochastic process is a sum of many independent random components, and none of the components dominate over the other. With a stationary Gaussian process which can be characterized by the auto-correlation function $R_{\Xi\Xi}(\tau)$. The wave amplitude can then be described by the relation between the spectral density function and the auto-correlation function $R_{\Xi\Xi}(\tau)$.

$$R_{\Xi\Xi}(0) = \int_0^\infty S_{\Xi\Xi}(\omega) d\omega = Var[\Xi(t)] = \sigma_\Xi^2 \quad (19)$$

The wave amplitude can then be expressed in a wave spectrum. Where one component carries the variance within that frequency bin, $\Delta\omega$ center around, ω_n [17].

$$\sigma_{\Xi}^2 = S_{\Xi\Xi}(\omega)\Delta\omega = \frac{1}{2}\xi_n^2 \quad (20)$$

$$\xi_n = \sqrt{2S_{\Xi\Xi}(\omega)\Delta\omega} \quad (21)$$

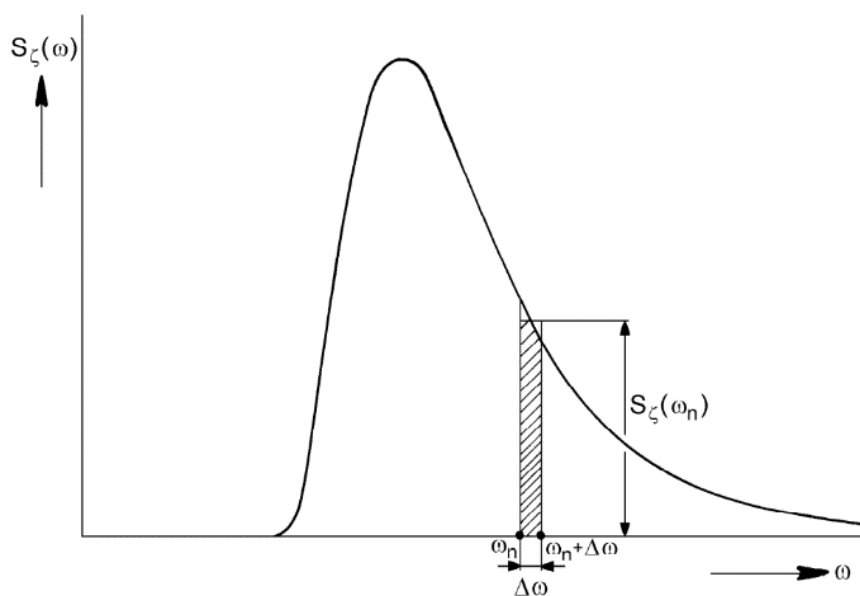


Figure 2 - 1 Wave spectrum [7].

One frequently used wave spectrum in the North Sea is the JONSWAP wave spectrum. The Joint North Sea Wave Project was a study of wave growth under growing wind conditions executed in the southern North Sea, which yielded the following equation given in hertz [20].

$$S_{\Xi\Xi}(f) = \underbrace{0.3125h_s^2 t_p^{-4} f^{-5} \exp\{-1.25t_p^{-4} f^{-4}\}}_{\text{Pierson-Moskowitz spectrum}} (1 - 0.287 \ln(\gamma)) \gamma^{\exp\left\{-0.5\left(\frac{f-f_p}{\sigma f_p}\right)^2\right\}} \quad (22)$$

γ is the non-dimensional peak shape parameter.

σ is the spectral width parameter.

The parameters can be calculated from DNV-RP-C205, where there is also a common directional function for wind sea. The typical values for n regarding wind sea are between two and four.

2.2 Rigid Body Motions in Waves

Dynamics for rigid body motions in waves are governed by the combined actions of different external forces, moments and by the inertia of the bodies themselves. These forces and moments for fluid dynamics cannot be defined as acting at a single point or a discrete point of the system. They must be regarded as distributed in a relative smooth or continues manner throughout the mass of the fluid particles [17].

2.2.1 Rigid Body Dynamics

Dynamic loads on a floating structure in fluid vary with time, where it has irregular characteristics. From section 2.1.3 irregular waves could be described as a superposition of regular waves the same can be done regarding floating structure. The irregular motions of a floating structure can be defined as the superposition of linear motions and can be obtained for a range of frequencies [17]. A linear transfer function between the waves and vessel motion describes the relations between input and output, can be defined as:

$$|H(\omega, \theta)| = \frac{\eta_a}{\xi_a} \quad (23)$$

The response amplitude operator can be used to determine the response spectrum by utilizing the transfer function. The RAO represent the relation between the amplitude and the wave for each given frequency [17].

$$S_{\eta}(\omega) = |H(\omega, \theta)|^2 * S_{\xi}(\omega) \quad (24)$$

For the motions concerning rigid bodies in fluids can be described by using the equation of motion.

$$(m + a)\ddot{x} + c\dot{x} + kx = 0 \quad (25)$$

m = Mass of the Object

a = Added mass

x = Displacement

c = Damping coefficient

k = Spring coefficient

For systems that require two or more coordinates to describe its motions is called multiple-degree-of-freedom system [15]. From Newton's second law of motion, it is derived a coupled equation of motion. Where the mass, damping and stiffness terms are expressed with matrices.

$$[m]\ddot{\vec{x}} + [c]\dot{\vec{x}} + [k]\vec{x} = \vec{f} \quad (26)$$

2.3 Wave Force on Slender Elements

Wave force on slender elements is based on slender cylinders, where the diameter is small relative to the wavelength. Where it is assumed that the motions of the water are the same all over the diameter of the cylinder. The Morrison equation is used to estimate inertia and drag loads per unit length for slender objects exposed to waves and/or current [17].

$$f(t) = \rho V(1 + C_a)\dot{v} + \frac{1}{2}\rho C_D A v |v| \quad (27)$$

The first term in the equation is the inertia force, where it's the sum of the mass of the displaced volume and the added mass times fluid acceleration. The second term is the drag force, where it's the density of the fluid times the projected area times fluid velocity and included the drag coefficient.

2.3.1 Added Mass Coefficient

When an object is accelerating in a fluid a force arises due acceleration of the nearby fluid particles. Newton's second law applies to Added mass. Where there is acceleration of the object times the hydrodynamic mass [17].

$$f = m_a \ddot{r} \quad (28)$$

m_a = Added mass

\ddot{r} = Acceleration

The added mass coefficient can be calculated by using the relationship between added mass per unit length divided by the density of the fluid and the area.

$$C_A = \frac{m_a}{\rho A} \quad (29)$$

2.3.2 Drag Coefficient

In general, the drag coefficient is dependent on the geometry of the object, Reynolds number and the Keulegan-Carpenter number. The drag coefficient changes when the Reynold number changes for various degrees of surface roughness [1].

It is assumed that the drag coefficient is constant with depth for the submerged object. The drag coefficient can be found by using Table B-2 in DNV-RP-H103 [1].

2.3.3 Slam Force

Slam forces or slamming occur during the impact between the object and the water surface. Large slamming force can be a problem with concern of snap loads and the strength of the object. The impulse loads are caused by the transfer of momentum from the water particles to the object [1].

$$f_s = v^2 * \frac{dm_a}{dz} \quad (30)$$

Slam force can also be written as:

$$f_s = \frac{1}{2} \rho C_S A_p v^2 \quad (31)$$

A_p is the waterplane area projected by the object. For the slamming coefficient it can be expressed as:

$$C_S = \frac{2}{\rho A_p} \frac{dm_a}{dz} \quad (32)$$

2.4 Probability Model

Probability models can be used to obtain estimates for exceedance probabilities. For marine operations in irregular waves, precise prediction of an event with high randomness is impossible. Selecting a probabilistic model is crucial to determine the exceedance probabilities for maxima and minima. When fitting a model, it is important to have sufficient data, this is needed for the distribution of an event. For instant the data can be historical or numerical simulation [21].

2.4.1 Extreme Value Distribution

Extreme value distribution is a limiting distribution for minimums or maximums, extreme values describe the extreme events. Extreme value is used to set realistic limiting sea states for an operation where the concern can be for instants snap loads. Of which the limiting sea state will be based on either exceedance of material strength or potential slack in the slings.

For the extreme values of a wave series, it is based on the absolute maxima or minima. Where data for different wave series need to be collected. The Gumbel distribution is a commonly used for determining extreme values for a system. The two Gumbel parameters are β and μ which are the scale parameter and the location parameter. The Gumbel distribution is given by [15]:

$$F_x(x) = e^{-e^{-\left(\frac{x-\mu}{\beta}\right)}} \quad (33)$$

When checking the extreme values, a Gumbel plot is used to verify how good the distribution fits a linear line where maxima is for $-\ln[-\ln(P)]$ and for minima $-\ln[-\ln(1 - P)]$ [22].

Another commonly used statistical method is the Weibull distribution. The Weibull distribution are usually based on two parameters, the scale parameter κ and shape parameter β . The Weibull distribution is commonly used when modeling possible failure rates for products to evaluate its reliability [15].

$$F_x(x) = 1 - e^{-\left(\frac{x}{\kappa}\right)^\beta} \quad (34)$$

The Weibull plot is found by the liner equation given in equation 35.

$$\ln[-\ln(1 - F(x))] = \beta \ln x - \beta \ln \kappa \quad (35)$$

Chapter 3

Hydrodynamic Analysis of Wavefields and Installation Vessel

3.1 Overview

OrcaWave is a diffraction analysis program that calculates the responses and loading for wet bodies using potential flow theory [23]. The governing equation used for OrcaWave is based on the fact that the fluid flow is assumed to be incompressible, inviscid, and irrotational. The fluid velocity is given by $\nabla\varphi$, where the velocity potential φ satisfies Laplace's equation in the fluid domain. Substituting Laplace's equation into the integrated Navier-Stokes equation yields the Bernoulli equation for the pressure [23].

$$p(X, t) = -\rho\left(\frac{\partial\varphi}{\partial t} + \frac{1}{2}(\nabla\varphi)^2 + gZ\right) \quad (36)$$

The governing equations can only be solved using the computational fluid dynamics approach. Since Laplace's equation is linear, the boundary conditions for the moving body surface and the free surface are nonlinear. In practical applications, wave steepness is often small, and it is standard to proceed with a perturbation expansion in this parameter [23].

$$\varphi(X, t) = \varphi^{(1)}(X, t) + \varphi^{(2)}(X, t) + \dots \quad (37)$$

OrcaWave solves these equations using the standard boundary integral equation method. Damping, added mass, and RAOs results from solving the first-order problem $\varphi^{(1)}$. Continuing the expansion to second-order and solving for $\varphi^{(2)}$ results in QTFs [23]

When solving the diffraction analysis in OrcaWave, it can use three types:

- **Potential formulation only:**

OrcaWave solves the potential formulation. The solution yields result for the velocity potential for all mesh panels. This enables the pressure to be evaluated on the surface for all bodies, and hence body results are generated for: damping, added mass, displacement RAOs, and load RAOs. In addition, the potential formulation can also evaluate the pressure in the fluid, which will yield the sea state RAOs for the fluid pressure [23].

- **Potential and source formulations:**

OrcaWave solves the source formulation, which yields the source function for all mesh panels. This enables tangential fluid velocity to be evaluated on the surface of all bodies; hence body results are generated for mean drift loads. In addition, Sea state RAOs are available for both pressure and fluid velocity [23].

- **Full QTF calculation:**

In addition to solving for both potential and source formulation, OrcaWave will also solve for the second-order potential at second-order frequencies, generating results for potential loads and quadratic loads, which together give the full QTFs [23].

3.2 Vessel Setup

The vessel setup in OrcaWave is imported from a WAMIT mesh file [24] and into OrcaWave with symmetry for XZ-plane. The vessel is imported as a “body” where the mesh position and orientation are specified in the mesh origin's X, Y, and Z coordinates [23]. The body mesh file must contain the wet body surface for the selected body. The calculation is only performed for the wet body panels.

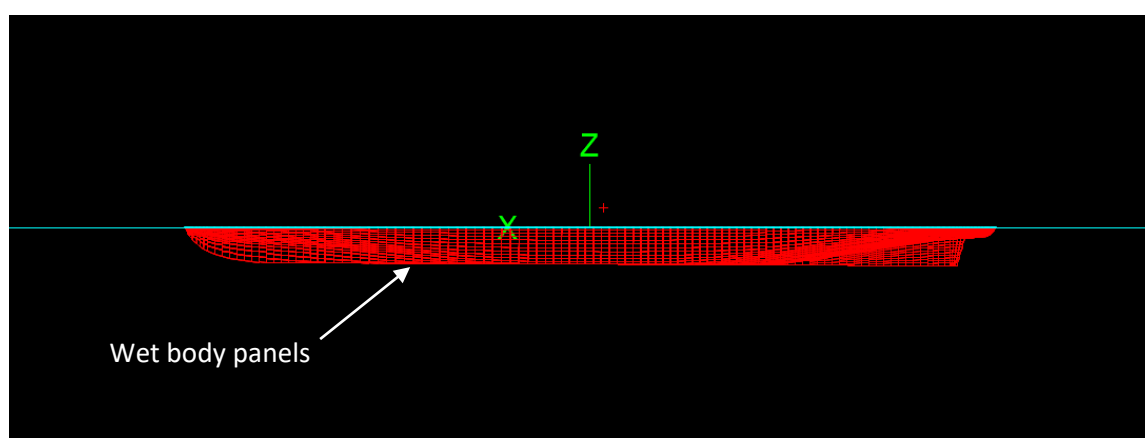


Figure 3 - 1 Vessel mesh in Orcawave

Calculation and output are set to potential formulation only. The potential formulation gives the most accurate values for the basic results computed directly from the values of φ : damping, added mass, load RAOs, and displacement RAOs. The source formulation obtains results depend on $\nabla\varphi$, such as mean drift loads and sea state velocity RAOs [23]. The waves are referred to by period for the given environment, and the data used is given in Table 3 - 1.

Table 3 - 1 data inputted for the environment.

	Value	Number specified
Water depth	200 m	1
Density	1025kg/m ³	1
Period	0,5s – 60s	66
Wave heading	0° – 180°	37

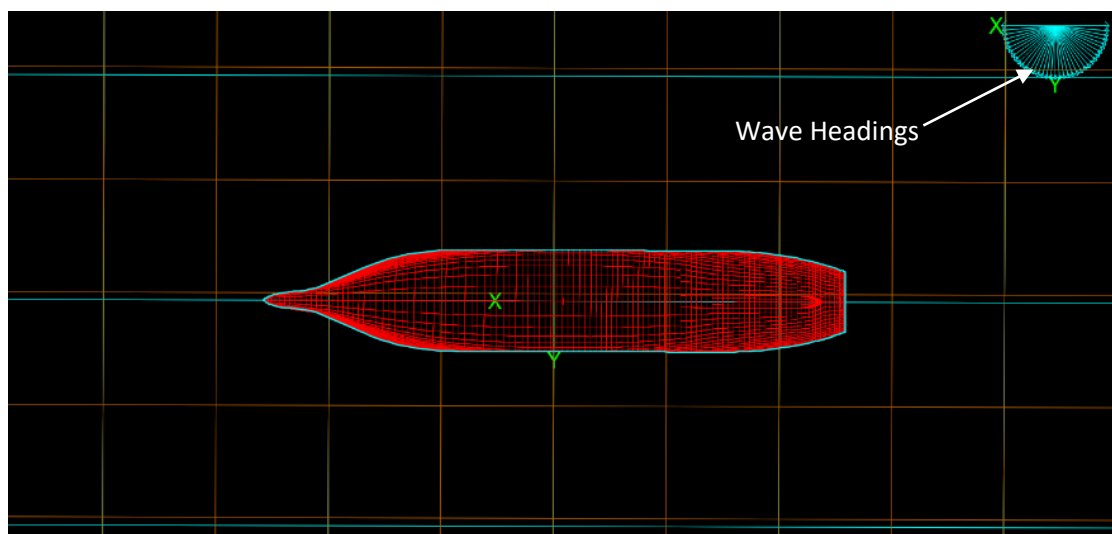


Figure 3 - 2 Vessel mesh with given wave headings

The data requirement needed from the vessel is the mesh file and the inertia. Constraints can also be implemented for specifying external stiffness or damping. The mesh file contains the draft, length, and beam data for the vessel setup. The inertia is defined as a matrix (for the general body) where the center of gravity, mass, and moment of inertia tensor must be specified. For constraint, roll damping has been specified due to the potential theory usually overestimating the roll motion of the ship. This is because, from the potential theory, the viscous effects are absent, such as skin friction and vortex shedding, which can contribute to the roll damping. Therefore, the constrain is used as a convenient measure for the damping effect [23]. The data inputted in Orcawave is given in Table 3 - 2.

Table 3 - 2 Vessel properties

	Value
Length	155 m
Beam	27 m
Draught	7,2 m
Mass	19539,2 t
CoG X	-2,5 m
CoG Y	0 m
CoG Z	3,9 m
Moment of inertia tensor Xx	2247000 t * m ²
Moment of inertia tensor Xy	0 t * m ²
Moment of inertia tensor Xz	192600 t * m ²
Moment of inertia tensor Yx	0 t * m ²
Moment of inertia tensor Yy	25920000 t * m ²
Moment of inertia tensor Yz	0 t * m ²
Moment of inertia tensor Zx	192600 t * m ²
Moment of inertia tensor Zy	0 t * m ²
Moment of inertia tensor Zz	25630000 t * m ²
D44	112500 kN * s * m

The last input for the vessel is the sea state RAOs, which will be used to calculate the shielding effect from the vessel. Sea state RAOs will give results at the location of the field points for the pressure in the fluid. The body potential is obtained by applying Green's theorem [23].

$$\varphi_B(X) = \frac{1}{4\pi} \int_{SB} \left\{ G \frac{\partial \varphi(\xi)}{\partial \eta_\xi} - \varphi_B(\xi) \frac{\partial G}{\partial \eta_\xi} \right\} dS_\xi \quad (38)$$

G is the Green's function.

SB is the surface of the body.

A grid of field points is specified in OrcaWave to simulate the shielding effect from the vessel. The water particles in the given location will have a different velocity potential RAO than the undisturbed sea. The sea state RAO is located and calculated for the splash zone crossing of the GRP cover.

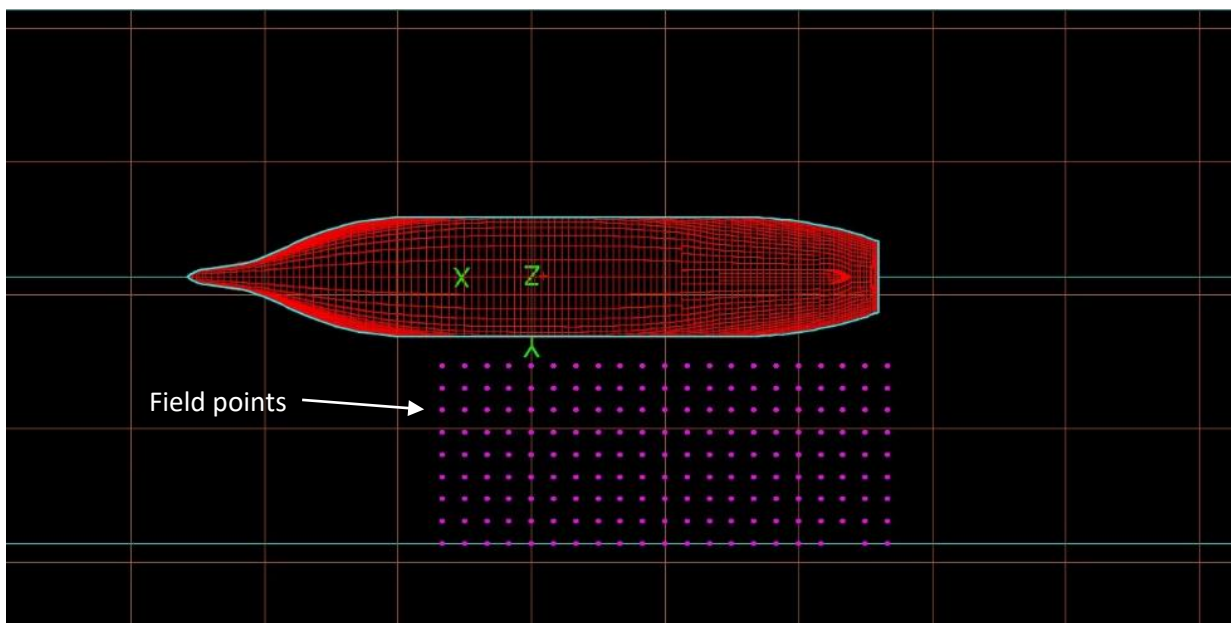


Figure 3 - 3 Vessel with field points for the calculation of sea state RAOs

3.3 Hydrodynamic Analysis Results

3.3.1 RAOs for Heave, Pitch, and Roll

Before the result have been extracted, the natural period for heave, pitch, and roll have been manually estimated to validate and compare with the simulation results. The manual calculation is based on the equations given below [19].

$$T_{Heave} = 2\pi \sqrt{\frac{m+m_a}{k}} \quad (39)$$

$$T_{Pitch} = 2\pi \sqrt{\frac{I_p+I_a}{k}} \quad (40)$$

$$T_{Roll} = 2\pi \sqrt{\frac{I_r+I_a}{k_r}} \quad (41)$$

The manually estimated natural period for heave, pitch, and roll yields:

$$T_{Heave} = 7.9 \text{ seconds} \quad (42)$$

$$T_{Pitch} = 6.9 \text{ seconds} \quad (43)$$

$$T_{Roll} = 14.8 \text{ seconds} \quad (44)$$

OrcaWave automatically makes an excel sheet from the simulation result, where all the simulation data is placed. The displacement RAOs simulation data have been extracted and plotted for pitch, roll (Figure 3 - 5) and heave (Figure 3 - 4).

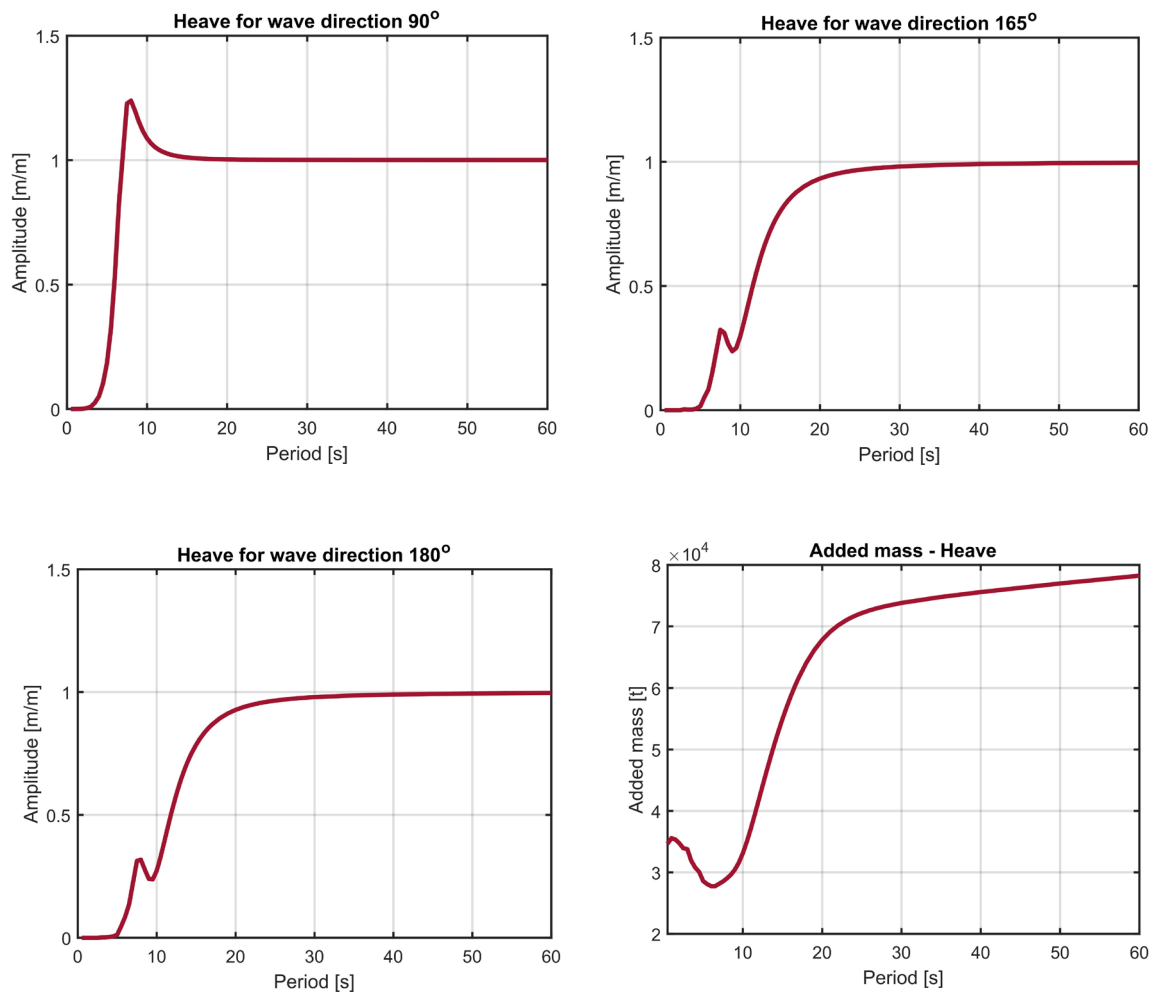


Figure 3 - 4 Heave RAO for wave direction 90°, 165°, 180°, and added mass.

The response amplitude operator for the vessel from OrcaWave clearly shows that the heave motion has the same peak at around eight seconds, corresponding to the calculated natural period. This is a good indication that the model is correct, of which the same exciting period is constant for the simulation and manually estimated natural period. Another good indication that the model is correct is due to no sudden drops in the heave motion or the added mass. The heave

RAO for the vessel is almost similar between 180 degrees and 165 degrees, which is slightly larger due to the small roll motion generated at 165 degrees.

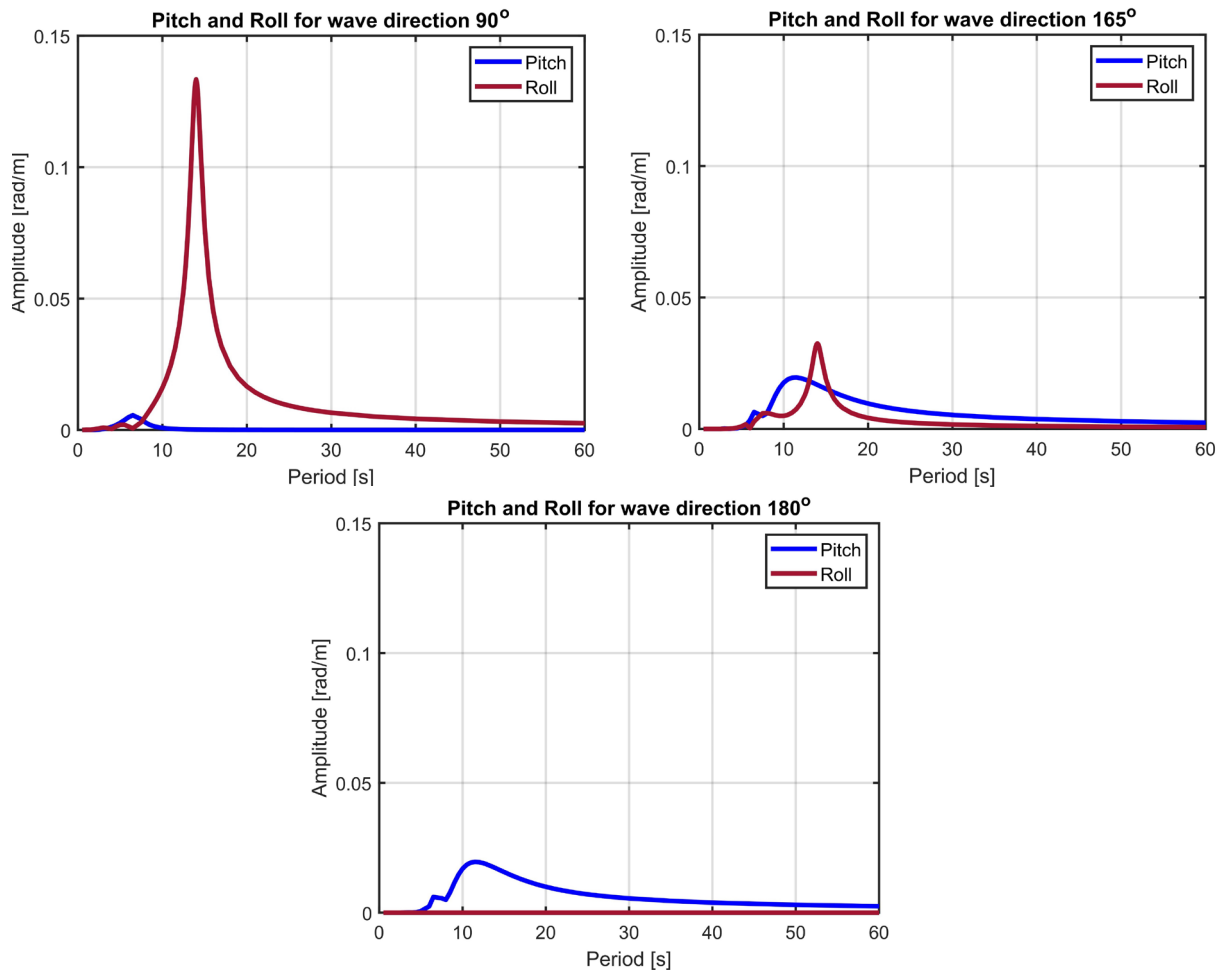


Figure 3 - 5 RAO for pitch and roll for wave direction 90°, 165°, and 180°

The same can be seen in the results for pitch and roll. The “sharp” peak from the simulated results is around seven seconds for pitch and 15 seconds for roll, which corresponds to the manually estimated natural periods.

3.3.2 Shielding Results

The shielding results have been plotted as a colormap, which shows how the velocity potential in the waves changes with respect to the distance from the vessel. The shielding effect has been estimated for all wave directions but only plotted for the wave heading used for the time-domain simulation.

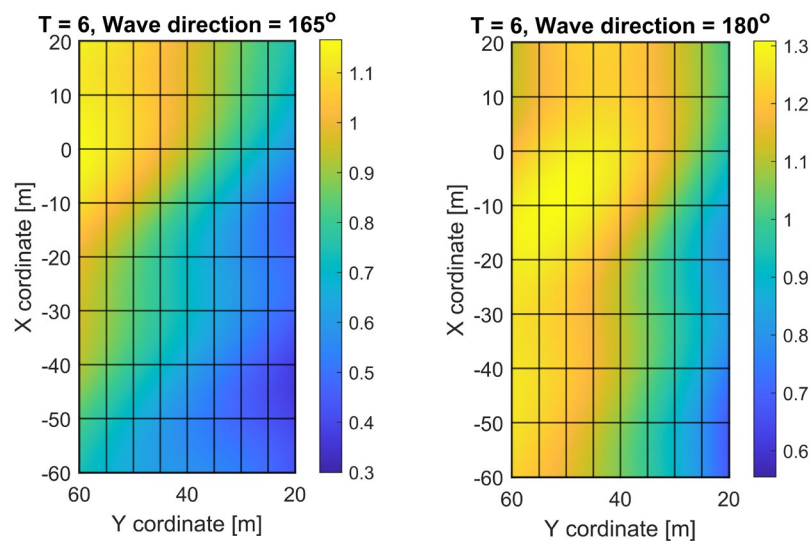


Figure 3 - 6 Shielding effect $T = 6$ s for wave direction 165° and 180°

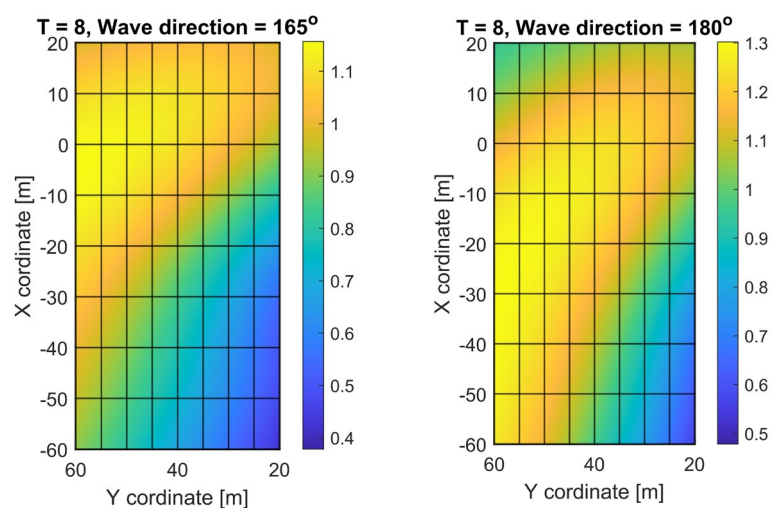


Figure 3 - 7 Shielding effect $T = 8$ s for wave direction 165° and 180°

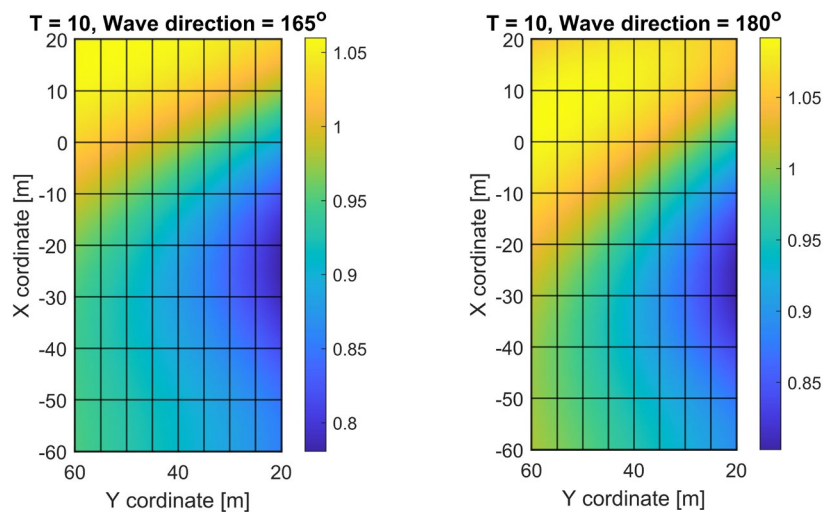


Figure 3 - 8 Shielding effect $T = 10$ s for wave direction 165° and 180°

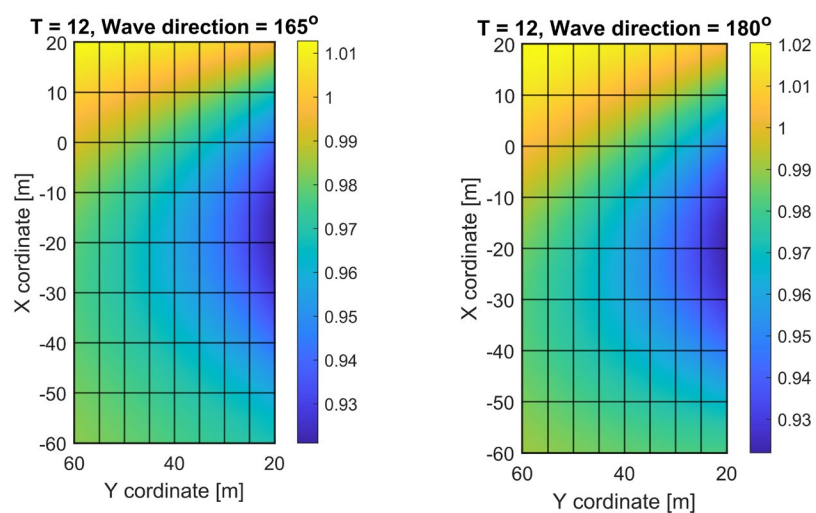


Figure 3 - 9 Shielding effect $T = 12$ s for wave direction 165° and 180°

As expected, the wave field around the floating vessel is different from the oncoming waves due to the presence and motion of the vessel. For Figure 3 - 6, there is a significant shielding effect for all directions, where for 165° , the incoming sea in some locations is lower than half of the given sea state. For 180° , the shielding effect is only prevalent close to the ship.

Figure 3 - 7 shows that the shielding area has decreased, but there is still some good location concerning lowering operations. For 165 and 180 degrees, the best positions are close starboard quarter. The best shielding results are observed close to the vessel. This may cause issues depending on the clearance between the vessel and the lifted object. For Figure 3 - 8, the shielding effect for 165 degrees decreases significantly compared to Figure 3 - 6. This can be attributed to longer wave periods reducing the shielding effect. In long waves, the ship will tend to follow the wave surface [17]. However, some shielding effects remain close starboard quarter for the vessel in the given directions.

For Figure 3 - 9, most of the shielding effects have dissipated, only small areas will give some benefits of shielding, but it is almost neglectable. The long periods as stated above will cause the vessel to follow the wave surface and diminish the shielding effect.

The different figures show that the vessel presence will reduce the incoming sea states for the given directions. The vessel for waves at 165 degrees will yield the greatest protection for most periods listed. For head waves, it is almost the same as 165 degrees, however, with a lower shielding effect and more emphasis on the location of the lifted object. In conclusion, the shielding from the vessel will reduce the sea state at proper vessel heading angles. The shielding effect is more prevalent for shorter periods than for longer periods. The lifted object must be correctly positioned according to the vessel to get the maximum effect of the provided shielding. Li et al. [11] have investigated the shielding effect for lowering an offshore wind turbine monopile from a floating installation vessel, with results similar to what's been discussed in this chapter.

Chapter 4

Numerical Model for Time Domain Simulation

4.1 Overview

This chapter presents the numerical model for the GRP deployment. The simulations are conducted in the simulation software OrcaFlex. OrcaFlex is a package for designing and analyzing a wide range of marine systems. Typical applications for offshore dynamics, mooring systems, marine renewables, and installation. A wide range of possible modeling objects can be chosen depending on the required level of complexity [9].

The GRP deployment model combines a vessel, six DOF buoys, lines, and a winch. The vessel is stationary using links as mooring lines with specified vessel motion. For the winch, it has been assigned a specific payout rate at a constant speed.

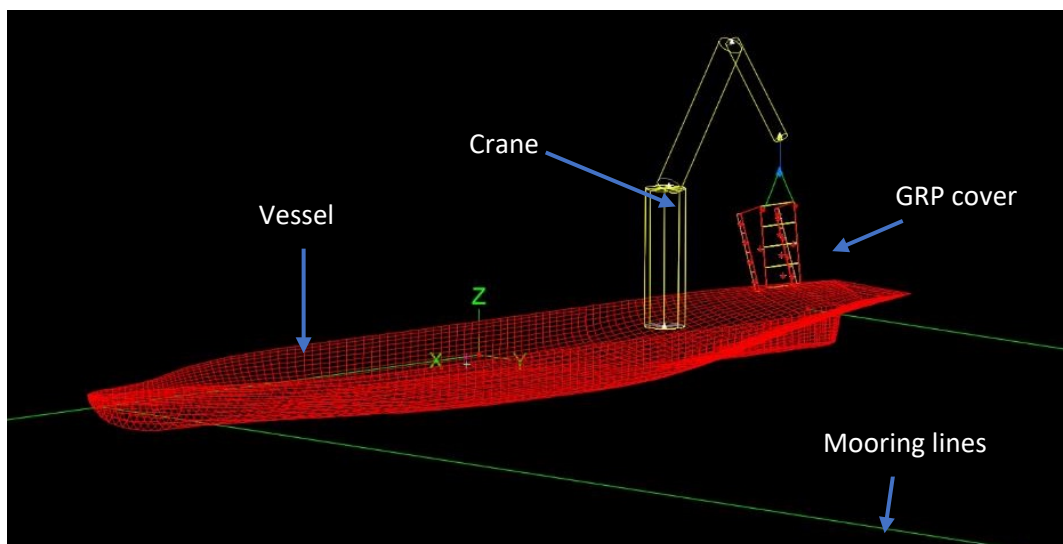


Figure 4 - 1 GRP deployment vessel in OrcaFlex.

The GRP cover is implemented into OrcaFlex as 14 lumped buoys connected to one main buoy. The numerical time-domain simulations are only done for the in-air and the splash zone crossing. The hydrodynamic forces for the GRP cover are based on DNV-RP-H103 modeling and analysis of marine operations [1]. This means amplitude-dependent hydrodynamics parameters are not implemented.

Main assumptions for simplified method [1]:

- The horizontal extent of the lifted object (in wave propagation direction) is relatively small compared to the wavelength.
- The vertical motion of the object follows the crane tip motion.
- The load case is dominated by the relative vertical motion between object and water – other motions can be disregarded.
- Increased heave motions of the lifted object due to the resonance effect are not covered.

For the manual estimations, it was assumed:

- Drag and added mass coefficients could be calculated based on a flat rectangular plate with an area equal to the projected area.
- Horizontal sea bottom and free surface for infinite horizontal extent.
- Pressure follows Bernoulli's equation for infinite water depth.
- Irrotational, incompressible, and inviscid flow.

4.2 Vessel Setup

The vessel is imported from OrcaWave into OrcaFlex, with all the properties collected from OrcaWave. The vessel setup will be equal for all the assessments of allowable sea states for hydrodynamics. The only difference is in the shielding case, where OrcaFlex will use the sea state RAO data for the vessel to implement a disturbance effect. This disturbance effect can be applied to nearby three DOF, six DOF buoys, and lines. The disturbance effect is only applied to the GRP cover and the shackle for the shielding case. The sea state RAO is the velocity potential disturbance RAOs, which OrcaFlex uses to calculate the fluid velocity, surface elevation, and fluid acceleration in the disturbed sea state [9].

For the vessel motion, there is a large variation to select from in the software OrcaFlex. The vessel setup will either be coupled or uncoupled motions to assess the allowable sea states. The vessel motion used to assess the sea states for the GRP protection cover will be determined in chapter 5 for the sensitivity study of coupled and uncoupled motion.

4.3 GRP Protection Cover

The GRP protection cover has been modeled in the CAD program Autodesk Inventor [25], using the cover dimensions from Solaas et al. [10]. In addition, Autodesk Inventor has been used to extract essential model data that can be used in OrcaFlex, such as mass, mass moment of inertia, volume, and different lifting angles.

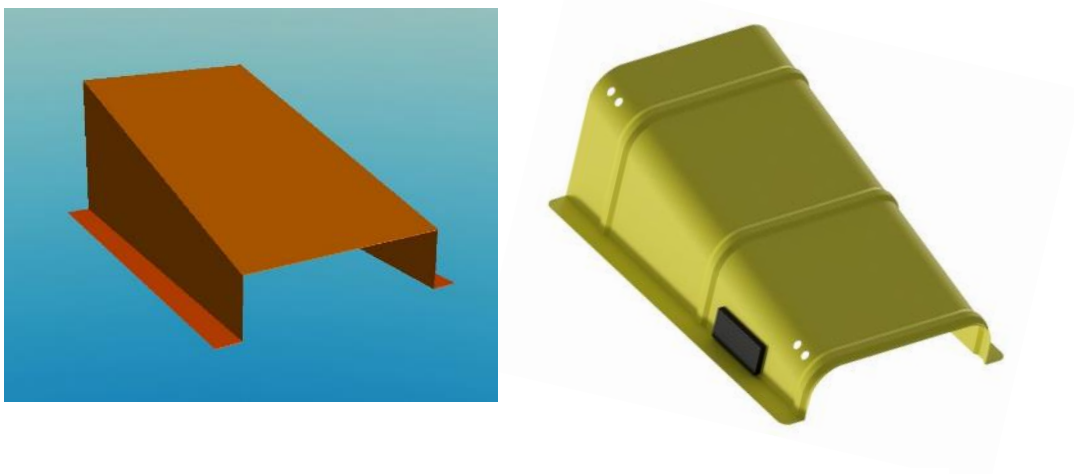


Figure 4 - 2 GRP Cover modeled in OrcaFlex and Autodesk Inventor.

From Figure 4 - 2, the GRP cover modeled in OrcaFlex looks simpler than the Autodesk inventor model. However, this is just a shaded drawing to project the cover in OrcaFlex. Of which the six DOF buoy contains all the data from Autodesk Inventor. The GRP cover dimension is given in Figure 4 - 3 and Table 4 - 1.

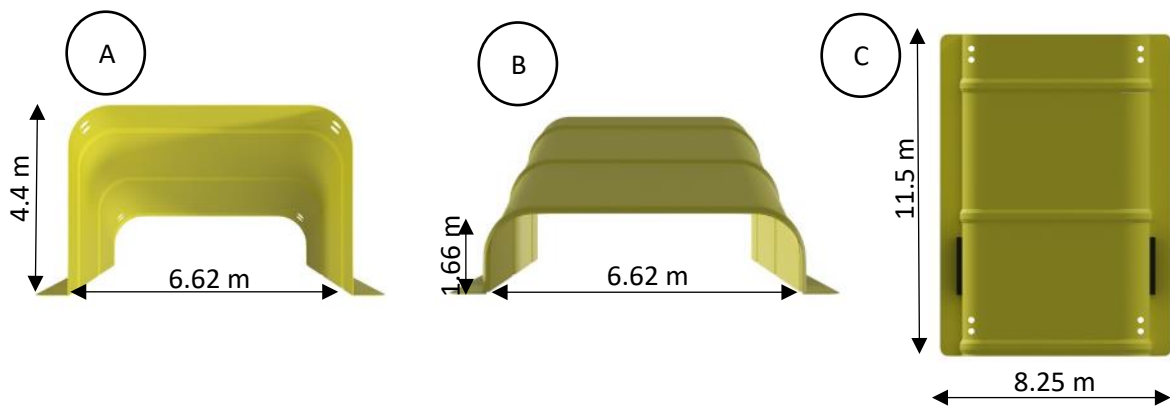


Figure 4 - 3 Dimensions for GRP cover, (A) view from the front, (B) view from the back, (C) view from above.

Table 4 - 1 Data extracted from Autodesk Inventor.

Parameters	Value
Length	11.5 m
Width included flanges	8.25 m
Width excluded flanges	6.62 m
Hight-a	4.40 m
Hight-b	1.66 m
Thickness	0.02 m
Vertical COG	1.846 m
Horizontal COG	6.665 m
Density cover	1 750 kg/m ³
Density ballast	7 850 kg/m ³
Volume cover	3.1184 m ³
Volume Ballast	0.8207 m ³
Mass	11900 kg

When creating a model in OrcaFlex, different types of buoys can be used to produce a model. For the GRP cover, 15 different lumped buoys have been used to represent a part or a function of the GRP cover. When using multiple lumped buoys to model the payload, they must be connected to create a single rigid body [9]. The side plate lumped buoys represent the flanges for the GRP cover, where one single side plate represents one part of the flange and contains all the hydrodynamic properties for that piece. The four mid plates represent the entire top cover and its hydrodynamic properties. The wall lumped buoy represents the side/wall of the GRP cover and contains the hydrodynamic properties of the wall. Finally, the main buoy has been used to connect all the buoys and create a single rigid body, of which the main buoy contains all the geometrical properties of the GRP cover. The GRP cover model is presented in Figure 4 - 4.

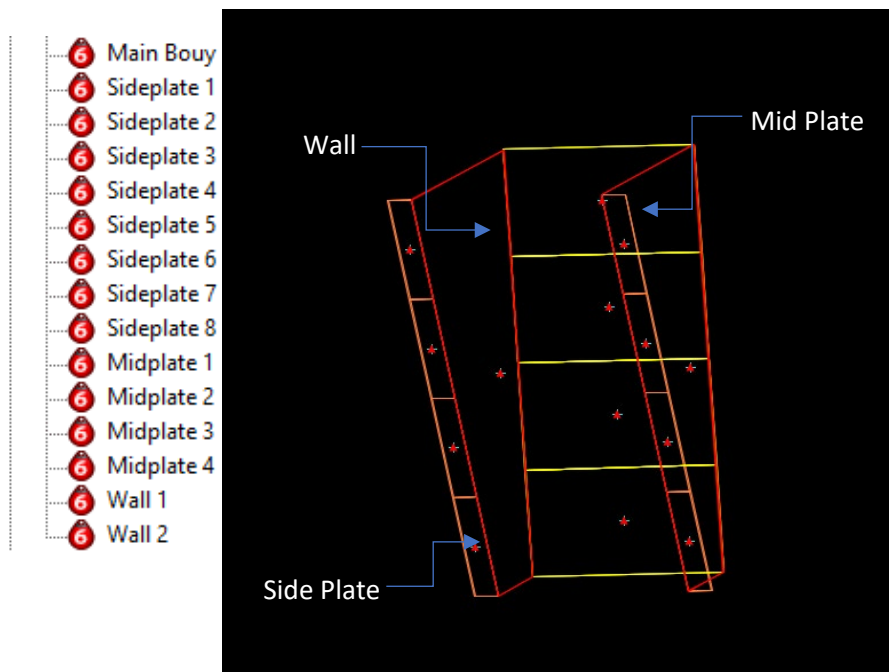


Figure 4 - 4 GRP model from OrcaFlex.

The red triangles from Figure 4 - 4 represent the connection point for the lumped buoys to the main buoy. The center of mass for this model is only dependent on the main buoy, which contains all the properties from Autodesk Inventor. In OrcaFlex, the center of mass for the main buoy is located at the center of the buoy. The center of mass can later be moved with inputs for

X, Y, and Z directions to the desired position. The center of mass has been placed such that the lifting angle for the cover is at 70 degrees. This will be the primary lifting angle of the cover used for most of the simulation. However, different lifting angles will be tested to assess the importance of the waterplane area for low-weight objects with large surface areas. All the lifting angles that will be used for simulations are given in Figure 4 - 5.

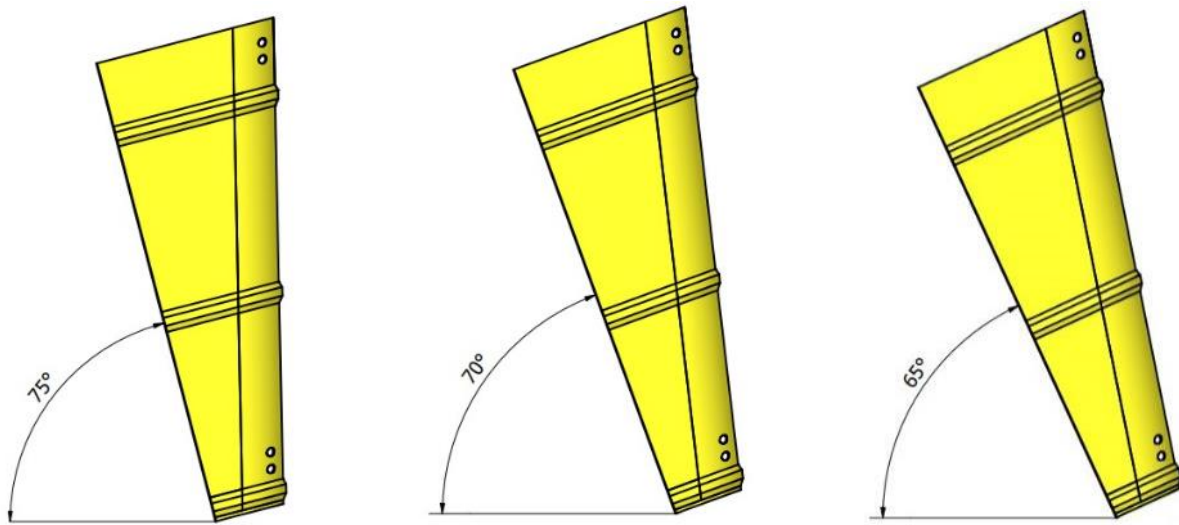


Figure 4 - 5 Lifting angles for GRP cover.

When using different lifting angles, the center of mass for the ballast needs to be moved in the correct position at the wall. The shifting position of the ballast will affect the mass moment of inertia, the center of mass for the cover, and the waterplane area for the slamming force. The mass and mass moment of inertia can be divided into each lumped buoy about its local center of mass. However, dividing it into many individual parts usually simplifies the structure. Therefore, Autodesk Inventor has been used to extract the mass moment of inertia for the entire structure. The general properties of the main buoy, side plates, mid plates, and walls are given in Table 4 - 2. The mass moment of inertia and center of mass for the main buoy is given in Table 4 - 3.

Table 4 - 2 Model dimensions in OrcaFlex.

Model	Value			Mass
	X	Y	Z	
Main buoy	8.25 m	3.03 m	11.5 m	11 900 kg
Side plates	0.815 m	0.02 m	2.875 m	0 kg
Mid Plates	6.62 m	0.02 m	2.956 m	0 kg
Walls	0.02 m	3.03 m	11.5 m	0 kg

Table 4 - 3 Model COG and mass moment of inertia in OrcaFlex.

Model	Center of mass			Mass moment of inertia		
	X	Y	Z	X	Y	Z
65°	0	0.75 m	- 0.91 m	95 573 kgm ²	196 174 kgm ²	134 533 kgm ²
70°	0	0.15 m	- 0.915 m	89 054 kgm ²	196 193 kgm ²	128 195 kgm ²
75°	0	0.05 m	- 2.05 m	131 665 kgm ²	239 077 kgm ²	127 922 kgm ²

The center of mass, as stated earlier, is located at the center of the representing lumped buoy. Therefore, the main buoy’s center is located at $X = 4.125$ m, $Y = 1.976$ m, and at $Z = 5.75$ m. This is the zero position for the main buoy, where it has been moved to its required position depending on the lifting angle, as shown in Table 4 - 3.

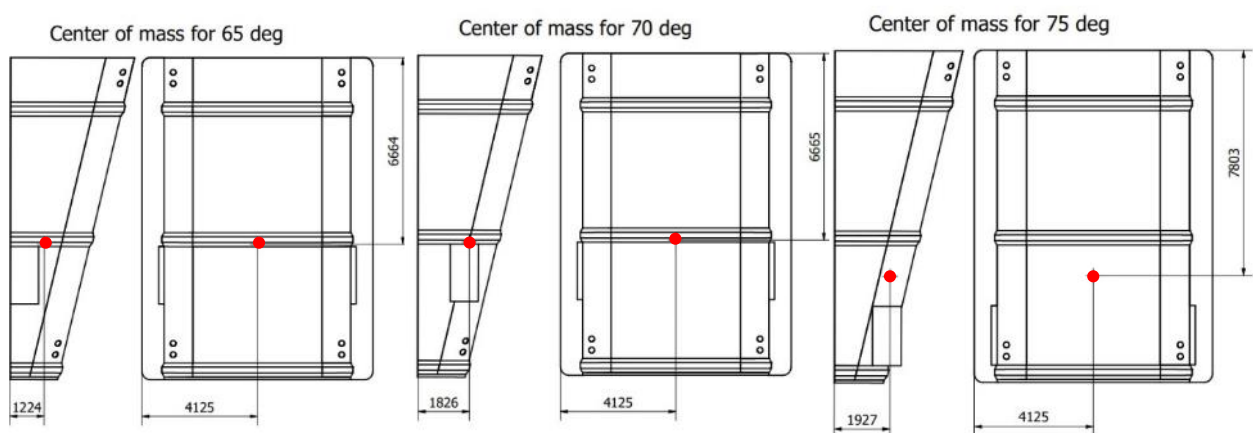


Figure 4 - 6 Center of mass from Autodesk Inventor.

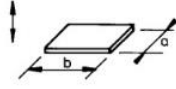
4.4 Analysis of Hydrodynamic Forces

The hydrodynamic forces have been calculated using simplified methods from DNV and verified by Solaas et al. [10]. In OrcaFlex, when using a single lumped buoy to model the payload, it can only handle changes in buoyancy and hydrodynamics in a simple way. Therefore, multiple lumped buoys have been used to model the payload to achieve a more accurate cover deployment analysis. When using more lumped buoys, volume, drag, and added mass properties must be split among the components for maximum accuracy [9].

4.4.1 Added Mass and Damping

The hydrodynamic parameters for added mass have been estimated using a simplified geometry, with the assumption of the cover being fully submerged. The simplified geometry assumes that the cover refers to a rectangular plate for the analytical added mass coefficient for three-dimensional bodies.

Table 4 - 4 Added mass for a rectangular plate Table 2-A DNV [1].

Rectangular plates 	Vertical	b/a	C_A	b/a	C_A	$\frac{\pi}{4} a^2 b$
		1.00	0.579	3.17	0.840	
1.25	0.642	4.00	0.872			
1.50	0.690	5.00	0.897			
1.59	0.704	6.25	0.917			
2.00	0.757	8.00	0.934			
2.50	0.801	10.00	0.947			
3.00	0.830	∞	1.000			

The added mass is calculated for A11, A22, and A33, then divided into the lumped buoys corresponding to their project area in X, Y, and Z directions. A11 represents the motion in Y-direction, A22 the motion in the X-direction, and A33 the motion in Z-direction. Figure 4 - 7 shows the selected projected area for each motion.

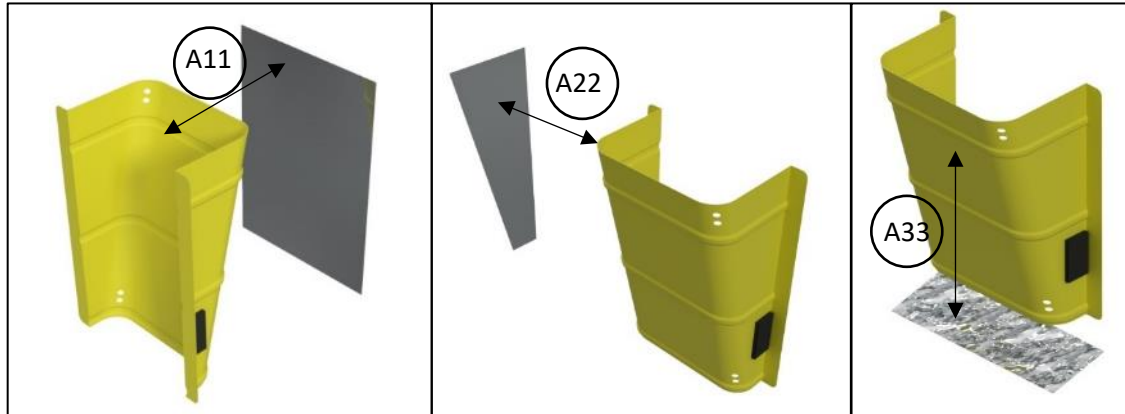


Figure 4 - 7 added mass for A11, A22, and A33, with the projected area marked in grey.

For the added mass A11, A22, and A33, it is assumed that the GRP cover position is as represented in Figure 4 - 7. However, when the GRP cover is submerged, the sea will disrupt the initial lifting angle, yielding different added mass for A11, A22, and A33 when crossing the splash zone. Therefore, the calculated added mass will better represent the motion for a fully submerged cover for the assumed GRP position.

For A22, it is assumed that it will have a large amount of “trapped” water inside the cover. However, there will be uncertainties regarding the volume due to the distance between the walls. Therefore, it is better to assume that the entire volume is filled with water rather than having a low prediction of the added mass for A22. Therefore, Autodesk Inventor has been used to fill the cover and extract the mass of the “trapped” water. The added mass and parameters for all directions are given in Table 4 - 5, of which the calculated added mass for the GRP cover is then compared with Solaas et al. [10].



Figure 4 - 8 GRP cover with trapped water from Autodesk Inventor.

Table 4 - 5 Parameters for added mass

Parameters	Value	Parameters	Value	Parameters	Value
a	8.25 m	a	3.07 m	a	2.76 m
b	11.5 m	b	11.5 m	b	6.66 m
b/a	1.39	b/a	3.75	b/a	2.41
C_A	0.67	C_A	0.86	C_A	0.79
		A22 water	223 900 kg		
A11	421 948 kg	A22	299 131 kg	A33	32 384 kg

Table 4 - 6 Comparison between added mass

	Calculated added mass	WAMIT added mass Solaas et al., (2017)	Difference (Calculated/WAMIT)
A11	421 948 kg	444 000 kg	5%
A22	299 131 kg	217 000 kg	27%
A33	32 384 kg	19 500 kg	40%

Comparing the simplified method and WAMIT shows some significant differences in the added mass for A22 and A33. The variation for A22 and A33 can be explained by Solaas et al. [10], which use a simplified GRP cover. Therefore, there may be some variations between the model design of the GRP covers, of which the only known dimensions are length, breadth, and height. In addition, the calculated added mass for this study uses DNV simplified method, which will produce differences in predicted added mass compared to a CFD simulation.

The calculated added mass has been divided into the corresponding lumped buoys. The hydrodynamic loads in OrcaFlex are calculated by an extended form of Morison's equation. The added mass load in OrcaFlex is given by [9]:

$$f_A = (\Delta_M + C_a^t \Delta_M) a_f - C_a^t \Delta_M a_b \quad (45)$$

Δ_M is the instantaneous reference mass given by $\rho_w M_{ref}$

C_a^t is the added mass coefficient for the component

a_f is the fluid acceleration relative to the earth.

$a_b = a_f - a_r$ where a_r is the fluid acceleration relative to the buoy.

When defining the added mass for the given buoys, it depends on the mass given by the submerged volume times the added mass coefficient (instantaneous reference mass times added mass coefficient), which yields the following equation for calculation of the added mass coefficient of the different lumped buoys.

$$M_a = C_a * \Delta_m \quad (46)$$

$$C_a = \frac{M_a}{\Delta_m} \quad (47)$$

The added mass coefficient is calculated for all lumped buoys with the given equation, and the extracted values are represented in Table 4 - 7.

Table 4 - 7 Parameters and added mass for lumped buoys.

	Δ_m		M_a			C_a	
		X	Y	Z	X	Y	Z
Side plates	48 kg	244 kg	10 421 kg	7 kg	5.083	217.104	0.146
Mid plates	401 kg	487 kg	84 645 kg	8 033 kg	1.214	211.085	20.032
Walls	1024 kg	147 617 kg	0 kg	97 kg	144.102	0	0.095

The added mass for each component is calculated based on the project area corresponding to the total added mass value for the given direction. For example, for A11, the project area for all the side plates corresponds to 19% of the total area. In addition, all the mid plates correspond to 81%. Therefore, the summation of all added mass for the lumped buoys will give the same value as A11, A22, and A33. The damping used for the cover has been extracted from Solaas et al. [10] and given in Table 4 - 8.

Table 4 - 8 Linear damping for cover

	B_1
Longitudinal (11)	2.4 kN/(m/s)
Transverse (22)	2.0 kN/(m/s)
Vertical (33)	89.1 kN/(m/s)

The linear damping in OrcaFlex applies the force in each local axis based on the given direction. The force applied on the lumped buoy depends on the portion of height submerged (portion wetted), where the damping forces will increase depending on the area of the lumped buoy submerged. The damping force in OrcaFlex is given by [9]:

$$f_{D_{x,y,z}} = -p_w UDF_{x,y,z} v_{x,y,z} \quad (48)$$

p_w refers to the portion of the lumped buoy wetted/submerged.

$UDF_{x,y,z}$ is the specified unit damping force for the component direction.

$v_{x,y,z}$ is the buoy velocity relative to the earth for the component direction.

4.4.2 Drag Coefficients and Inertia

OrcaFlex uses an extended form of Morison's equation regarding inertia and drag force. The inertia term is reduced by the amount $C_a \Delta a_b$ and the drag term uses the body-relative velocity [9].

$$f = (C_m \Delta a_f - C_a \Delta a_b) + \frac{1}{2} \rho C_d A |v_r| v_r \quad (49)$$

f is the fluid force per unit length on the body.

C_m is the inertia coefficient for the body, which is equal to $1 + C_a$.

v_r is the fluid velocity relative to the body.

Δ is the mass of fluid displaced by the body.

The inertia force is dependent on the added mass coefficient, which was calculated previously. Implementation in OrcaFlex is “~,” which takes the added mass coefficient of the body and adds one to get the inertia coefficient ($C_a + 1$) [9].

The representative drag coefficient for three-dimensional bodies is based on $Re > 10^4$ with the following equation for rectangular plate $Area = LD$ [18].

$$C_d = 1.10 + 0.02 \left(\frac{L}{D} + \frac{D}{L} \right) \quad (50)$$

For $1/30 < (L/D) < 30$

The calculated drag coefficients and drag area for the lumped buoys are represented in Table 4 - 9.

Table 4 - 9 Drag coefficient and drag area for lumped buoys.

Model	A_d			C_d		
	X	Y	Z	X	Y	Z
Side plates	0.058 m^2	2.343 m^2	0.016 m^2	1.162	1.142	2.5
Mid plates	0.059 m^2	19.57 m^2	0.132 m^2	1.162	1.142	2.5
Walls	34.85 m^2	0 m^2	0.060 m^2	1.162	1.142	2.5

The drag coefficient is calculated for the entire GRP cover for X, Y, and Z, where the difference in drag for the lumped buoys is dependent on their respective drag area.

4.4.3 Slamming Force

The calculation for slam force on lumped buoys is a special case of the general cylinder-based model. The problem regarding lumped buoys is that they do not have a specific geometry. Therefore, it is not possible to calculate their waterplane area [9]. Thus, the slamming area must be defined as a constant value when using the constant slam coefficient model. The issue in OrcaFlex is that it cannot simply apply the resultant slam force the instant the buoy enters the waterplane area. That would give a discontinuous step change in the load applied to the buoy, which may preclude the existence of a dynamic equilibrium position [9]. The same reasoning also holds for the end of slamming forces when the buoy is completely submerged. OrcaFlex avoids this problem by ramping up the slamming area to its full value over the first 10% of the lumped buoy submergence. The same solution is used for the last 10% of the lumped buoy submergence. This is done to avoid a discontinuous step in the load [9]. Figure 4 - 9 refers to the ramping function applied in OrcaFlex.

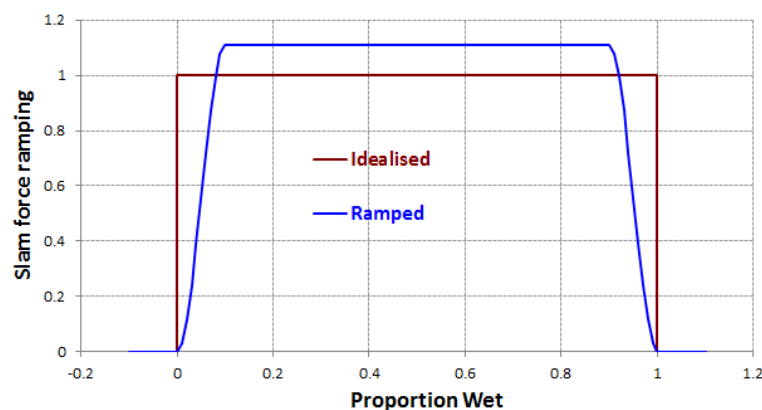


Figure 4 - 9 Ramping of slam force for lumped buoys [24].

Proportion wet refers to the ratio between the total buoy volume and submerged buoy volume. The slamming load is applied to the center of the wetted volume of the lumped buoy [9]. To ensure the slamming load is correctly applied, the slamming load is split amongst all the lumped buoys for the hydrodynamic properties. The slamming coefficient and waterplane area define

the slamming data in OrcaFlex. To define the slamming coefficient, DNV-RP-H103 can be used to calculate it based on [1]:

$$C_s = \frac{2}{\rho A_P v_s} \frac{dA_{33}^{\infty}}{dt} \quad (51)$$

Which can be rewritten as:

$$C_s = \frac{2}{\rho A_P} \frac{dA_{33}^{\infty}}{dh} \quad (52)$$

dA_{33}^{∞}/dh is the rate of change of added mass with submergence, which is dependent on the added mass and height for the given lumped buoy. The slamming area will differ depending on the lifting angle for the cover. The waterplane area for the different angles has been extracted from Autodesk Inventor and is shown in Figure 4 - 10.

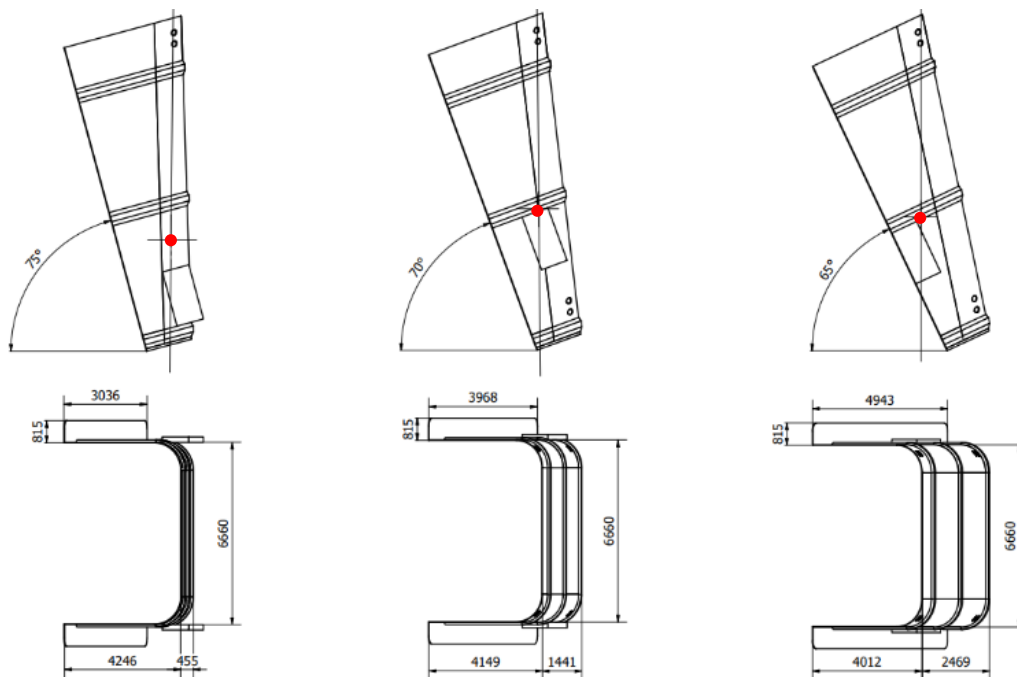


Figure 4 - 10 Slam area for GRP cover at different angles.

From Figure 4 - 10, the center of mass is in red to display the lifting angle for the cover. Underneath the lifting angles is the view of the GRP cover from below, representing the slam area.

The projected slam area has been divided into each lumped buoy based on their corresponding projected area. The slam coefficient and projected area for different angles are given in Table 4 - 10.

Table 4 - 10 Slam coefficient and waterplane area for lumped buoys.

Model	A_p	C_s
GRP Cover 65°		
Side plates	0.982 m ²	5
Mid plates	4.862 m ²	5
Walls	0.130 m ²	5
GRP Cover 70°		
Side plates	0.789 m ²	5
Mid plates	2.385 m ²	5
Walls	0.112 m ²	5
GRP Cover 75°		
Side plates	0.603 m ²	5
Mid plates	0.753 m ²	5
Walls	0.094 m ²	5

The slamming coefficient is extracted from DNV-RP-H103 between the theoretical values of π (von Karman) and 2π (Wagner). Therefore, for smooth circular cylinders, C_s should not be less than 3. Otherwise, C_s should not be taken as less than 5 [1].

4.5 Lifting Setup

The assembly of the lifting arrangement starts from the crane, which is fixed to the deployment vessel. The vessel motion will affect the crane arm and induce motion on the GRP protection cover. The crane arm model contains a line element, which is used as a support to connect the winch wire and to induce correct motions on the cover. Finally, the GRP cover is connected to the winch via a shackle and a two-legged sling arrangement. The total mass for the lifting operation is approximately 15 000 kg, where the lifting setup is based on Gunnebo 2-legged wire rope sling, which is in accordance with NORSOK R-002 [26].

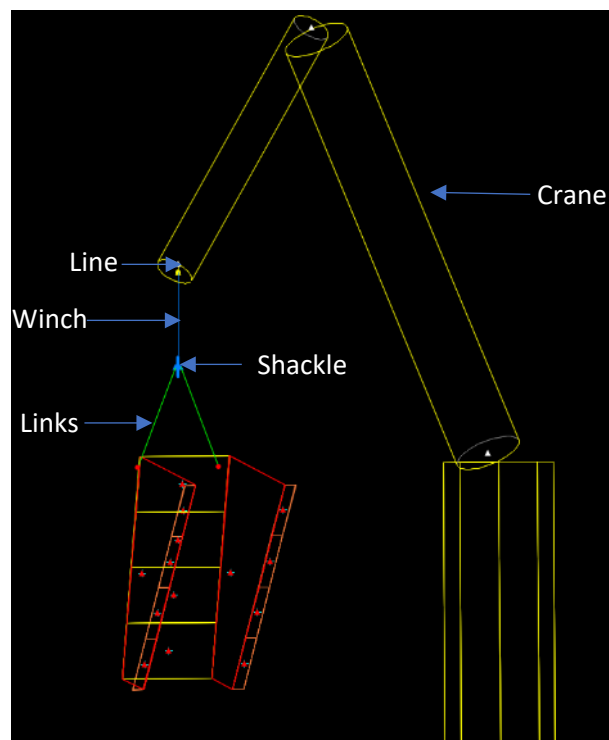


Figure 4 - 11 Lifting arrangement in OrcaFlex.

The crane is modeled with the use of constraints and shapes. The constraints are used to manipulate the crane to enforce the desired position. The shapes are just visual representations of the crane with no effect on the numerical model. The constrain position and orientation corresponding to the crane and crane tip position relative to the RAO origin. The line is fixed inside the crane arm to constrain the winch wire in the correct position for the lifting setup.

The winch has an initial length of five meters and a constant stiffness of 236 000 kN. The winch will have a set payout rate for the different simulation stages, where the lowering speed for the GRP cover is set to 0.2 m/s until the whole body and slings are deeply submerged.

Table 4 - 11 Winch setup in OrcaFlex.

	Stage duration	Stage end	Mode	Value
Stage 0	40 s	0 s	Payout rate	0 m/s
Stage 1	90 s	90 s	Payout rate	0.2 m/s
Stage 2	150 s	240 s	Payout rate	0.2 m/s

The slings are modeled as links. Links are massless and without hydrodynamic loads, which connect two objects. Links are useful for modeling wires where mass and hydrodynamic loads are small and can be neglected [9]. For the links, they are defined as tethers which are simple elastic ties that can take tension but not compression. The tensions for tethers are described with a variation in the tether's length and a stiffness component [9].

$$T = \begin{cases} \frac{k(l-l_0)}{l_0} & \text{for } l > l_0 \\ 0 & \text{for } l \leq l_0 \end{cases} \quad (53)$$

The sling data is extracted from Gunnebo datasheet for 2-legged wire sling and given in Table 4 - 11.

Table 4 - 12 Sling data from Gunnebo (Appendix B)

Sling type	Nominal Ø	WLL (0° - 90°)	Unstretched length	Axial stiffness
6x19- fiber core	0.032 m	16 800 kg	6 m	37 580 kN

The working load limit is given at 16 800 kg for a sling angle between 0 and 90 degrees. Based on the shackle position, the unstretched length of six meters will give an angle of 60 degrees for the slings connected to the GRP cover. The same method used for the center of mass has been applied to constrain the slings in the correct position to the GRP cover. The sling connection points for the GRP cover in OrcaFlex are given in Table 4 - 13.

Table 4 - 13 Sling connection to the GRP cover in OrcaFlex.

Model	X	Y	Z
Sling 1	- 3 m	-2.015 m	5.03 m
Sling 2	3 m	-2.015 m	5.03 m

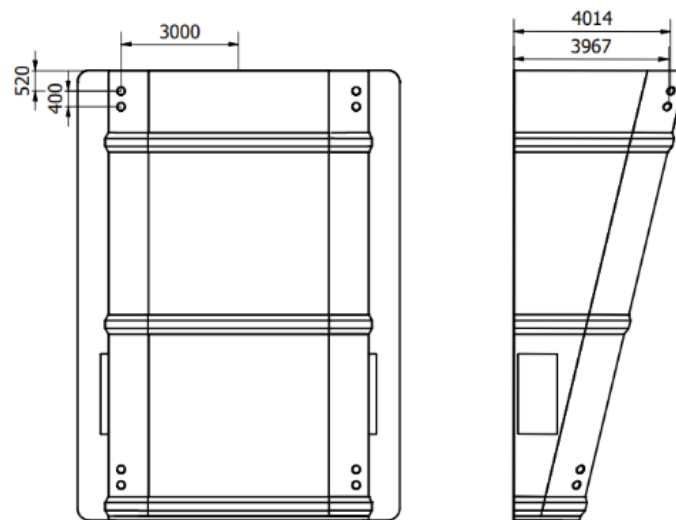


Figure 4 - 12 Sling position from Autodesk Inventor.

4.6 Environmental Conditions

The waves for the simulation are randomly generated as a wave train using JONSWAP. In OrcaFlex, there are three options for the parameters when specifying the wave train. Automatic, which will define all the given parameters. Partially specified, which will specify α , σ_1 , and σ_2 . Last is the fully specified, where all the parameters must be manually defined.

Partially specified is used where T_p , H_s , and γ will be defined before the simulation. The other parameters will automatically change when different inputs are given to T_p , H_s , and γ . For reference, the peak shape parameter γ is given by DNV-RP-H103 in section 2.2.6.6 [1].

$$\begin{aligned} \gamma &= 5 \quad \text{for} \quad T_p/\sqrt{H_s} \leq 3.6 \\ \gamma &= \exp\left(5.75 - \frac{1.15T_p}{\sqrt{H_s}}\right) \quad \text{for} \quad 3.6 < T_p/\sqrt{H_s} < 5 \\ \gamma &= 1 \quad \text{for} \quad T_p/\sqrt{H_s} \geq 5 \end{aligned} \quad (54)$$

Li et al. [14] concluded that in different description sea states, such as Torsethaugen, the allowable H_s values for the vessel are significantly less compared to JONSWAP. In the disturbed wind sea and swell, the spreading coefficient is set to the value of two with the number of directions equal to eleven. Therefore, only wind sea is considered, even if swell usually has a greater peak period than local wind waves. However, swell is based on long waves independent of the local environment, which is not included in these simulations. Therefore, the sea state description used for these simulations will only be for the JONSWAP wind sea.

4.7 Simulation Setup

The simulation is performed as an implicit time-domain simulation, where the default time step of 0.1 seconds was used. The simulation stage is set up with a time duration of 280 seconds and divided into three sections. The first section is dedicated to building the environmental conditions and lasts 40 seconds to remove asymmetry in the loading. From OrcaFlex, it is recommended to set the build-up period to at least one wave period [9]. The remaining sections are for lowering the GRP cover to deeply submerged and last 240 seconds.

The simulation sets that will be performed to assess the allowable sea states are given in Table 4 - 14.

Table 4 - 14 Time-domain simulation.

Simulations	Lifting Angle	Shielding	Wave direction	T_p
Set 1	70°	No	165° – 180°	5 – 12 s
Set 2	65° – 75°	No	180°	5 – 12 s
Set 3	70°	Yes	165° – 180°	5 – 8 s

The primary lifting angle for the cover is at 70 degrees and will be used to assess the sea states with and without shielding. The remaining lifting angles will be tested for head waves to assess the influence different lifting angles may have on the system. The shielding effect will only be tested for the shorter wave periods based on the results from sea state RAOs, where it was observed that there is no beneficial shielding effect for long periods.

Chapter 5

Sensitivity Study on Numerical Methods

5.1 Overview

In chapter 5, two sensitivity studies will be conducted for the numerical model. The first sensitivity study will focus on the number of wave seeds needed to achieve reliable results. The second part will focus on coupled and uncoupled motion to determine the vessel approach for assessing the allowable sea states.

5.2 Numbers of Wave Seeds

5.2.1 Seeds

When performing simulations on a numerical system in a time-domain software, it relies on using enough random wave seeds, emphasizing enough seeds. If too few wave seeds are used, it may limit the predicted extreme value and risk an operation of proceeding without the comprehensive knowledge of the risk involved. For example, the ramification of a marine operation with a small sample size can lead to severe injuries/damage in the context of personnel, equipment, or the environment. On the other hand, an extensive number of wave seeds are also not desired when doing simulation. Every wave seed takes time to simulate and complete, and the data must be extracted after completion. Lengthy simulation holding back deadlines and operations may terminate the entire project/contract. The wave seeds needed to acquire trustworthy results within the project time limit may differ depending on the numerical system.

In some cases, only ten seeds are needed to acquire good predictions for the extreme values. For other systems, it may be more than 50 seeds. The analysis for this study is based on a continuous lowering simulation for a short duration.

According to DNV-RP-H103 section 3.4.3.7, analyses like these needs a minimum of ten simulations where the minimum and maximum values for all simulation should be documented [1]. However, Li et al. [27] conducted a sensitivity study on the number of seeds needed for the monopile lowering and landing operations. They stated that 30 seeds were sufficient to assess and predict the extreme values reliably.

5.2.2 Simulation

The simulation setup is as described within chapter 4, where the GRP cover will be continuously lowered down after stage one. A statistical method is required to estimate the extreme values for the predicted estimations. From subchapter 2.4.1, Gumbel and Weibull were discussed as two statical methods for extreme values. Gumbel is a widely used method for predicting extreme response for offshore structures [28]. By using the maximum likelihood method, the parameters are estimated based on the data for each condition. Weibull will also be used to determine the best fitted statistical method when assessing the predicted extreme values.

The focus of the sensitivity study will be on the extreme values for minima and maxima tension. The predicted extreme values for sling tension are evaluated and used to determine the number of seeds needed. The issue with deploying an object with low weight and a large surface area is that the hydrodynamic forces can easily exceed the submerged weight. This can result in slack in the slings, generating large snap loads. Snap loads are unwanted and are one of the limiting factors for the allowable sea states. Therefore, the deciding criteria are determined by the extreme minima values, but the distribution for maxima will also affect the number of seeds used. Due to the large sample size of wave seeds, only one sea state is used for the simulations. The environmental data and numbers of seeds are listed in Table 5 - 1.

Table 5 - 1 Sea state description for the sensitivity study for seeds.

Seed number	Wave direction	Wave height	Wave period	Wave Spreading
30	180 deg	2 m	8 s	Short-crested (n = 2)
50	180 deg	2 m	8 s	Short-crested (n = 2)
100	180 deg	2 m	8 s	Short-crested (n = 2)

5.2.3 Maxima Sling Tension

The average maxima for 100 seeds have been plotted to indicate the possible numbers of seeds needed. The cumulative average value for each seed has been included to assess if or when the sling tension will converge. Finally, the average maxima for slings 1 and 2 have been plotted with the mean value of 30, 50, and 100 seeds. The mean value is included to outline the possible best fits depending on the cumulative average value.

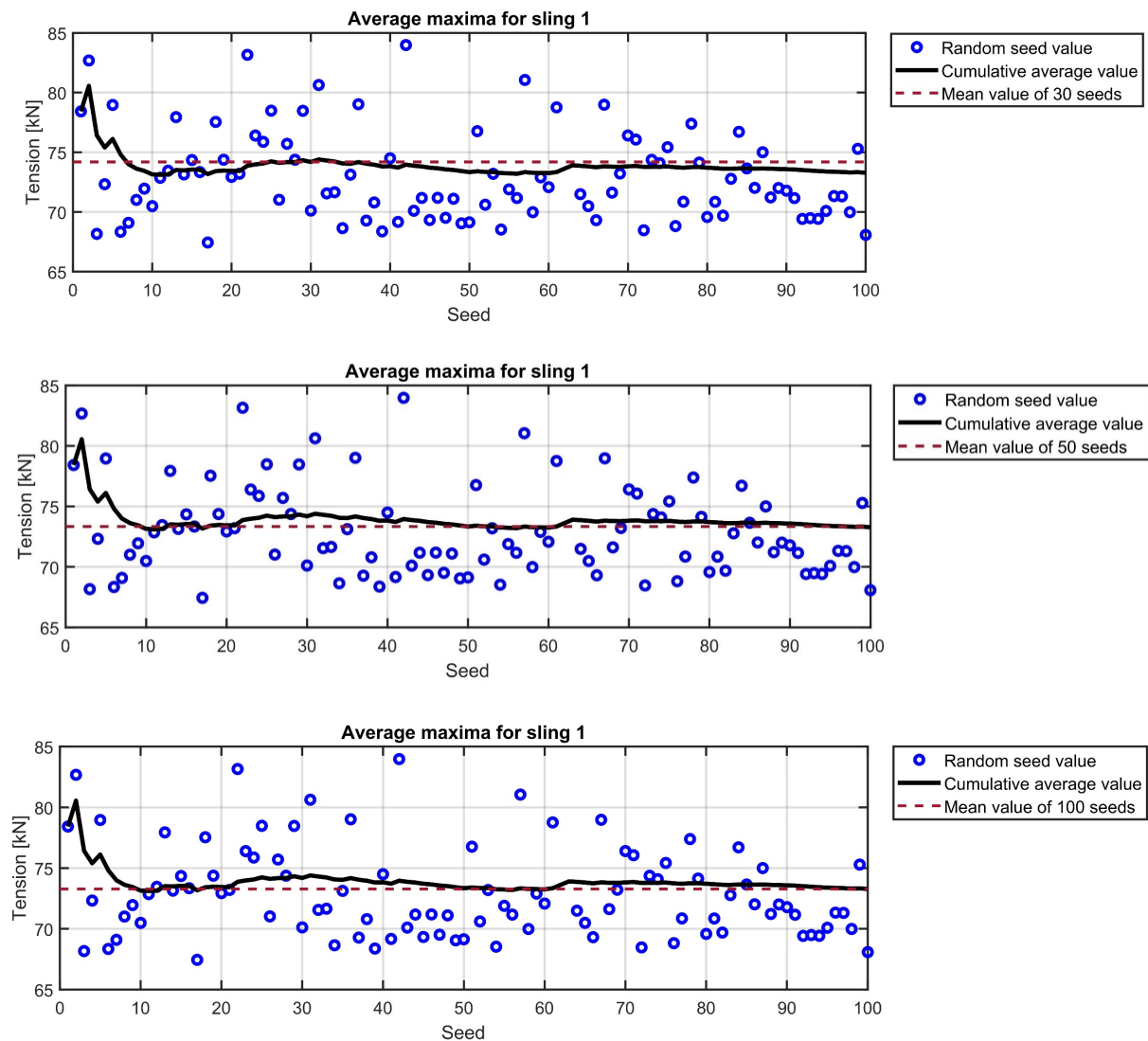


Figure 5 - 1 Average maxima tension for sling 1.

The average maximum value given in Figure 5 - 1 converges at around 15 seeds with some fluctuation in the tension. This fluctuation for the cumulative average value will continue for the 100 seeds. From the mean values, the trend for sling 1 shows that for larger volumes of seeds, the predicted tension of the mean value will be lower than the given cumulative average value. Only the mean value of 30 seeds captures the higher tensions observed.

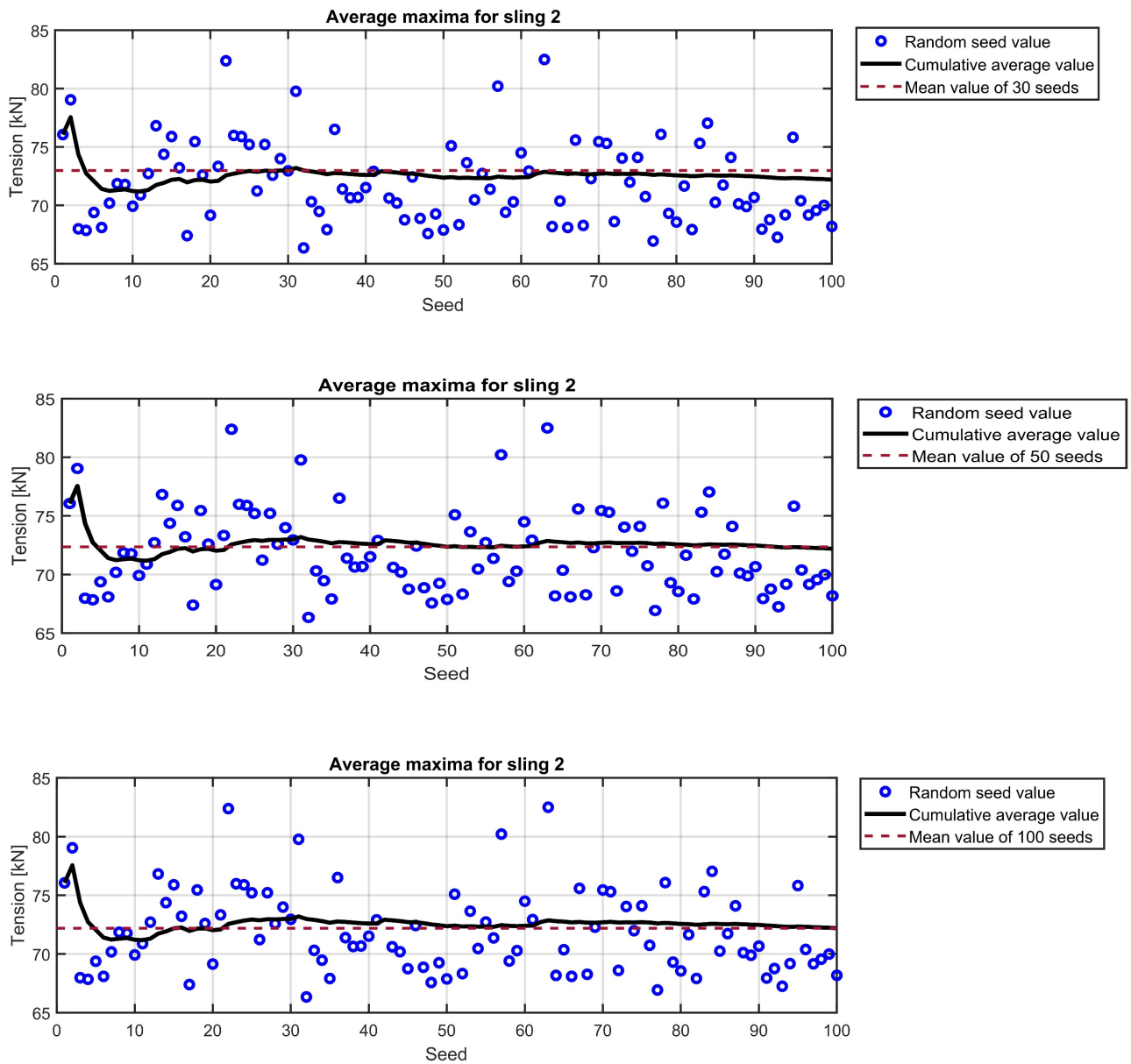


Figure 5 - 2 Average maxima tension for sling 2.

The cumulative average value for sling 2 flattens out later than sling 1. After 25 seeds, the cumulative average value will start to converge, with some fluctuation in the tension. However, the cumulative average value for sling 2 is more stable compared to sling 1. For the different mean values, the behavior is similar to sling 1, where it is still only the mean value of 30 seeds that captures the higher tensions.

From Figure 5 - 1 and Figure 5 - 2, the number of seeds needed to acquire consistent predictions for maximum can be extracted from the cumulative average value. The cumulative average value for sling 2 will yield the minimum required seeds. This is due to the slow convergence of sling 2, which will yield a minimum requirement of 25 wave seeds. However, the difference between the mean values shows that for a low number of wave seeds, the predicted extremes, in this case, will yield a more conservative assessment. From the mean values of slings 1 and 2, there is a clear trend that the numbers of seeds used to simulate the sea states will yield different assessments for the sea states. However, the largest observed difference between the mean values is only 800 Newtons. Therefore, the difference between the number of seeds used should yield similar predictions for the extreme values.

A statical method must be used to estimate the trend for the extreme values at 30, 50, and 100 seeds. For sling 1, Gumbel and Weibull plot to determine which statistical method yields the best fitted distribution. For sling 2, only the Gumbel plot has been used to identify the best fit of 30, 50, and 100 wave seeds. Therefore, given the look of the tail for the extreme values, the numbers of seeds needed can be identified by the best fitted distribution.

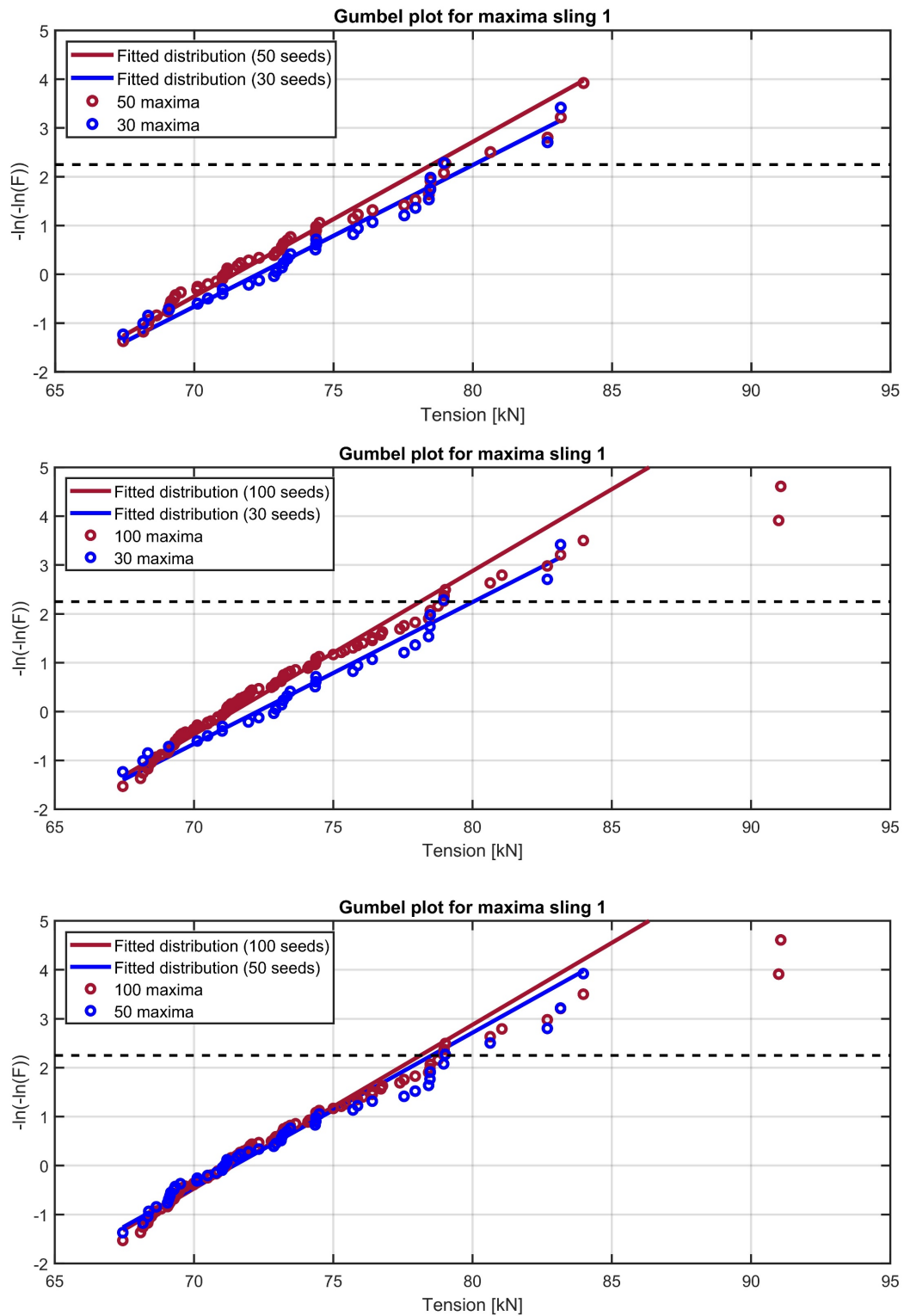


Figure 5 - 3 Gumbel plot for maxima tension sling 1 (30, 50, and 100 seeds).

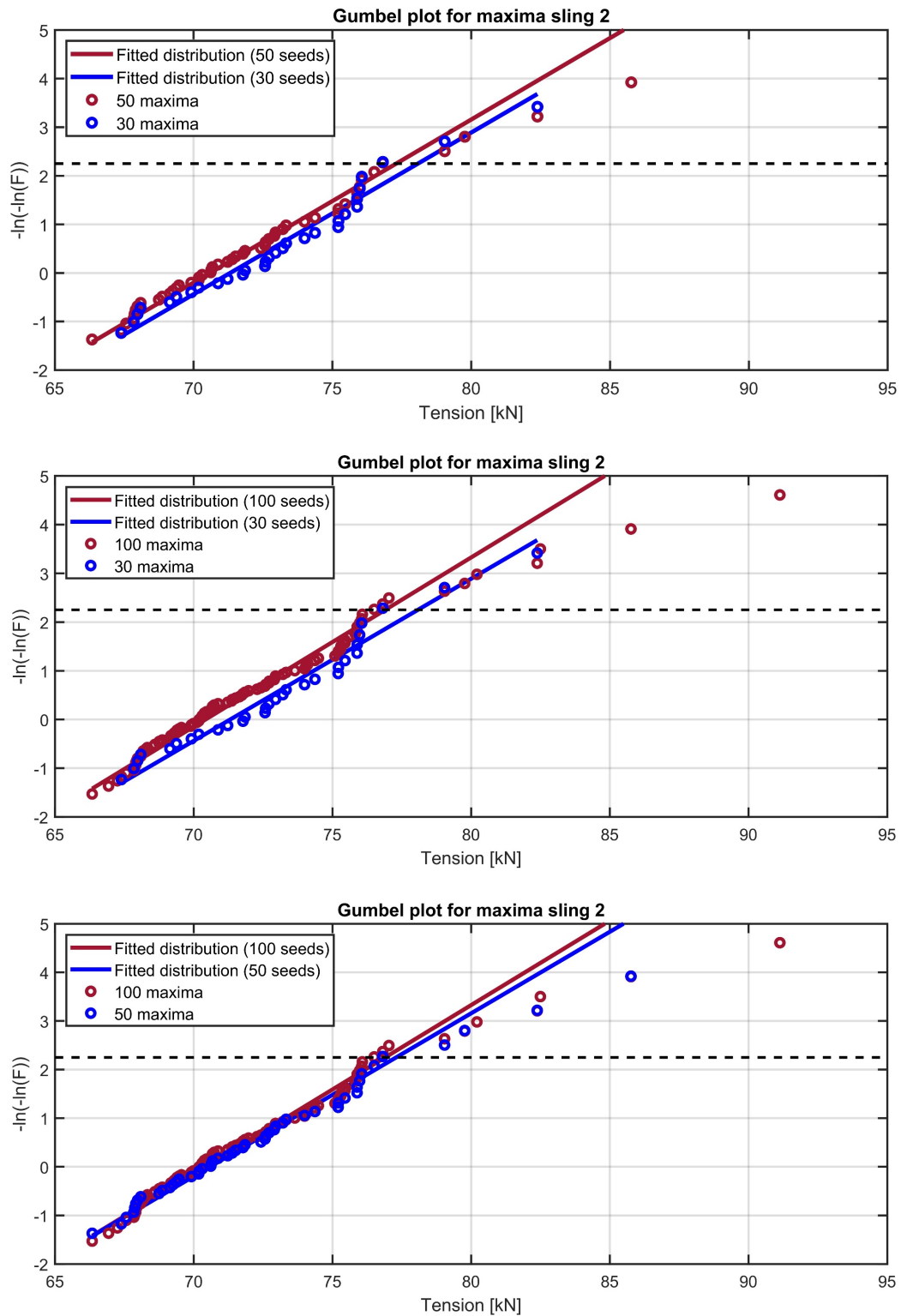


Figure 5 - 4 Gumbel plot for maxima tension sling 2 (30, 50, and 100 seeds).

The Gumbel plots for different numbers of seeds are given in Figure 5 - 3 and Figure 5 - 4. The black dotted line represents the non-exceedance probability given at 0.9. The non-exceedance probability is used in this chapter to assess the difference in the number of wave seeds. For slings 1 and 2, the wave seeds of 50 and 100 will yield a similar prediction for the non-exceedance probability, with the difference being almost neglectable. For the fitted 30 wave seeds, the difference is more noticeable. The use of 30 wave seeds yields the most conservative prediction and may limit the sea states, where 50 or 100 seeds may have given acceptable results. However, based on the tail fitting observed from sling 1 and sling 2. The distribution of 30 wave seeds will yield the most reliable estimate for the specified wave seeds used. For sling 1, the fitted distribution of 50 seeds will also yield a great fit for the predicted extremes. However, this only applies for sling 1, where for sling 2, the fitted distribution of 50 seeds misses the most significant predicted extreme value.

There is also a possibility to fit the distribution for the maxima tail, as shown in Figure 5 - 5. For non-linear processes, it is recommended to fit the distribution to the tails instead of using all the data when predicting the extreme values. However, this may introduce large uncertainties in the estimation due to the limit of the sample size [12].

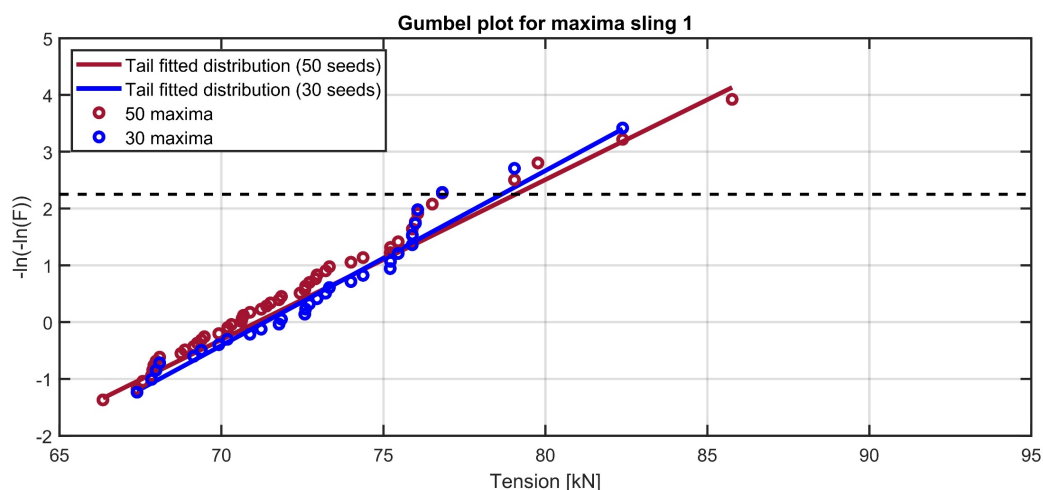


Figure 5 - 5 Tail fitted Gumbel plot.

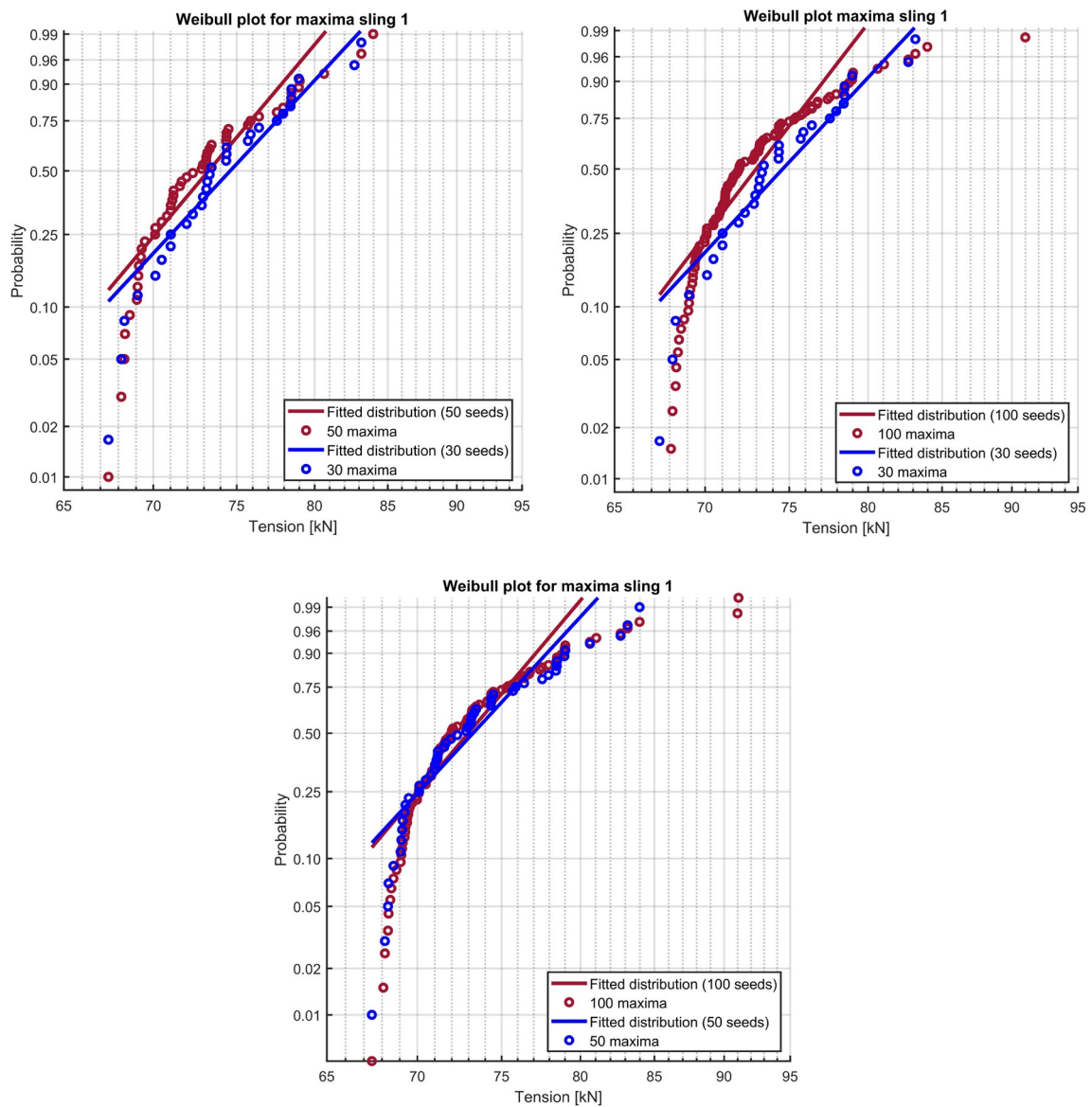


Figure 5 - 6 Weibull plot for maxima tension sling 1 (30, 50, and 100 wave seeds).

The fitted Weibull distribution is given in Figure 5 - 6. The main concern for the different Weibull distributions is that it misses the crucial tails required to assess the allowable sea states. As a result, the fitted Weibull distribution is a terrible fit for evaluating and assessing the sea states for the extreme maxima values. Using Weibull instead of Gumbel for the given extreme values will yield large uncertainties for the operation due to the poorly fitted data.

5.2.4 Minima Sling Tension

The same procedure as for maxima has been used for the minima sling tension. First, the cumulative average value of 100 wave seeds has been plotted to indicate the number of seeds needed. Next, the cumulative average value for each seed has been included to assess when the sling tension will converge. Finally, the average minima for slings 1 and 2 have been plotted with the mean value of 30, 50, and 100 seeds. Again, the mean value is included to outline the possible best fits for the number of seeds tested.

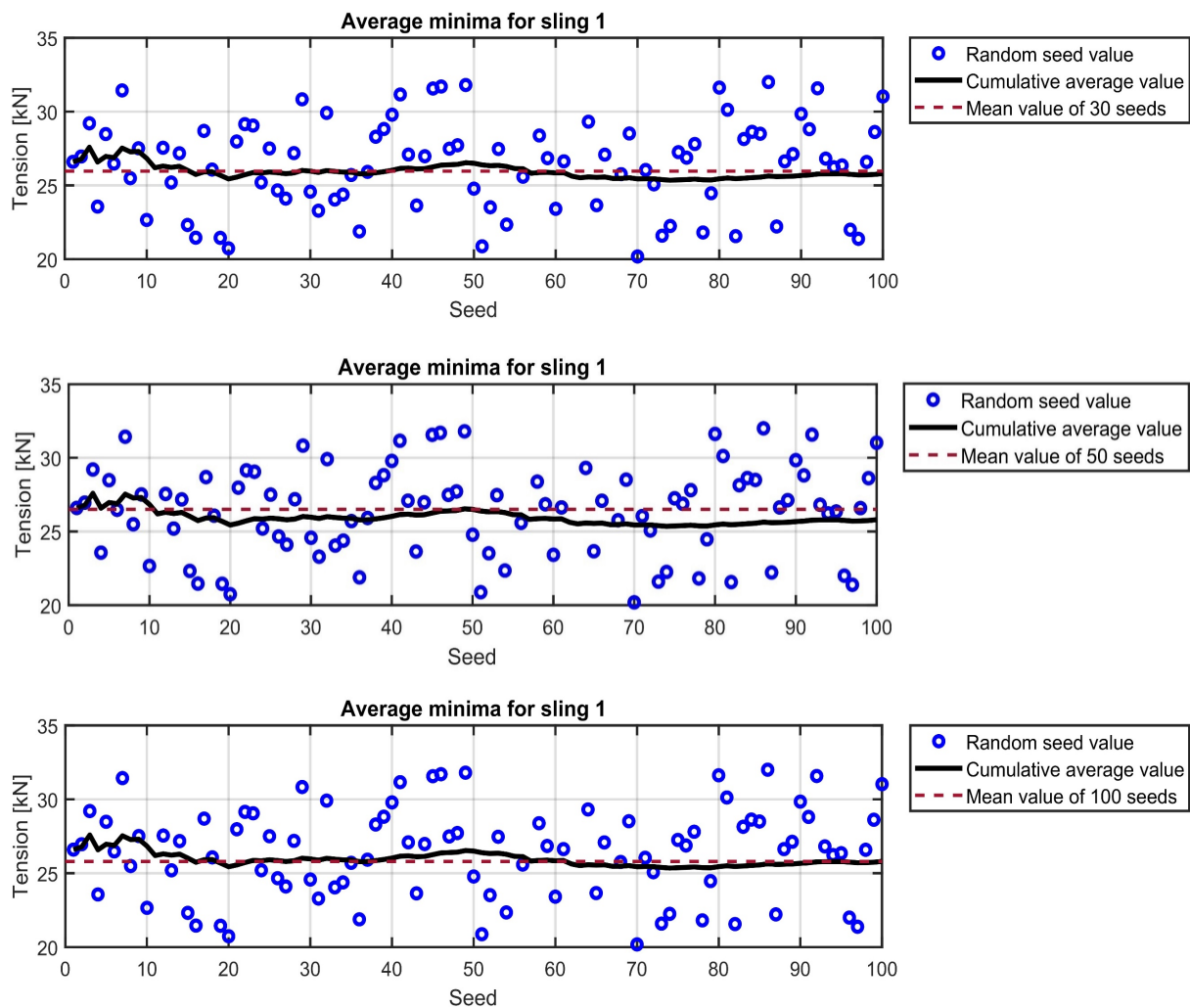


Figure 5 - 7 Average minima tension for sling 1.

From Figure 5 - 7, the cumulative average value behaves more steadily from the first seeds and converges sooner compared to the cumulative average value for maximum. The cumulative average value converges at around 15 seeds, which will fluctuate in tension for the 100 seeds. From the mean values, the best fit for sling 1 would be 30 or 100 seeds. The mean value of 50 seeds will give a slightly higher value for minimum tension. However, the largest difference observed between the mean values is only 700 Newtons. For sling 2, given in Figure 5 - 8, similar results and trends are observed as to sling 1, with the foremost difference being a slightly higher average tension for sling 2.

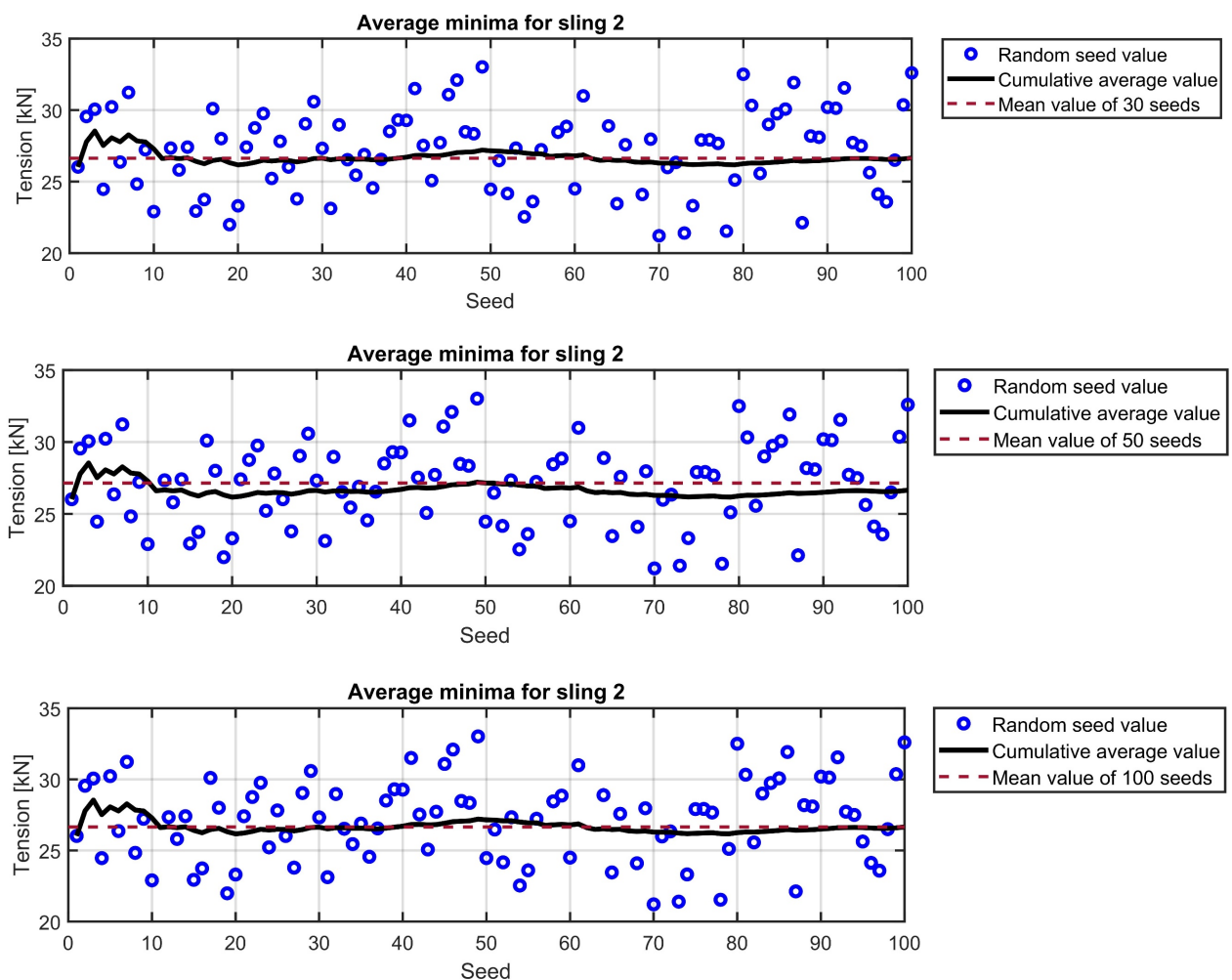


Figure 5 - 8 Average minima tension for sling 2.

As was done for maxima, The same statistical methods have been used for minima. For sling 1, Gumbel and Weibull have been plotted to determine which statistical method gives the best fitted distribution. For sling 2, only the Gumbel plot has been used to categorize the best fit of 30, 50, and 100 seeds.

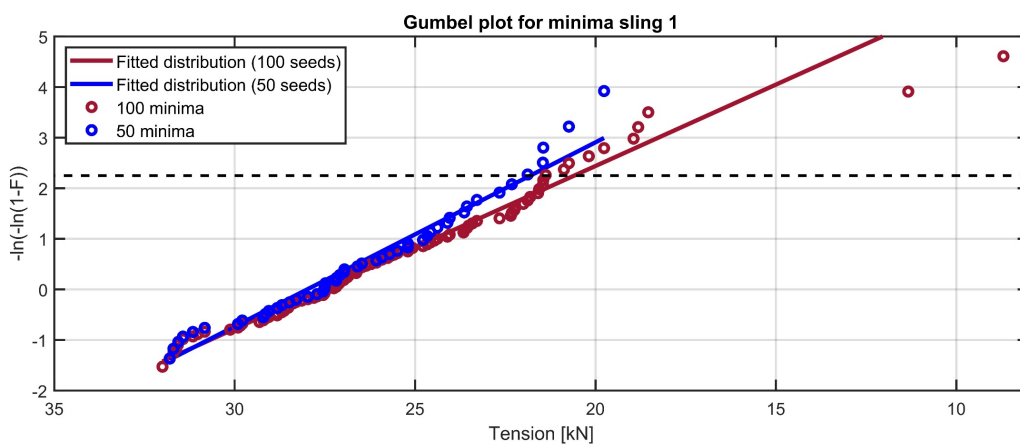
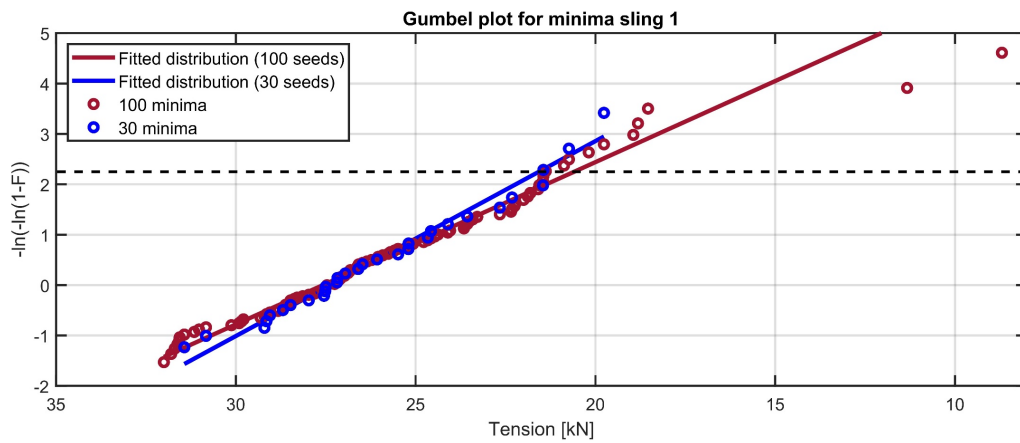
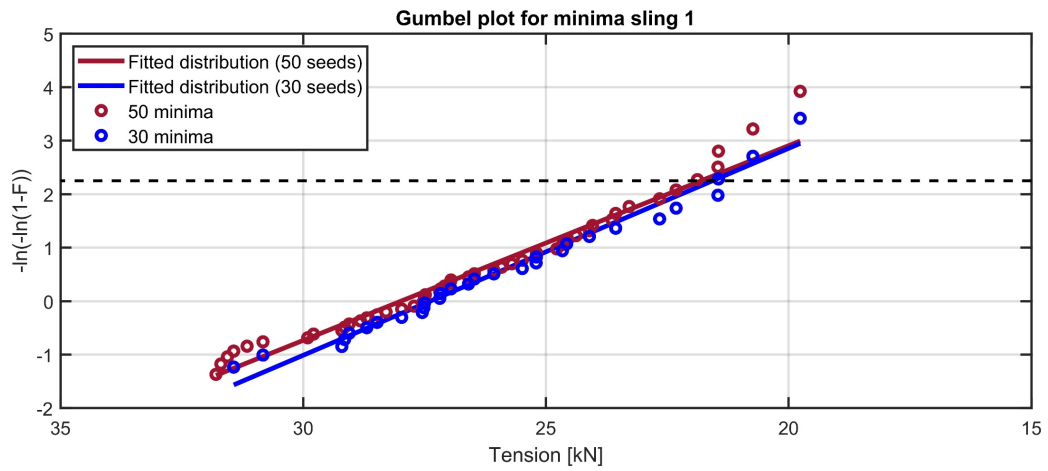


Figure 5 - 9 Gumbel plot for minima tension sling 1 (30, 50, and 100 seeds).

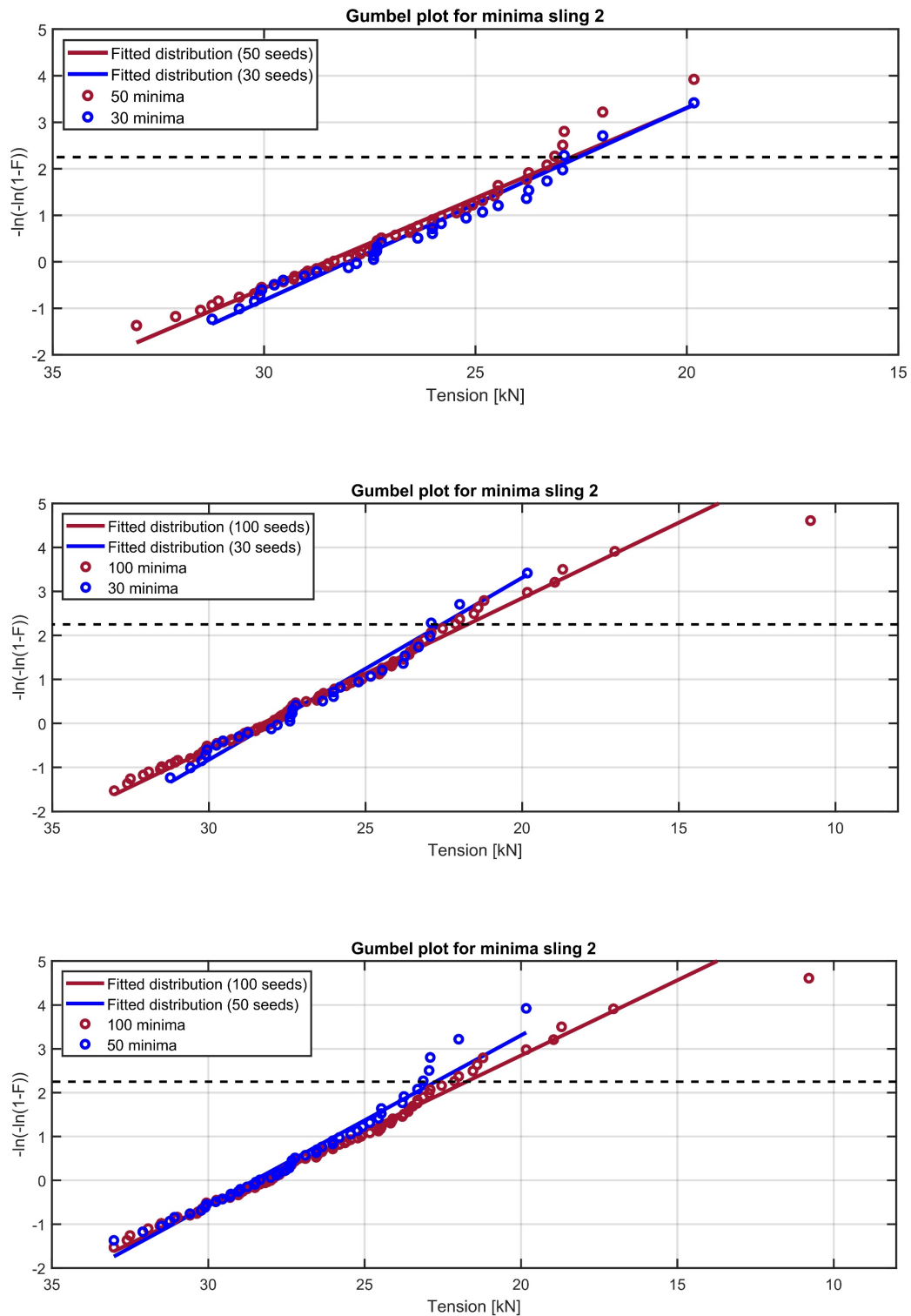


Figure 5 - 10 Gumbel plot for minima tension sling 2 (30, 50, and 100 seeds).

The Gumbel distribution for minima has been plotted in Figure 5 - 9 and Figure 5 - 10. The fitted distribution of 100 seeds tends to follow the minima values better than the Gumbel maxima. However, due to the large sample size and proximity in tension, the fitted distribution of 100 seeds will have issues following the extreme minima tail. The same can be seen for the fitted distribution of 50 seeds, but with minor deviation for the tail extreme.

From the non-exceedance limit at 0.9, the conservative number of seeds can be determined as the fitted distribution of 100 seeds, which will give the lowest predicted tension for both sling 1 and sling 2. The fitted distribution of 30 and 50 seeds will yield a similar result for the non-exceedance limit. This can be seen from the Gumbel distribution, where the distribution of 50 seeds tends to diverge towards the tail end value of 30 seeds.

It is clear from both minima and maxima sling tension that the number of seeds used will affect the fitting of the Gumbel plot. From both minima and maxima, the best fitted distribution regarding the tails is the fitted distribution of 30 seeds. However, based on the conservative number of fitted seeds, the numbers of seeds needed will differ depending on the predicted extreme value.

The fitted Weibull distribution is given in Figure 5 - 11 for the minima tension in sling 1. The Weibull probability paper for minima is a definitive improvement compared to the maxima extreme values. The fitted Weibull distribution follows the predicted extreme minima values better. However, compared to the Gumbel distribution, the tail fitting is still lacking for the Weibull distribution. The Gumbel distribution will yield a better tail fitting, which will give a more reliable prediction of the assessment of sea states.

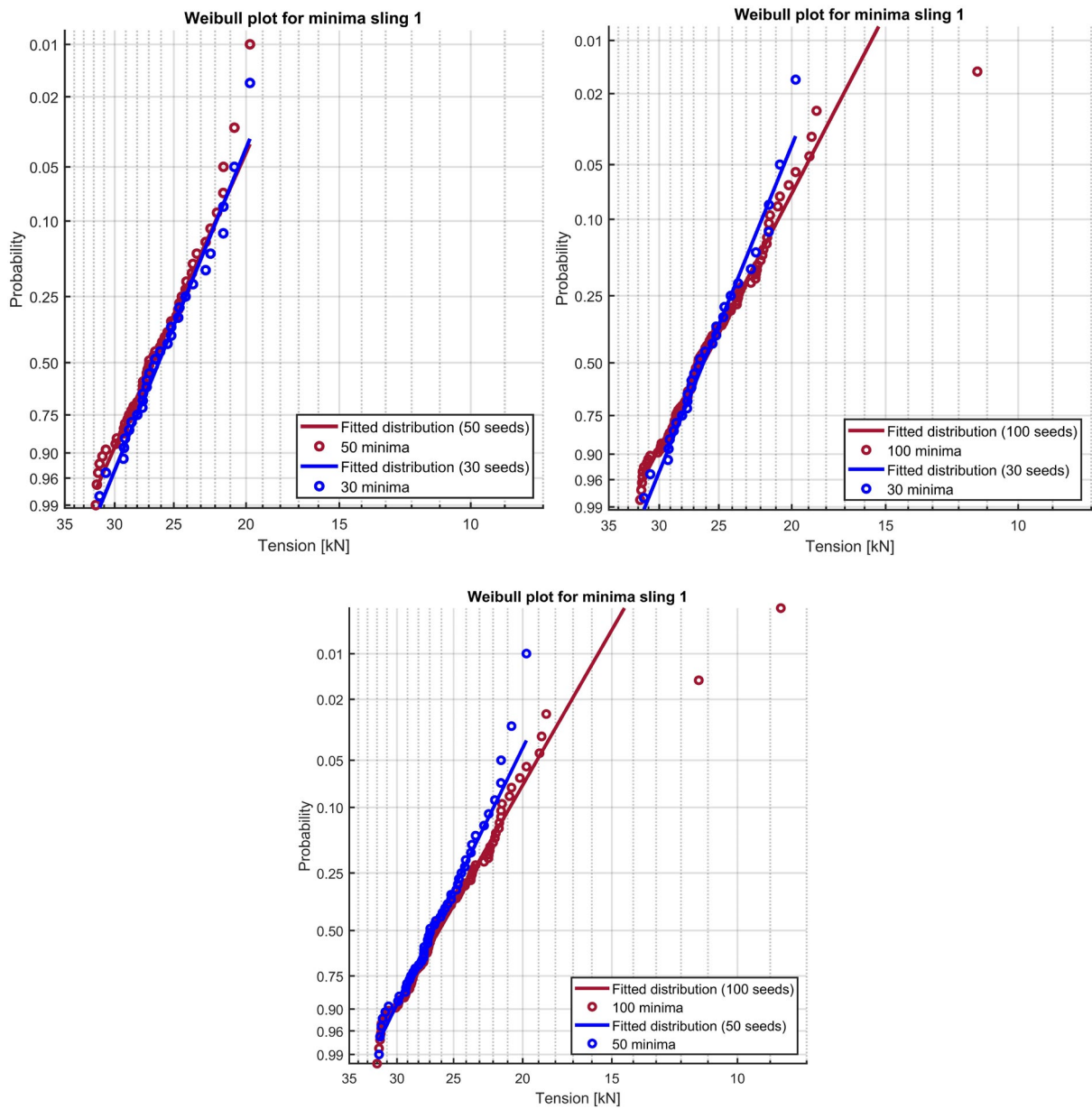


Figure 5 - 11 Weibull plot for minima tension sling 1 (30, 50, and 100 wave seeds).

5.2.5 Discussion of the Numbers of Seeds

The number of wave seeds used to assess the allowable sea states is based on the results extracted from the maximum and minimum tension of slings 1 and 2. Given the extreme values for maxima, there is a clear indication that for slings 1 and 2, the fitted distribution of 30 seeds will give the best tail fitting for the used wave seeds. However, For the larger sample size, the tail fit for the wave seeds was lacking, resulting in the possibility of fitting the distribution after the tail extremes.

From the extreme values, with only regard to the fitted Gumbel distribution, 30 seeds appear to be sufficient to provide a reliable estimation for the numerical model. The main benefit of using 30 seeds versus 50 or 100 seeds is the lower computational cost for evaluating the allowable sea states. However, large sample size is desired with concern for the extreme maxima values and the possible need for tail fitting. Therefore, a larger quantity of seeds, such as 50 and 100, is more beneficial when a tail fitting is required.

From the observed convergence of the cumulative average values, there is a clear indication that 30 seeds should be enough to acquire reliable predictions to assess the allowable sea states. This applies to both the observed minima and maxima sling tension. However, it is difficult to assess the number of seeds needed. From the observed prediction, the number of seeds used will yield either over- or under- estimations of the predicted extreme values. Therefore, based on the result from the cumulative average values and the Gumbel fitting, 30 wave seeds are selected to be used for the assessment of sea states. The 30 seeds from the extracted data seem to reliably predict the sea state without requiring large computational power.

The Gumbel probability plot fits better for the given extreme value. The fitted Weibull distribution for minima is still usable. However, compared to the Gumbel distribution, it is missing some of the substantial extreme values. There is always the possibility of tail fitting, but this can also be done with the Gumbel distribution. For the continuation of the study, only the Gumbel distribution will be used as the primary statistical method.

5.3 Coupled and Uncoupled Motion

5.3.1 Simulation

The simulation setup is the same as in chapter 4, the only difference being the input selected for the vessel. The calculated data for the vessel from a time-domain analysis depends on primary and superimposed motion. As the name suggests, if superimposed motion is selected, then the motions of primary and superimposed are applied concurrently, with the latter being imposed on the former [9].

The selection that can be chosen from primary motion is as follows:

- **None:** The primary position of the vessel remains fixed at the position determined by static analysis [9].
- **Prescribed:** allows to model the vessel moving station during the simulation [9].
- **Calculated (3DOF):** Calculates Surge, Sway, and yaw based on the included effects plus loads from lines or objects connected to the vessel [9].
- **Calculated (6DOF):** Calculates the vessel motion for all six degrees of freedom, based on the included effects plus loads from lines or objects connected to the vessel [9].
- **Time history:** The primary motion is given by a time history defined as a function of time and the vessel's primary motion [9].
- **Externally calculated:** The primary motion is defined by an external function [9].

For superimposed motion, the inputs that can be selected are as follows:

- **None:** There is no offset, and the vessel will follow the primary motion [9].
- **Displacement RAOs + harmonic:** The vessel moves harmonically in all six degrees of freedom, where the wave-generated harmonic motions are specified by the RAOs [9].
- **Time history:** The offset is defined by a time history as a function of time and the vessel's primary motion [9].

For this sensitivity study, the focus is on the uncoupled and coupled motion. The combination of the primary and superimposed motion determines how the vessel will behave at varying seas. The paring will be calculated (6DOF) for primary and none for the superimposed motion for coupled motion. For the uncoupled motion, the paring will be none for primary and displacement RAOs + harmonic for superimposed. For the uncoupled system, the predefined response from the vessel is used to calculate the motion based on the incoming wave train. This, in return, means that any forces acting on the GRP cover will not affect the vessel's motion. The vessel will be uncoupled to the GRP cover, and the superimposed motion gives a steady/moored vessel with motions due to only first-order waves effects [9].

For the simulation of coupled and uncoupled, the environment has been altered compared to subchapter 5.2.2 and given in Table 5 - 2. In addition, the increase in wave height is done to compare the motions in a more extreme environment and evaluate the difference among them.

Table 5 - 2 Sea state description for coupled and uncoupled.

Vessel motion	Wave direction	Wave height	Wave period	Wave Spreading
Coupled	180 deg	2.5 m	8 s	Short-crested (n = 2)
Uncoupled	180 deg	2.5 m	8 s	Short-crested (n = 2)

Even though this is a light lift, DNV has concluded that the coupling effects may be significant even for small objects. From DNV-RP-H103 subchapter 7.3.3.3, “the object tends to dampen the vessel motion with reduced force in the hoist wire as a result. An uncoupled analysis will therefore be conservative.” [1]. For the GRP cover, lower values for the tension using coupled motion are expected, which may make it the conservative motion. The lower expected tension for coupled motion will yield a larger probability of triggering snap loads.

5.3.2 Shackle Position

The first point of interest is the difference in shackle movements between the two motions. The shackle position for Z-direction has been used as a “fixed” point to validate the difference between the motions. The average maxima and minima of 50 seeds have been plotted for coupled and uncoupled shackle positions and are given in Figure 5 - 12

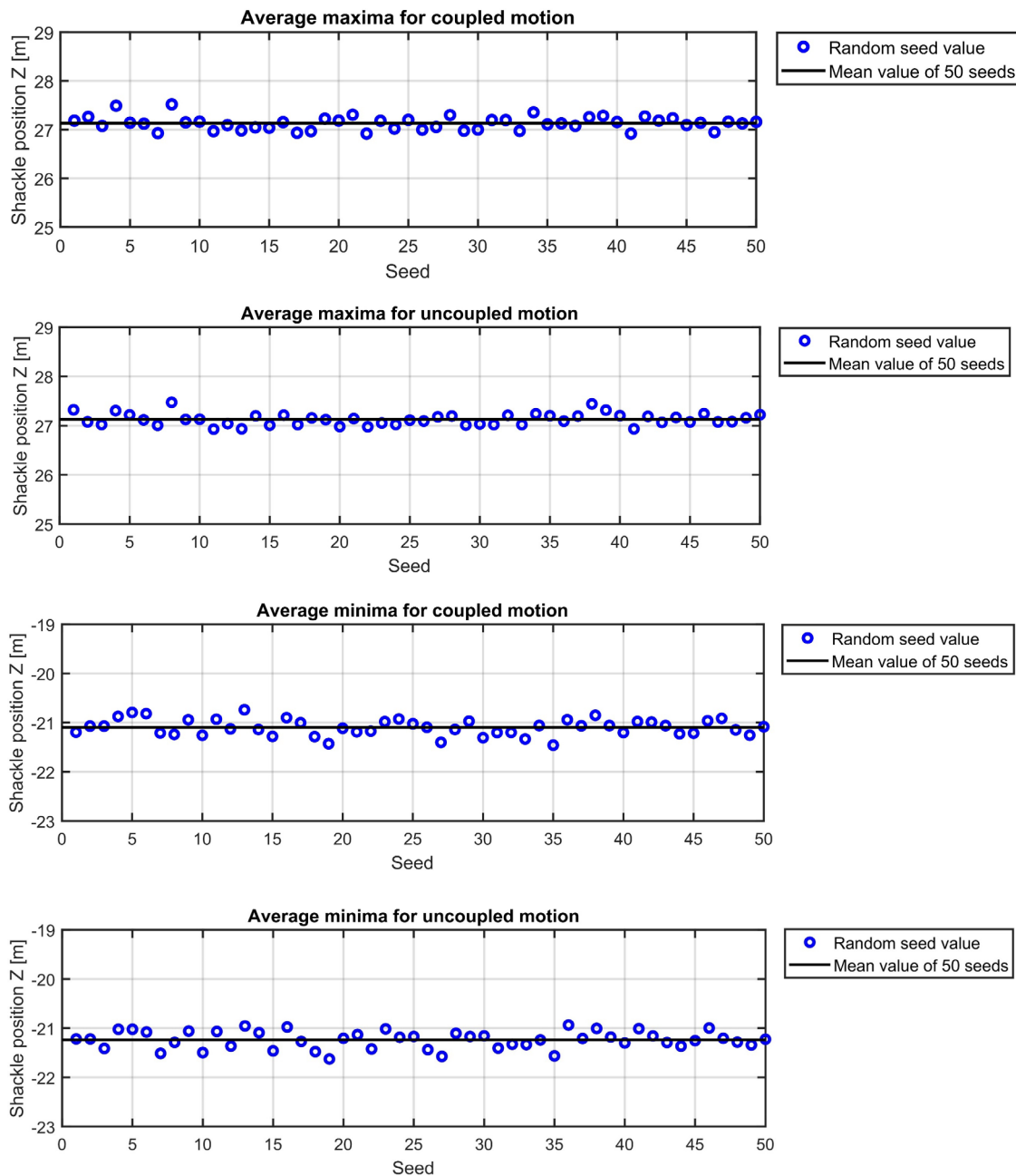


Figure 5 - 12 Average maxima and minima for shackle position.

From the average max and min values of the shackle position, there is a slight difference for every seed, which is reflected in the mean value of 50 seeds. The main occurrence for the coupled and uncoupled shackle position is that the differences can be substantially diverse for any given seed. For seeds 6 and 20, there is a notable disparity between the initial position of the shackle for the two seeds. For seed 6, the initial maxima position of the shackle is 27.120 m for coupled and 27.117 m for uncoupled, which yields a difference of 0.01%. For seed 20, the initial maxima position is 27.185 m for coupled and 26.981 m for uncoupled, yielding a difference of 0.75%. This difference in the motions for the shackle position is due to the links connected to the vessel. For coupled motions, the forces on the vessel from the links can affect the initial position, which varies with the given wave seed. This will result in slightly different positions for the shackle for the coupled system. However, these links are needed for the coupled motion as they act as mooring lines to keep the vessel in position. The mean value of 50 seeds and the difference between coupled and uncoupled shackle positions are given in Table 5 - 3.

Table 5 - 3 Shackle position for the mean value of 50 seeds.

Shackle Z Coupled	Shackle Z Uncoupled	Difference	Preential
27.13 m	27.126 m	0.004 m	0.01%
-21.23 m	-21.096 m	0.134 m	0.66%

The issue with having a slight difference in the starting position of the shackle is due to the splash zone crossing for the GRP cover. This may affect the result because the simulation will not be exactly similar with a slight difference in the splash zone crossing.

5.3.3 Maxima Slings Tension

For the sling tension for the different motions, the cumulative average value for maxima has been plotted in Figure 5 - 13. From DNV-RP-H103 subchapter 7.3.3.3, it is expected lower values for the coupled motion [1]. However, the coupled motion for slings 1 and 2 will yield slightly larger tension than uncoupled for the cumulative average value.

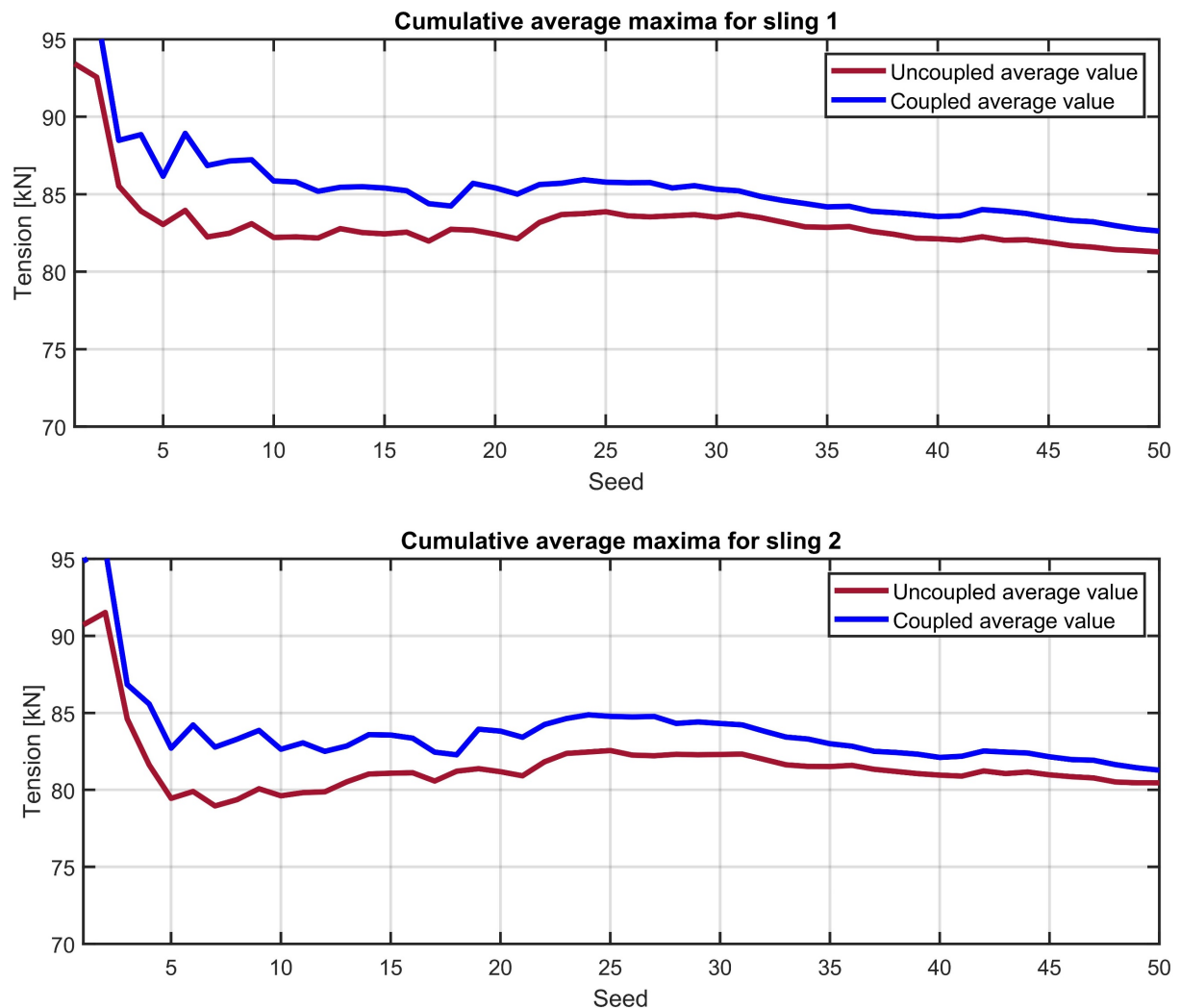


Figure 5 - 13 Cumulative average maximum for coupled and uncoupled motion.

From the behavior of the different graphs, there is a small spike in tension for seed 19, which may indicate some form of snap load in the coupled system. The cumulative average value for the different motions follows almost the same trend/path. The combined average value of 50 seeds for the different motions will only yield slight differences in maximum tension. For sling 1, the difference in tension for the given motions is only 1.3 kN, which yields a difference of

1.6 %. For sling 2, the difference between the motion is even less, at 0.8 kN, which yields a difference of approximately 1 %.

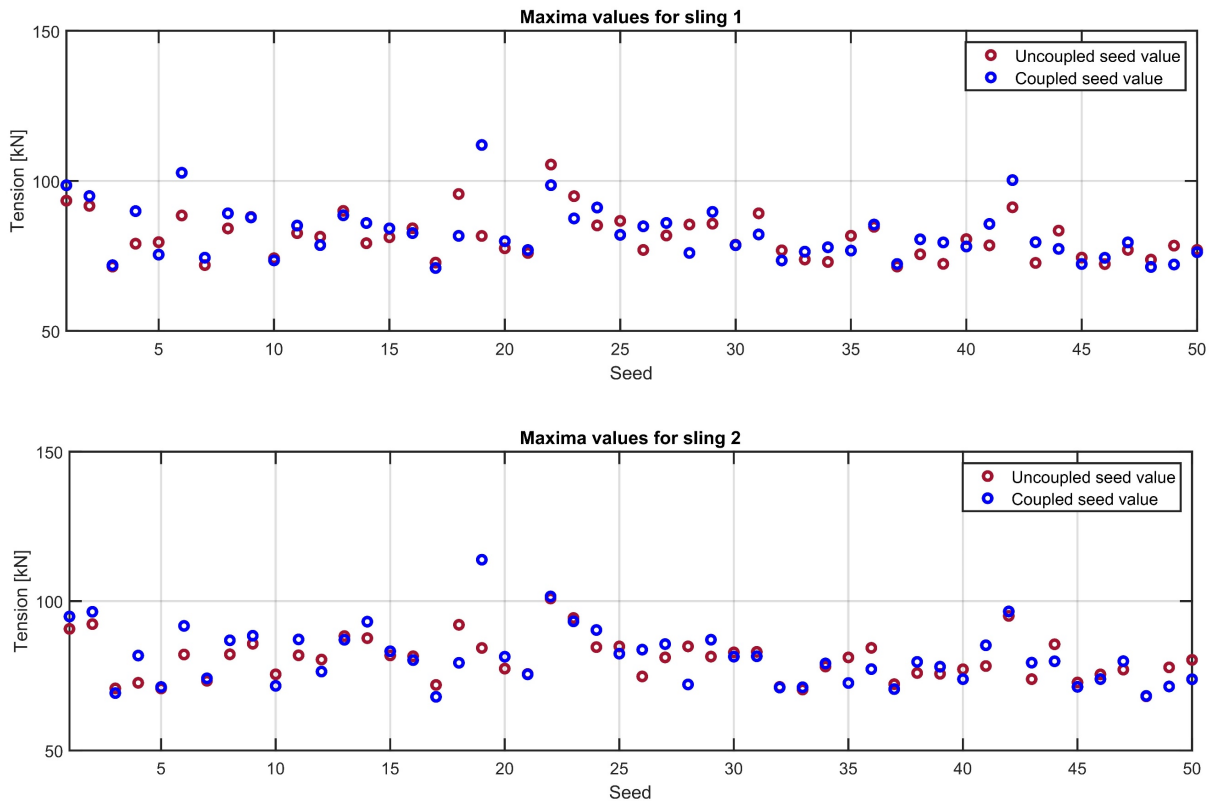


Figure 5 - 14 Maximum tension for individual seeds.

From Figure 5 - 14, the individual value for each seed has been plotted for slings 1 and 2. From the different individual seeds, only one significant deviation was observed for seed 19. For seed 19, the difference between coupled and uncoupled motion is almost 25%. The large difference in magnitude for seed 19 is likely due to snap loads that only ensue for the coupled motion. Only 40% of the individual seeds yield a greater magnitude for the uncoupled motion. Of which the average difference between the individual seed is approximately 4%. The low number of uncoupled seeds, which are greater in magnitude than coupled, explains why the coupled motion will yield slightly conservative values. However, the difference in magnitude between the motion is greater than it should be due to the considerable tension for seed 19.

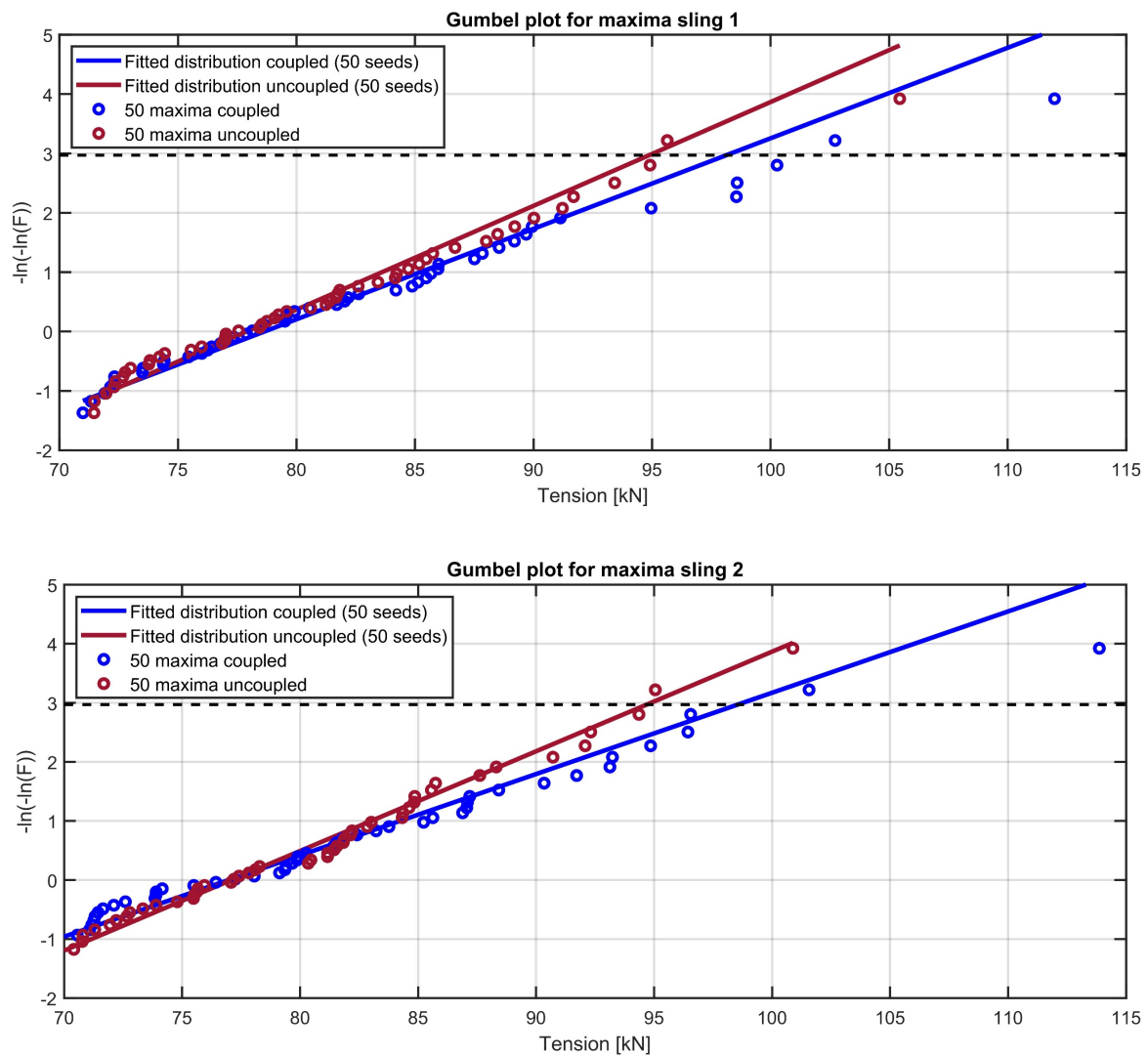


Figure 5 - 15 Gumbel plot for maxima tension, coupled and uncoupled motion.

The fitted Gumbel plot in Figure 5 - 15 shows for slings 1 and 2 that the non-exceedance limit of 0.9 yields larger tension for the coupled motion. These values for coupled motions were not expected regarding DNV-RP-H103 subchapter 7.3.3.3. However, the lower expected tension for the coupled system will give a greater probability of snap loads, which is the probable cause for the “conservative” values observed for coupled motion.

5.3.4 Minima Sling Tension

The same procedure is done for minima tensions for the different motions as of maxima. The cumulative average value for minima has been plotted in Figure 5 - 16 for slings 1 and 2. As expected, the coupled motion yields a lower value for the tension due to the slightly larger forces observed from the maxima coupled system.

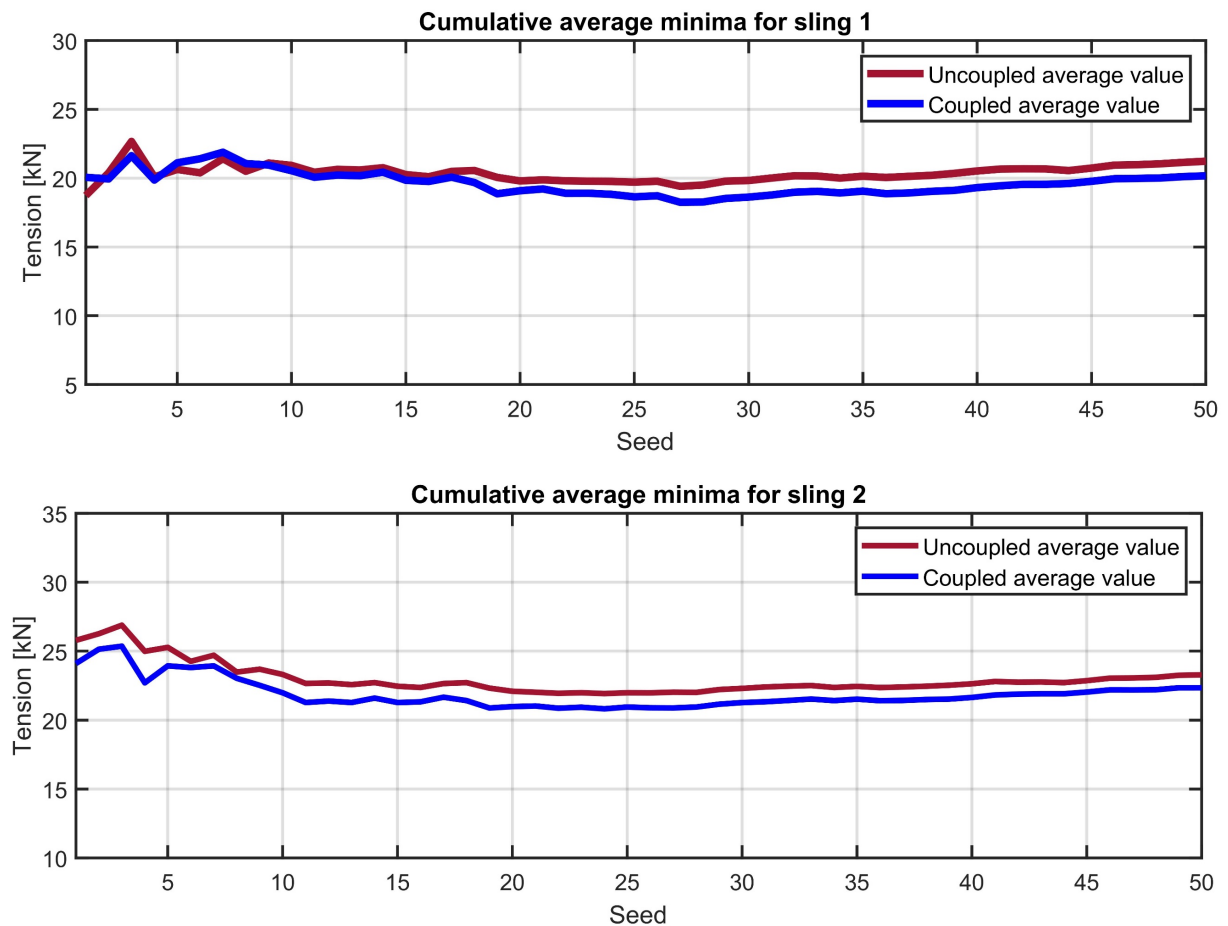


Figure 5 - 16 Cumulative average minima tension for coupled and uncoupled motion.

For the cumulative average minima, the most significant difference in tension observed between the motions is approximately 0.8 kN, which yields a difference of 4%. Figure 5 - 16 shows that the cumulative average tends to follow the same trend/path. Therefore, the coupled motion will still yield the most conservative prediction. However, the difference between the motion is almost neglectable.

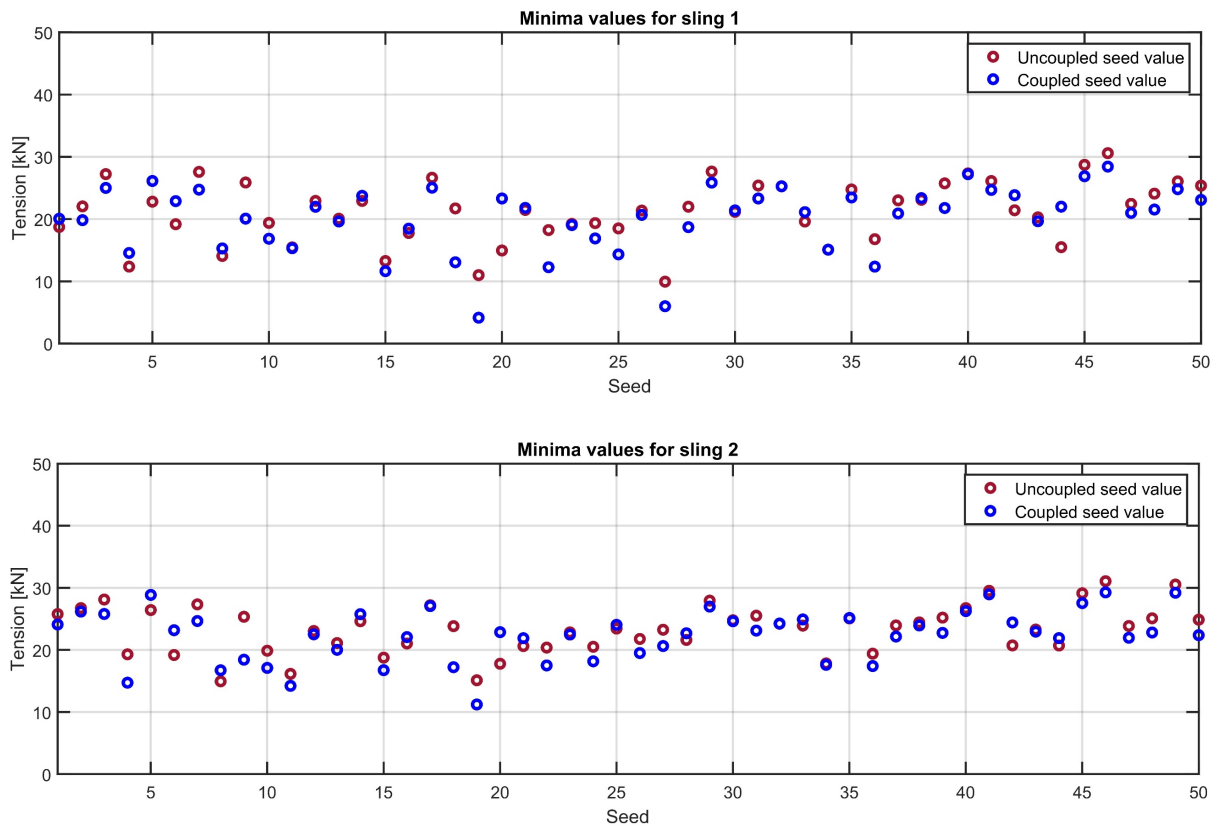


Figure 5 - 17 Minimum tension for individual seeds.

From Figure 5 - 17, the individual value for each seed has been plotted for slings 1 and 2. There is no significant deviation between the motions for the different individual seeds. The average difference between the individual seeds is approximately 12%. However, there are many seeds for coupled motion, which yields lower tension than uncoupled. For the coupled motion, less than 30% of the individual seeds will predict sling tension larger in magnitude than uncoupled. Therefore, the coupled motion has a greater risk of snap loads.

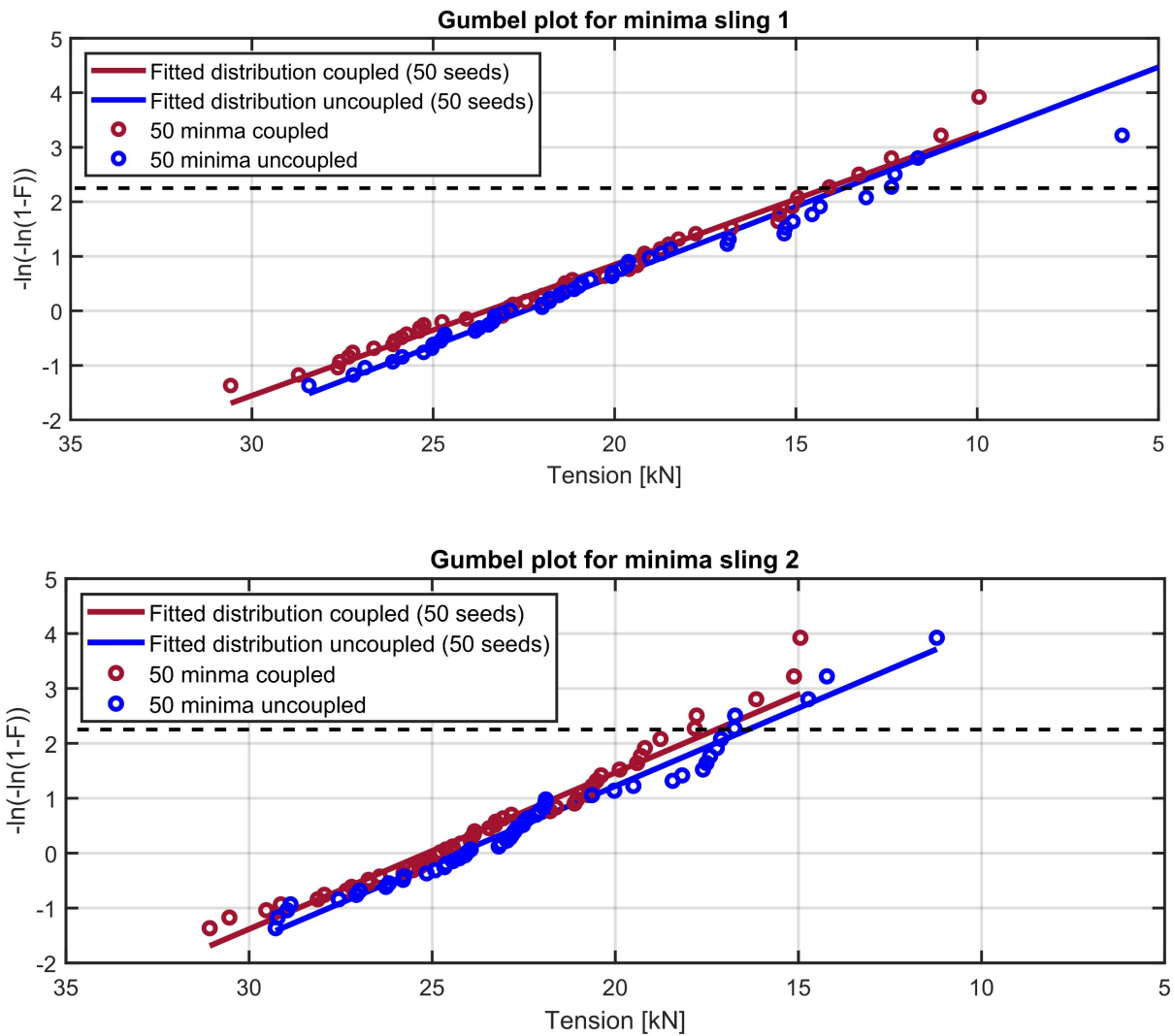


Figure 5 - 18 Gumbel plot for minima tension, coupled and uncoupled motion.

From the given minima Gumbel plot for slings 1 and 2, using either coupled or uncoupled motion will yield similar results when assessing the allowable sea states. This is because the difference in the fitted distribution for sling 1 is neglectable, where sling 1 from the assessment of the number of wave seeds yields the lowest predicted tension. Therefore, based on the minima, the difference is so small that it will not affect the assessment of sea states for the cover.

5.3.5 Comparison of Different Seeds

Two seeds with significant variations between the individual vessel motions have been selected for further investigation. The seeds that will be used for further investigation are 18 and 19, which obtain the largest deviation of tension observed among the different motions. In order to understand the large difference, the tension for slings 1 and 2 have been plotted and given in Figure 5 - 19.

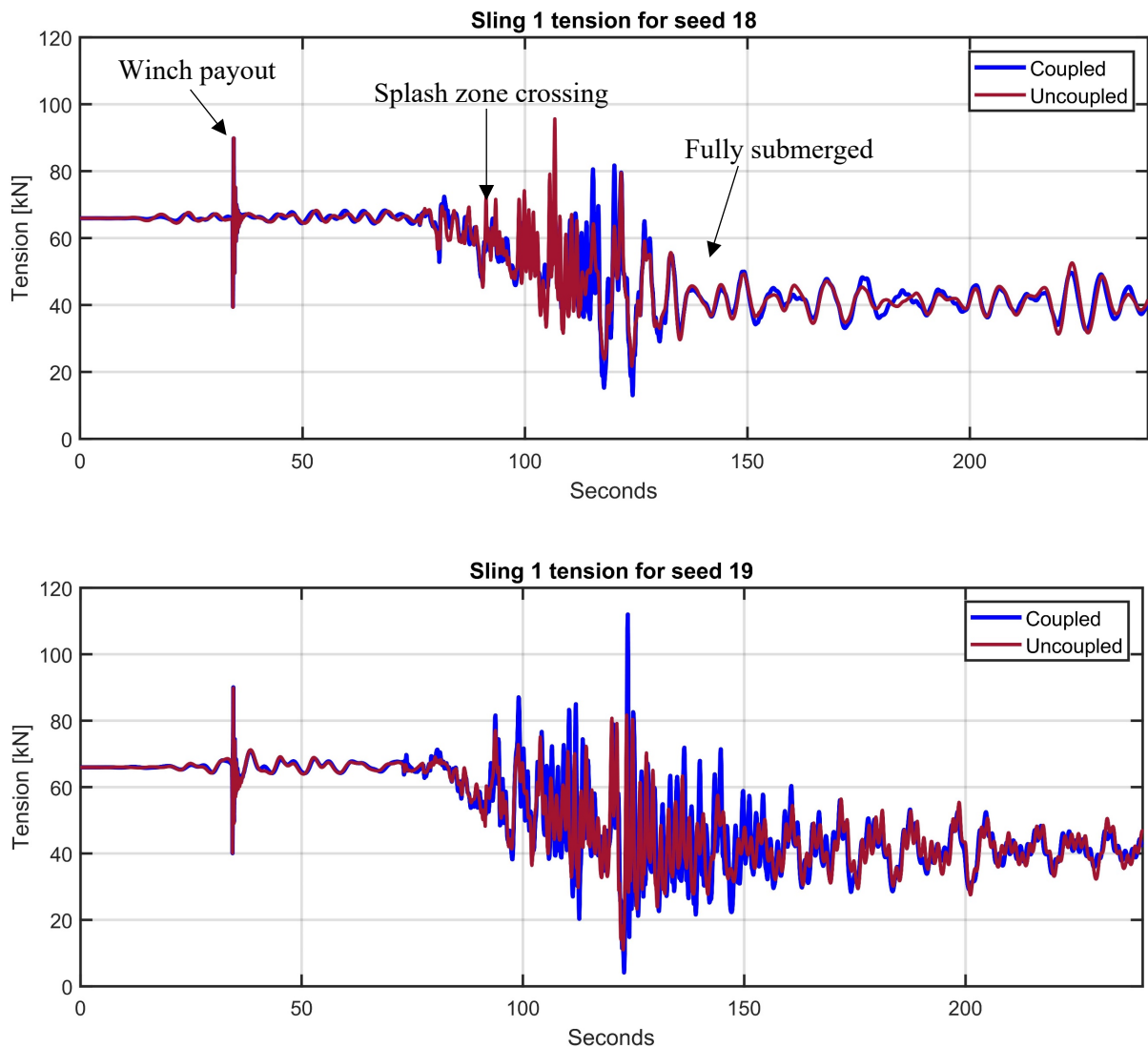


Figure 5 - 19 Sling 1 tension for seeds 18 and 19.

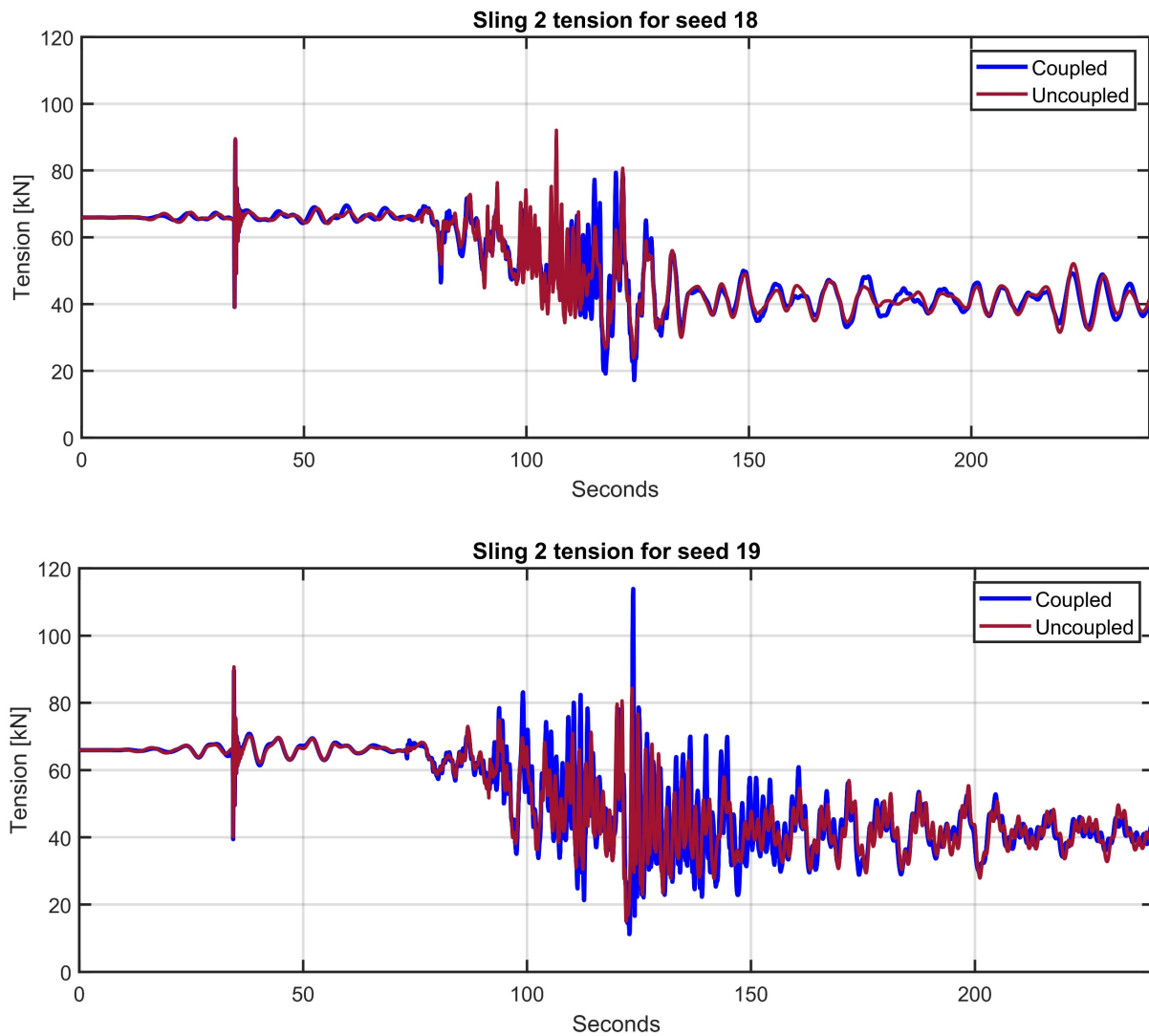


Figure 5 - 20 Sling 2 tension for seeds 18 and 19.

For seed 18, the maximum tension occurs after the center of mass of the cover crosses the splash zone. The early spike in tension for the uncoupled motion for seed 18 does not indicate any form of snap or slam loads. For seed 18, the most significant slam loads occur close to fully submergence. The slam loads should be greater for the coupled motion due to the lower observed tension. For seed 19, the largest tension occurs close to the full submergence of the cover. The significant spike in tension for seed 19 is due to snap loads occurring for the coupled system. However, the most significant tension observed for sling 2 ensues even if the minimum sling tension is above the snap load criteria.

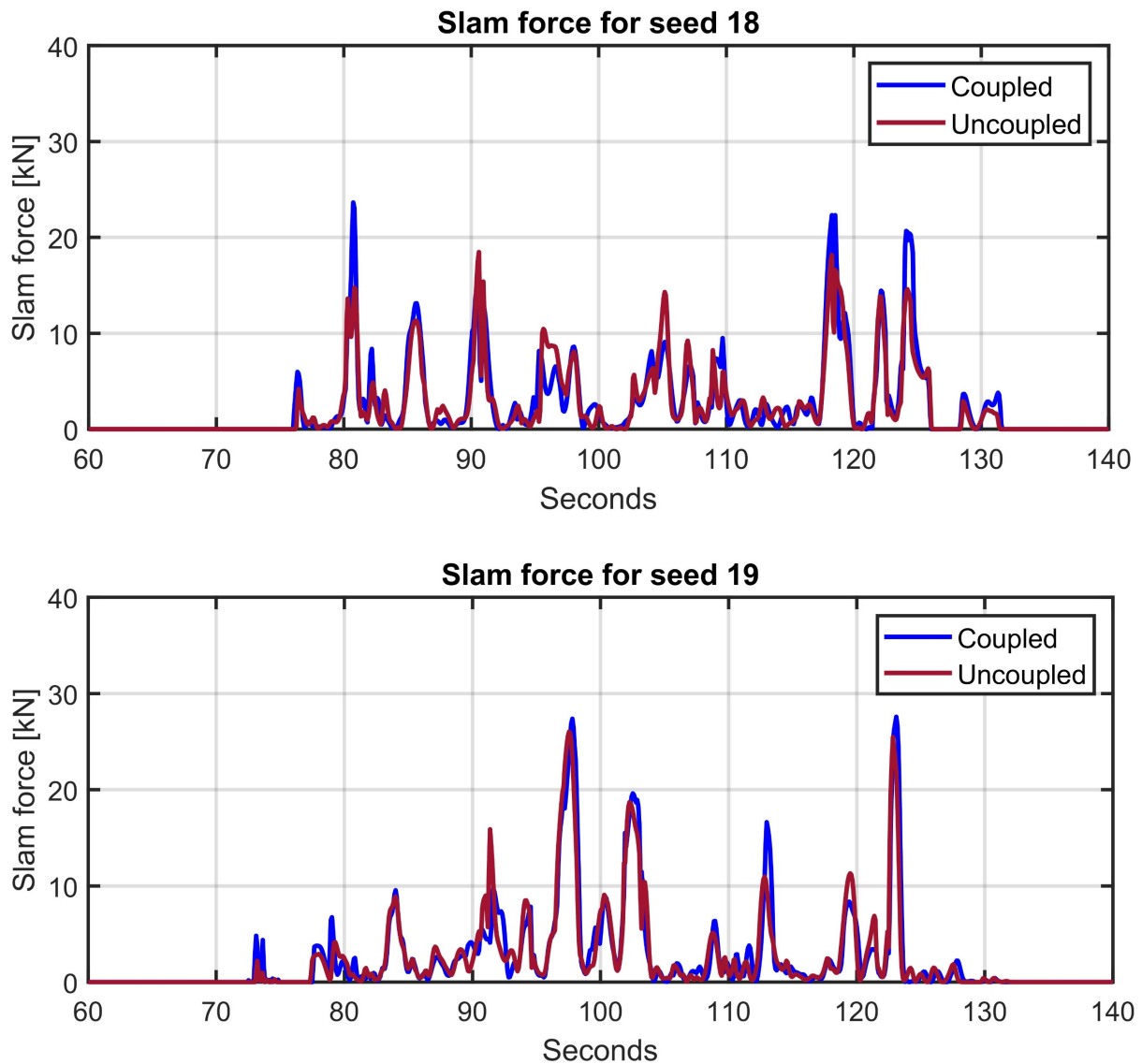


Figure 5 - 21 Slam force for seeds 18 and 19.

The slamming force given in Figure 5 - 21 shows a correlation between low tension and large slamming loads [29]. The cover at coupled motion will experience slightly larger slamming forces, which explains why the sling tension tends to be lower for coupled motion. As expected for seed 18, the significant spike in tension for uncoupled motion is not correlated to slamming forces. For seed 19, the slamming loads for coupled and uncoupled motion are almost similar in magnitude. However, the large difference in tension between the motion is not correlated to the slamming force, which was not expected.

From chapter 3, the eigenvalues for the vessel were calculated, of which the natural period of heave corresponds to the applied wave period. This may influence the difference in tension observed for the coupled and uncoupled motion. The natural periods for the coupled system can be obtained with manual estimation by solving the following equation [30]:

$$[-\omega^2(\mathbf{M} + \mathbf{M}_a) + \mathbf{K}] \cdot x = 0 \quad (55)$$

The manual estimated natural periods will yield identical eigenvalues as the uncoupled system. As expected, due to this being a light lift, the object will not affect the eigenvalues of the vessel. The heave motion for seeds 18 and 19 is given in Figure 5 - 22.

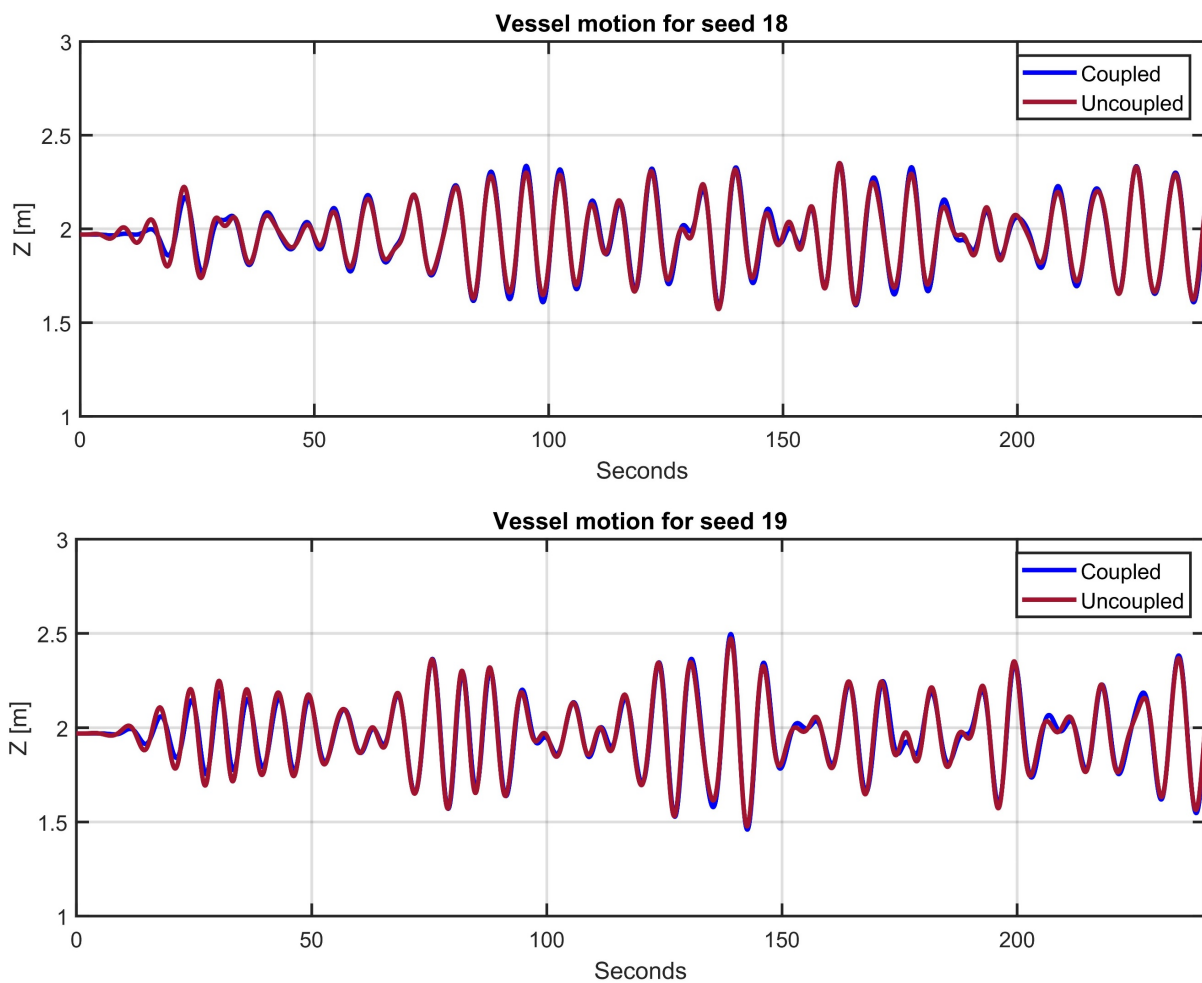


Figure 5 - 22 Heave motion for seeds 18 and 19.

From the heave motion of the vessel, there is nothing to indicate the large differences in tension observed in seed 19. Instead, the vessel's response is almost identical between the motions, with only a slightly larger response for the coupled motion due to the added forces applied to the vessel from the mooring lines and cover.

The shackle position for the different seeds is given in Figure 5 - 23. The same result is observed for the shackle position/motion as for the vessel motion. The shackle position is almost identical between the coupled and uncoupled motions.

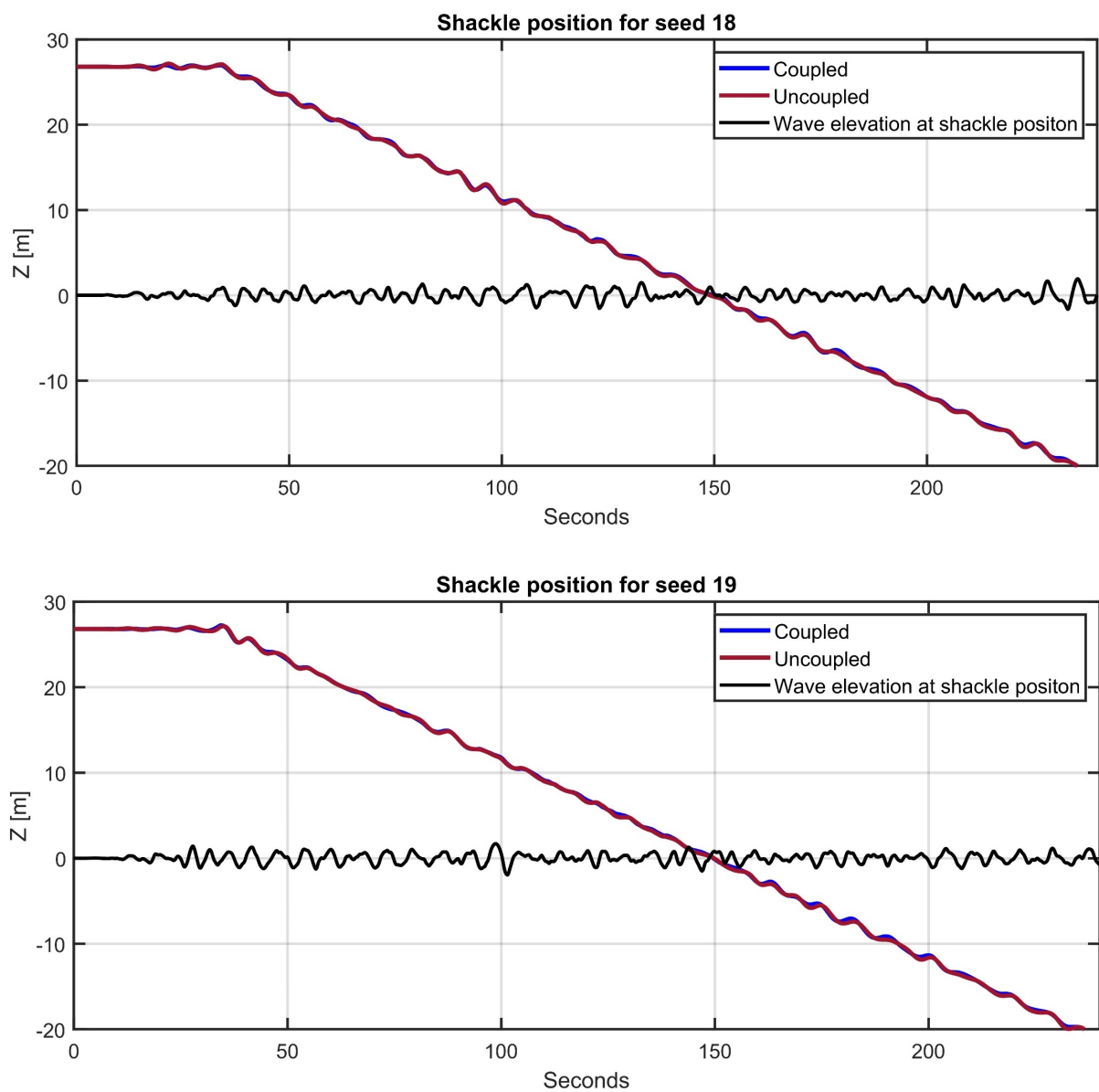


Figure 5 - 23 Shackle position for seeds 18 and 19.

For seed 18, there is nothing to indicate a large spike in tension that only occurs for the uncoupled motion. The same can be seen for seed 19, where the shackle motion/position is almost identical for the large snap load at the coupled motion. An investigation of the model in OrcaFlex is needed to identify the large differences in tension.

One of the most considerable differences observed from the model in OrcaFlex is the yaw rotation of the cover for the individual motions. For seed 19, the yaw rotation for coupled motion is 10 degrees larger compared to the uncoupled motion. More extensive yaw rotations on the cover for coupled motion increase the risk of lowering the cover at an undesired position. As a result, the cover will experience larger hydrodynamic forces than the intended crossing position. The yaw motions of the cover from seed 19 can be seen in Figure 5 - 24.

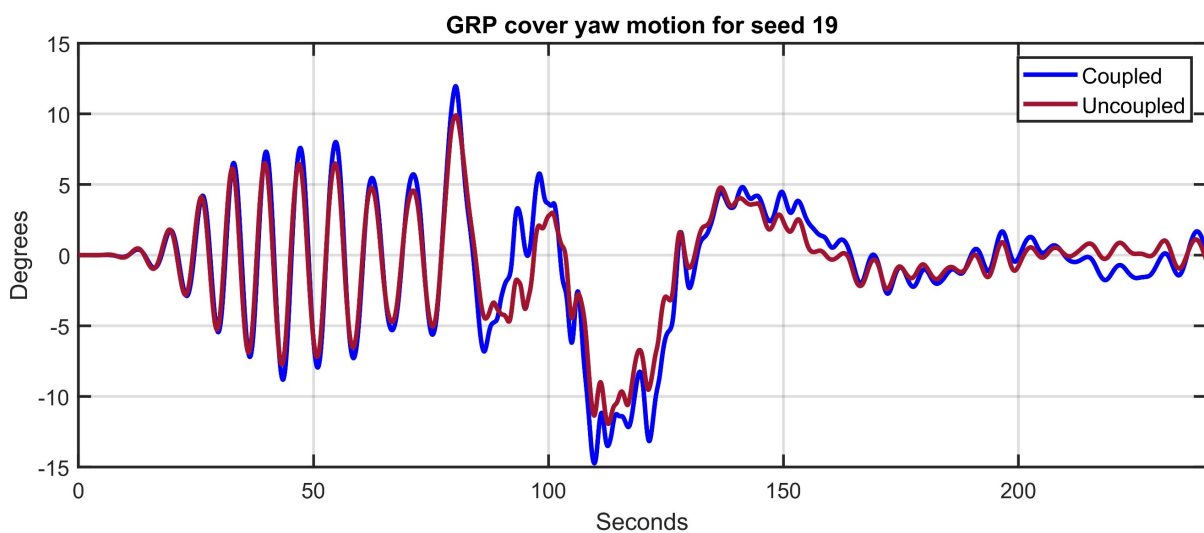


Figure 5 - 24 Seed 19 yaw cover rotation for uncoupled and coupled motion.

Another issue observed from the simulations is large pendulum motions on the lifting wire. These pendulum motions occur at the splash zone crossing and contribute to slack and considerable sling tension. For seed 18, the spike in tension for uncoupled motion is due to this observed pendulum motion. The pendulum motion is present for both the coupled and uncoupled motion.

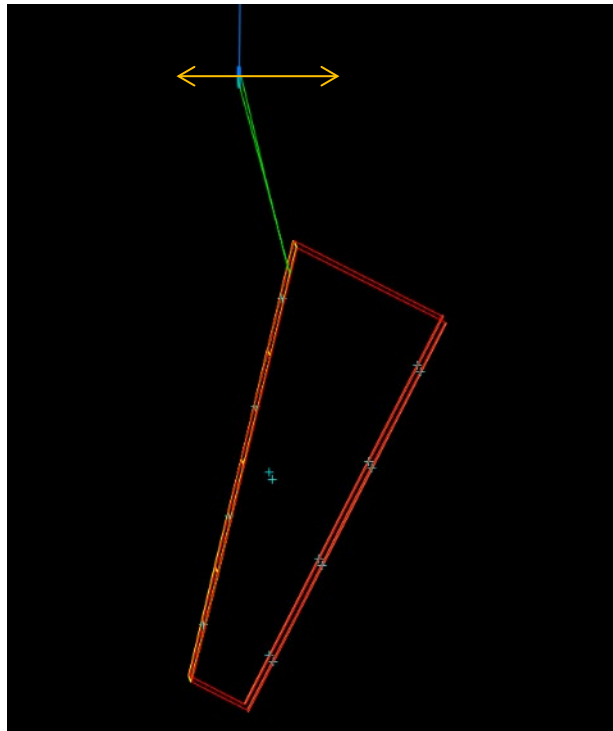


Figure 5 - 25 Example of pendulum motion from OrcaFlex.

From Figure 5 - 27, the pendulum motion for seed 19 has been plotted for both coupled and uncoupled motion. The largest shackle motion corresponds to the observed lowest sling tension value. Even if the shackle behavior is similar between the coupled and uncoupled motion, the forces applied will differ. Figure 5 - 26 shows that the shackle for the coupled motion will experience a greater compression force than the uncoupled motion, which may influence the tethers, which cannot handle compression forces [9]. However, the difference in tension is not just from the pendulum motion but a combination of the previously stated yaw and pendulum motions.

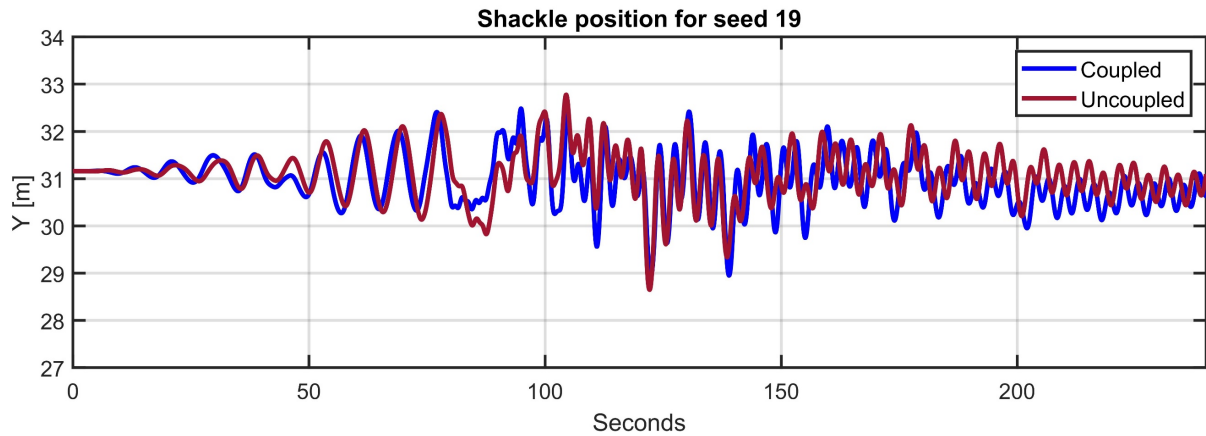


Figure 5 - 27 Pendulum motion for shackle.

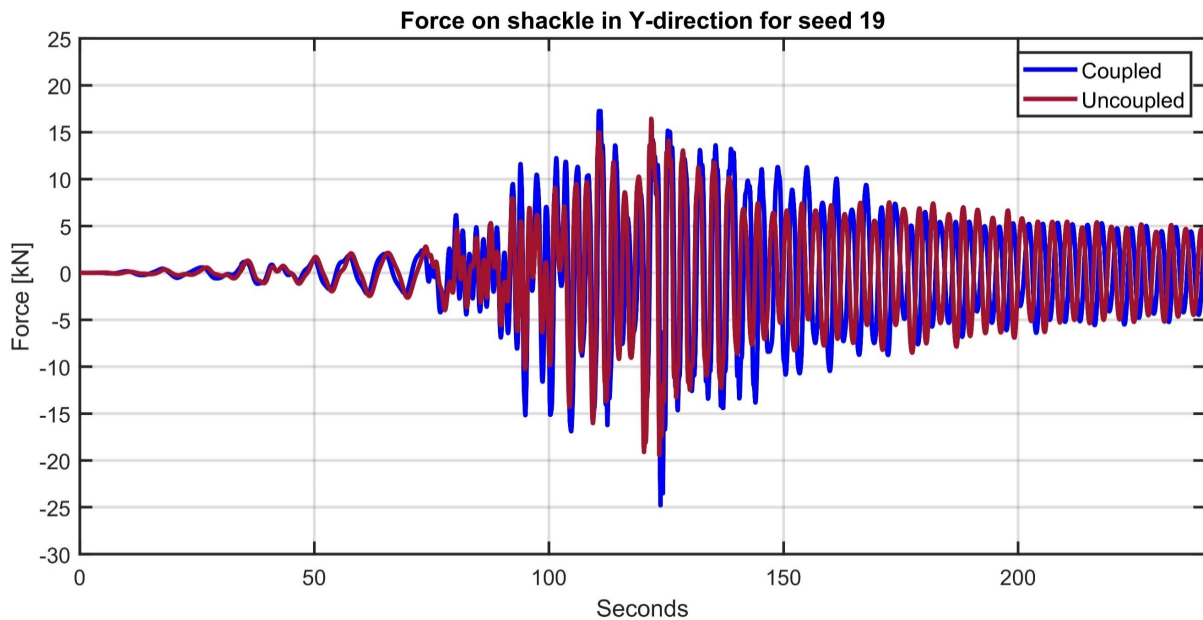


Figure 5 - 26 Shackle force in Y-direction.

The last observed difference between coupled and uncoupled systems is the vessel's roll motion. The GRP cover will apply a moment force on the vessel for the coupled system, and the moment force will change the behavior of the roll motion for the coupled system. For example, from Figure 5 - 28, the vessel's roll motion for the coupled system will be slightly larger and shifted due to the applied moment from the cover.

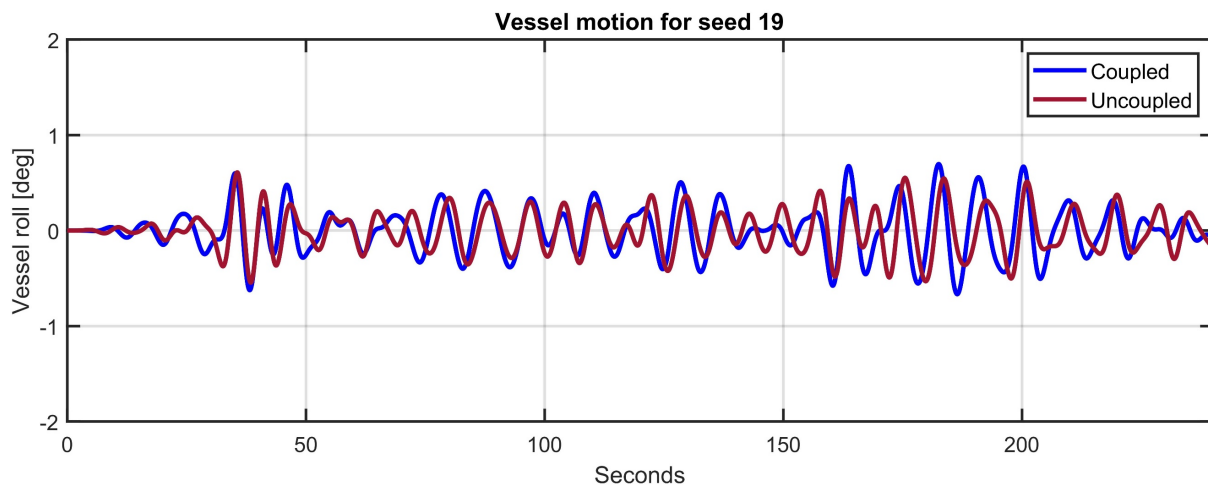


Figure 5 - 28 Roll motion for seed 19.

The significant differences in tension for seed 19 are due to a combination of events that all happens concurrently. First, the cover rotates to the vessel for the coupled motion at the minimum observed tension, increasing the hydrodynamic forces. The motion of the shackle is also towards the vessel, while the roll motion is towards the cover. These co-occurring events increase the possibility of large snap loads, which was the case for seed 19.

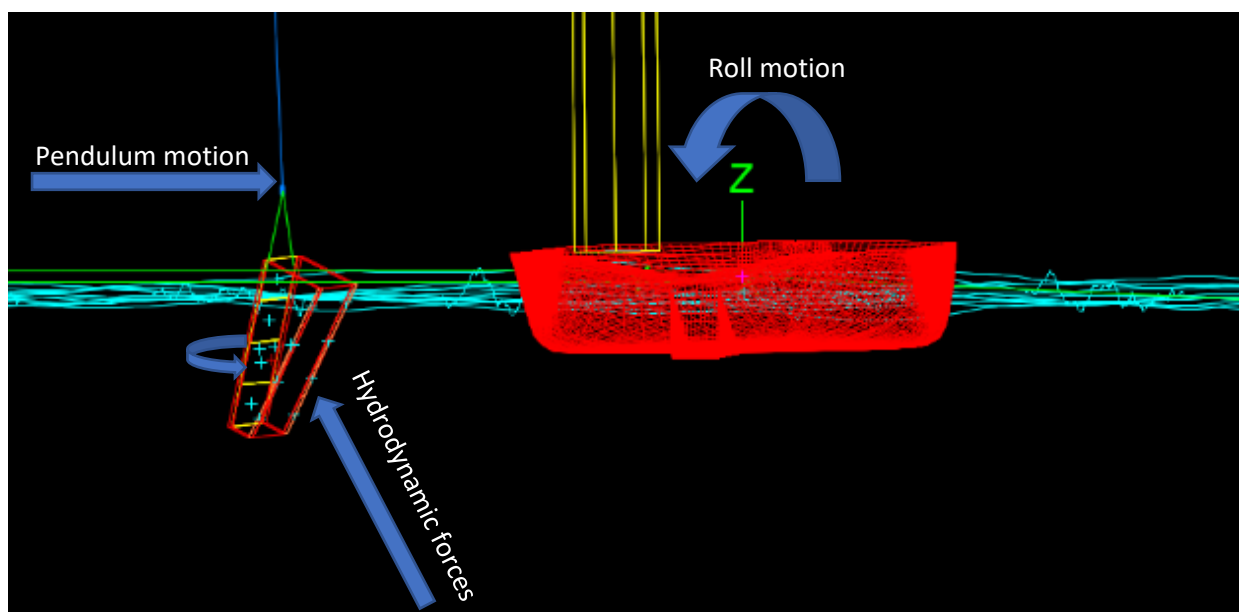


Figure 5 - 29 Example of different events co-occurring for seed 19

5.3.6 Discussion of Coupled and Uncoupled Motion

The conservative motion for the vessel will be the coupled system. The coupled motion will experience larger and lower sling tension than the uncoupled motion. From DNV-RP-H103 subchapter 7.3.3.4, it is concluded that with the increased size of the object, the coupled analysis will better describe the vessel behavior more precisely [1]. The cover's large size and low weight warrants large hydrodynamic forces, which will be more prevalent as seen from the slamming loads for the coupled motion. However, the difference in tension between the motions is almost similar, of which seed 19 contributes mainly to the differences.

The GRP cover will experience larger yaw rotations using the coupled motion when in air, which results in greater impact between the cover and the sea surface, as seen from the slamming loads. This can yield an undesired position, where more of the cover surface area is present, which will increase the hydrodynamic forces on the cover. Lastly, the coupled system will also experience a shift in the roll motion due to the moment applied from the GRP cover, which in some circumstances will affect the sling tension, as shown from seed 19.

For the assessment of allowable sea states, it is decided to continue using uncoupled motion. The slight observed difference between the motions in sling tension should yield closely related sea states. Also, for longer wave periods it has been observed large yaw rotations for the coupled vessel in the numerical time-domain simulation (Appendix C). In real life, the dynamic positioning system will contradict these motions and keep the vessel steady for yaw, surge, and sway. In order to contradict these motions in OrcaFlex, extra mooring lines or artificial constraints are needed. This will make the simulated coupled model in this subchapter obsolete, with the main assumption that the responses on the new coupled model will yield almost identical results as the uncoupled motion. This is because yaw motions for the vessel are also present in the uncoupled model. However, using displacement RAOs and harmonics will better constrain the vessel for the motions of yaw, surge, and sway without any modification to the model.

Chapter 6

Assessment of Allowable Sea States

6.1 Operational Criteria

The operational criteria are conditions that need to be met to determine if the marine operation can be conducted. The criteria are compared with the result of the time-domain simulation by fitting a statistical model to the sample. In addition, the difference between lifting angle and use of shielding may affect the operational limits. When assessing the allowable sea state, the target probability of non-exceedance will influence the extreme values. Usually, the probability of non-exceedance is in the range of 0.9 to 0.99. However, this is determined by the risk associated with the operation. Selecting a high limit of non-exceedance probability will increase the uncertainty regarding whether an incident will happen or not. A too low value may reduce the reliability of the predicted extremes if the sample size is too small [12]. Based on Chapter 5, the non-exceedance probability will remain at 0.9. This exceedance probability will be implemented to investigate the three different extreme values criteria:

- Snap loads
- Working load limits of the slings
- Clearance between the cover and the vessel

The operational criteria are based on the working load limits of the slings, DNV-RP-H103 for allowable snap load, and vessel clearance. From DNV-RP-H103, the allowable tension for the sling shall never be lower than 10% of the minimum static tension to avoid snap loads [1]. The safe working load for the slings shall never surpass a mass of 16 800 kg [32]. The vessel clearance is set to five meters to avoid potential collision between the cover and the vessel, with an initial clearance of 16.5 meters. The operational limit will never exceed a wave height above three meters to ensure safe working conditions for the deck crew that will execute the operation.

6.2 GRP Cover Lifting Angle

6.2.1 Operational Limits

When assessing the allowable sea states, it must be validated against the operational criteria to determine the limits. This has been done for all the extracted results and validated using a Gumbel distribution. The operational criteria from subchapter 6.1 define the three extreme values criteria, which will give the allowable sea states. From the simulation result, the extreme value limiting the sea states for the GRP cover is only the minimum sling tension. From all the simulations conducted, only two seeds surpassed the working load limit. This only occurred for one sea state for the cover at 75 degrees, and the Gumbel plot is given in Figure 6 - 1.

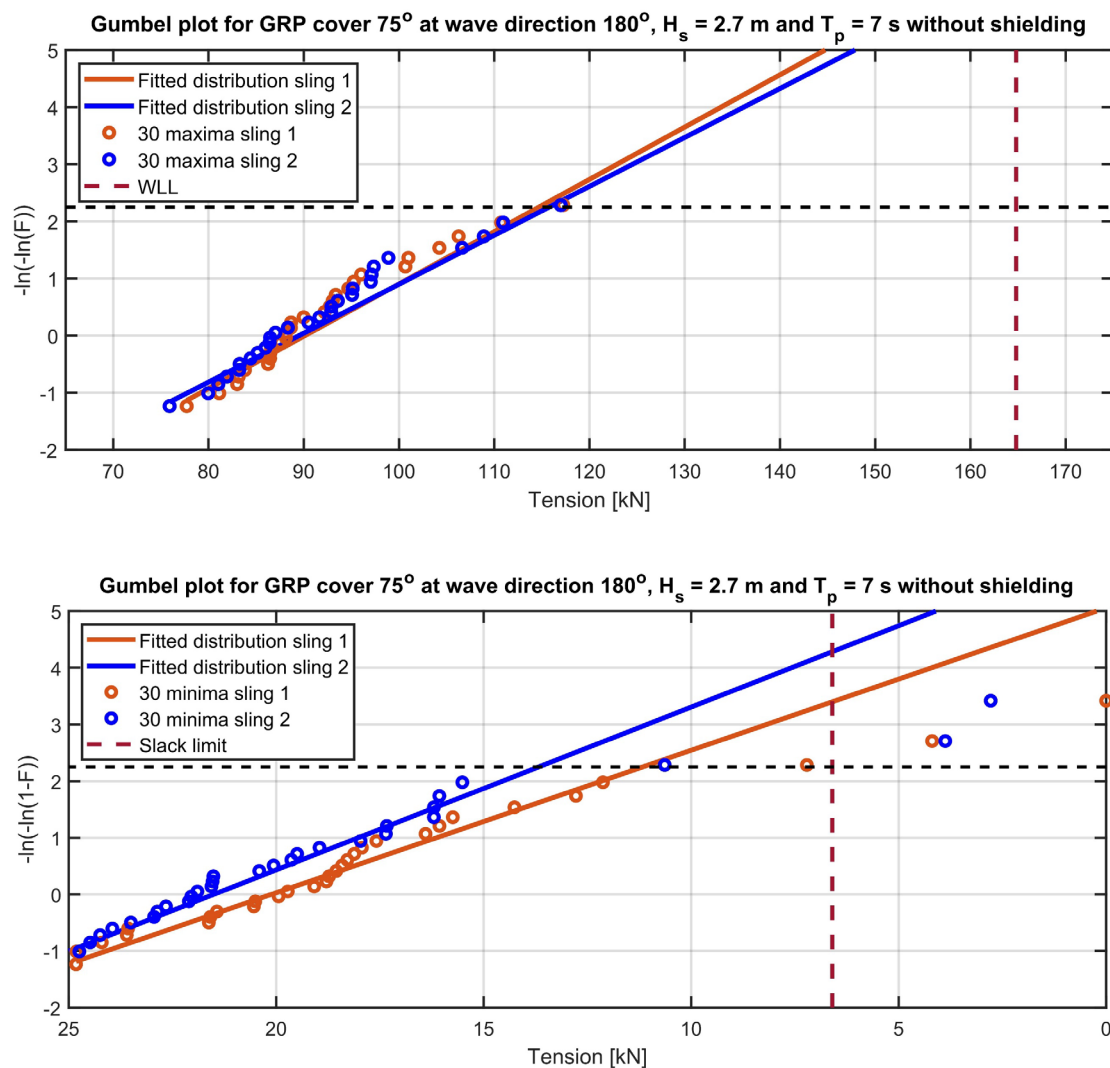


Figure 6 - 1 Gumbel plot for maxima and minima for grp cover at 75°.

As seen from the fitted distribution, the limiting factor for the allowable sea states will be the minimum tension of the slings. From the observed results, large snap loads rarely occur even if the sling tension is well below the snap limit. However, a significant fluctuation in the sling tension will cause large strains in the material, which may damage the slings even if the load limit is never reached.

For the last operational criteria regarding minimum clearance, the observed results indicate that clearance between the vessel and the cover will not be an issue or a limiting factor. The lowest observed clearance between the vessel and the cover was found for the allowable sea state of the cover at 75 degrees and given in Figure 6 - 2.

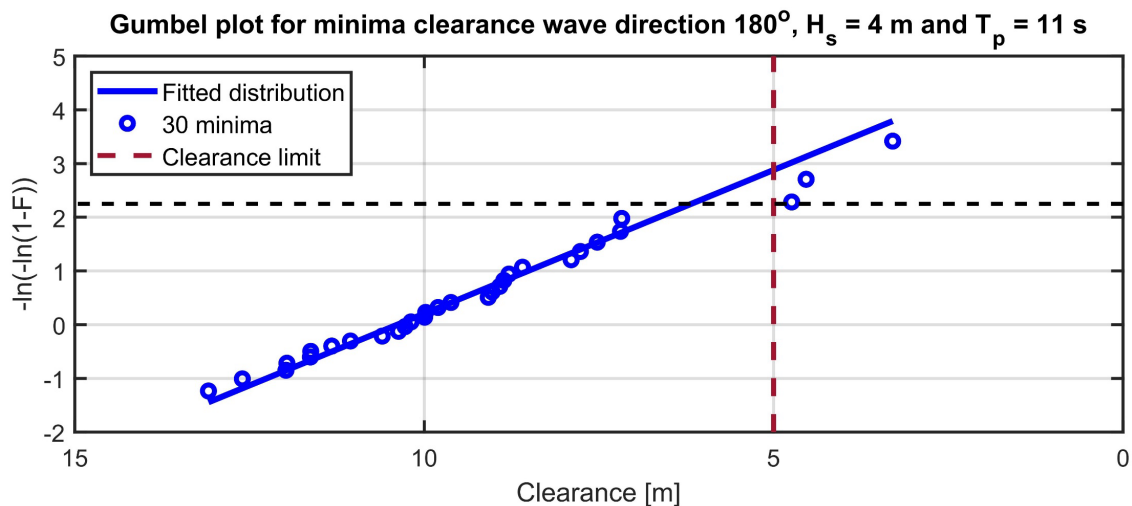


Figure 6 - 2 Gumbel plot for minima clearance.

The minimum clearance has been verified from the fitted distribution at a wave height of four meters, which is greater than the pre-defined limit of three meters. Therefore, the fitted distribution shows that minimum clearance does not limit the allowable sea states. As a result, the assessment of the allowable sea state will not be limited by the clearance when there is no possibility of collision between the objects.

As stated earlier and shown in Figure 6 - 1 and Figure 6 - 2, the limiting factor for the GRP cover will depend on the allowable snap loads. Low sling tensions for the cover are common for all the tested sea states, of which the fitted distribution compared to the slack limit determines the acceptable sea states.

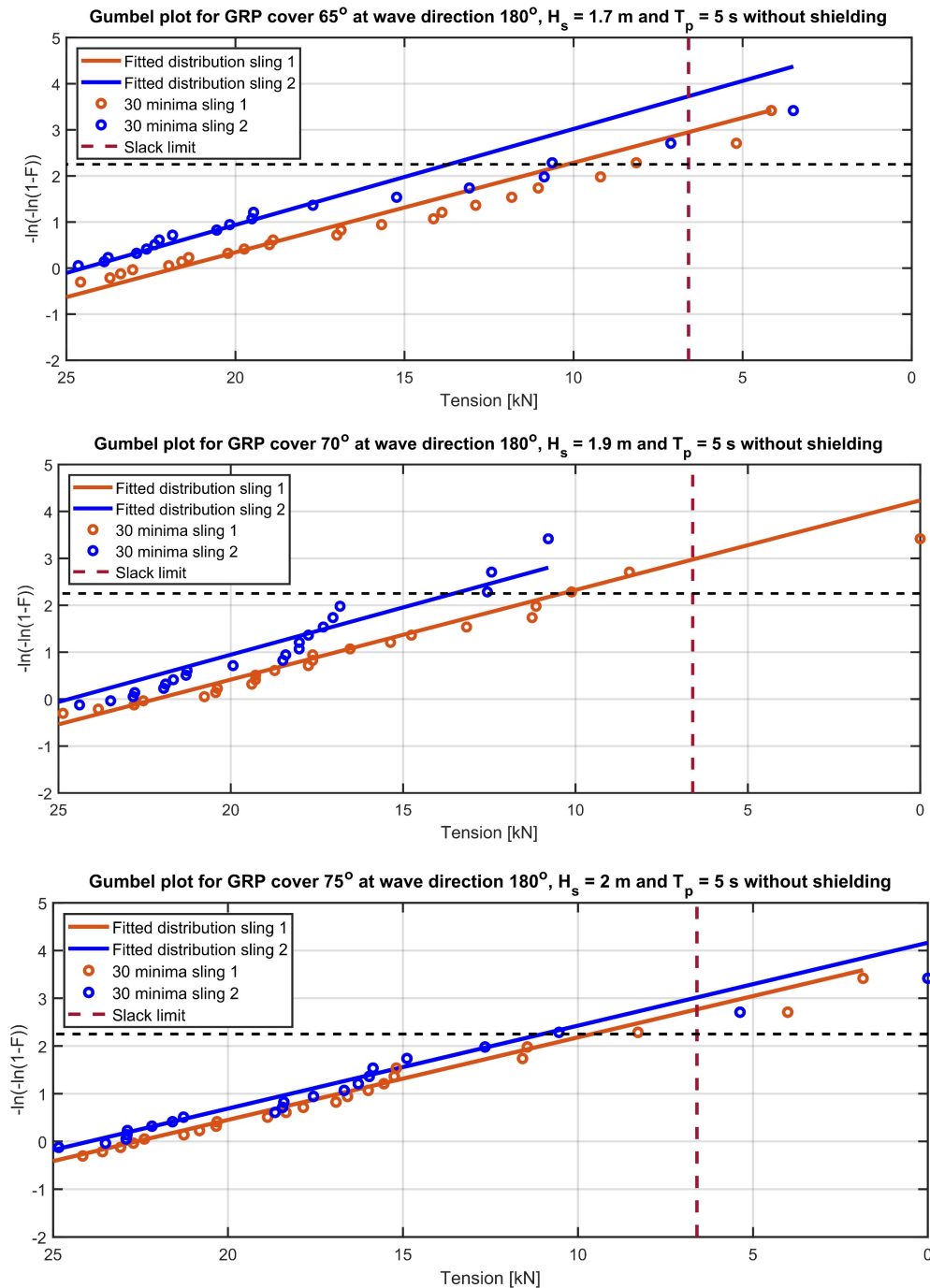


Figure 6 - 3 Gumbel plot for minimum tension for lifting angles 65°, 70°, and 75°.

From Figure 6 - 3, shows that the minimum tension for five seconds has been plotted for all the lifting angles. Then, based on the slack limit and the fitted distribution, the allowable sea states are given for the different angles. Finally, the same procedure has been conducted for all the tested wave periods, giving the allowable sea states.

6.2.2 Allowable Sea States

The allowable sea states are presented in Figure 6 - 4. The area underneath the lines represents the allowable wave height and wave period, where it can be lowered through the splash zone. The allowable sea states for the different angles must not be mistaken as limits for the entire operation. This study only focuses on the limits of lowering through the splash zone.

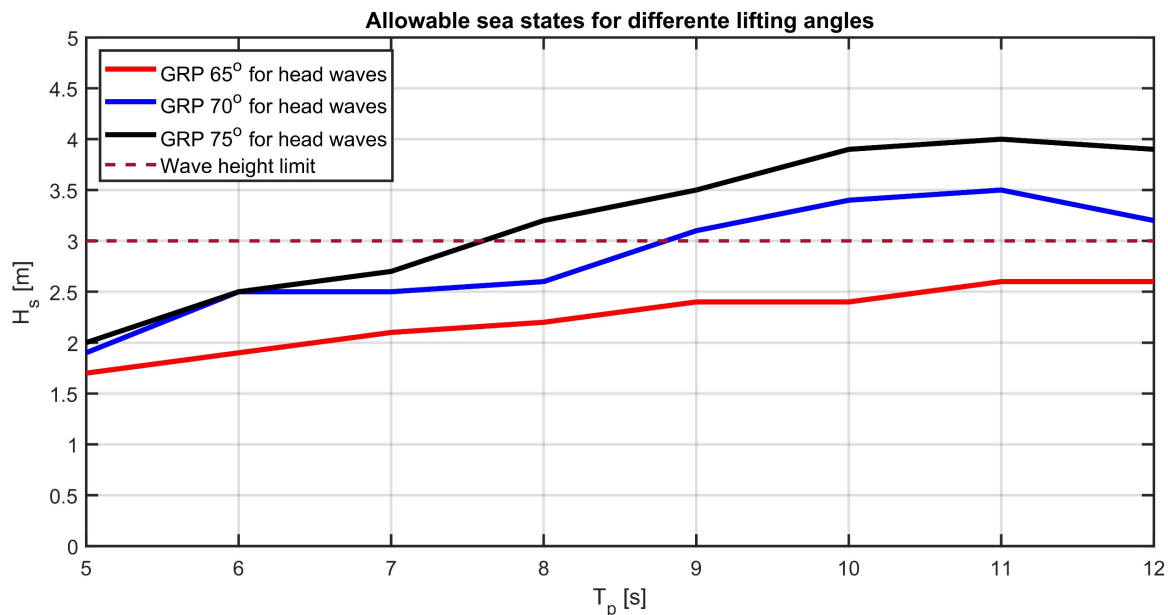


Figure 6 - 4 Allowable Sea state for different lifting angles.

The lifting position of the cover for the splash zone crossing contributes significantly to the allowable sea states. The preferable lifting angle for the cover is 75 degrees, which is expected due to the smallest waterplane area. The limiting factor for the cover at lower lifting angles is the larger slamming forces, which greatly increase the hydrodynamic forces. This can be observed from the allowable sea states for the cover at 65 degrees, which contains the largest waterplane area and the lowest sea states.

The most considerable differences between the lifting angles can be seen from longer wave periods. For shorter wave periods, the small difference is due to the low weight and the large surface area of the GRP cover. A shorter interval between the waves will generate larger motions on the cover, which increases the hydrodynamic forces. Therefore, for shorter wave periods, there is a higher probability that the hydrodynamic forces surpass the submerged weight, which can cause snap loads. This applies to all the tested lifting angles for shorter wave periods.

As stated previously, there is a clear correlation between the slamming loads and the sling tension. As shown in Figure 6 - 5 and Figure 6 - 6, the lowest sling tension occurs at the peak of the slamming force, which is consistent for all the lifting angles. The observed result for all the different lifting angles shows that maximum sling forces occur when the cover is almost fully submerged. At nearly fully submergence is also where the largest magnitude of slamming force is observed, which generates slack and snap loads in the slings. This can be seen in Figure 6 - 6, where the cover at an angle of 65 degrees is below the 10% minimum static tension limit. However, the maximum tension after slack stays well below the working load limit.

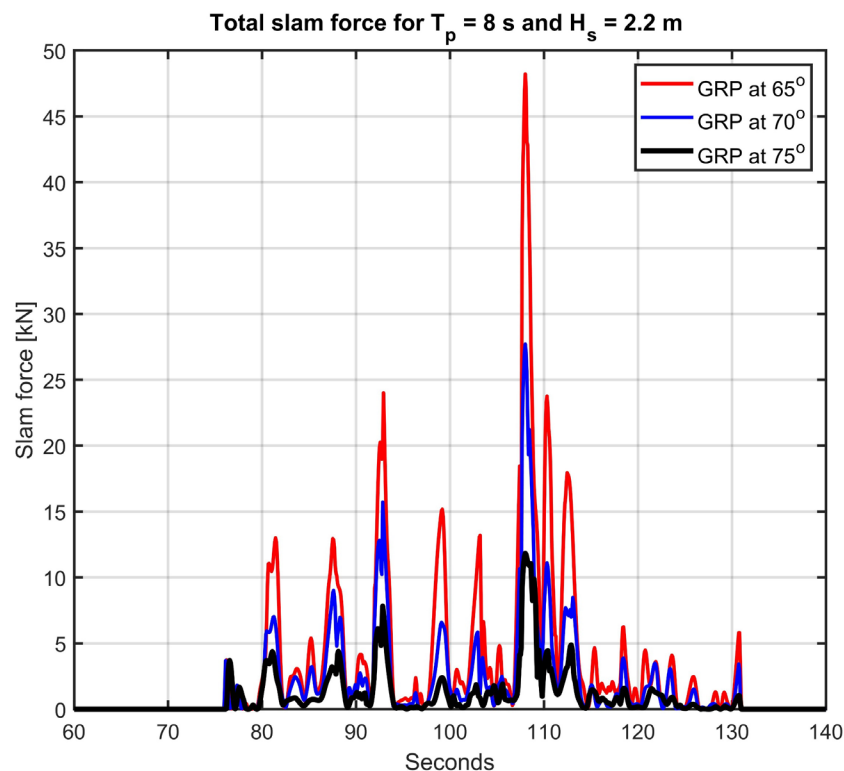


Figure 6 - 5 Example of slam forces at different lifting angles

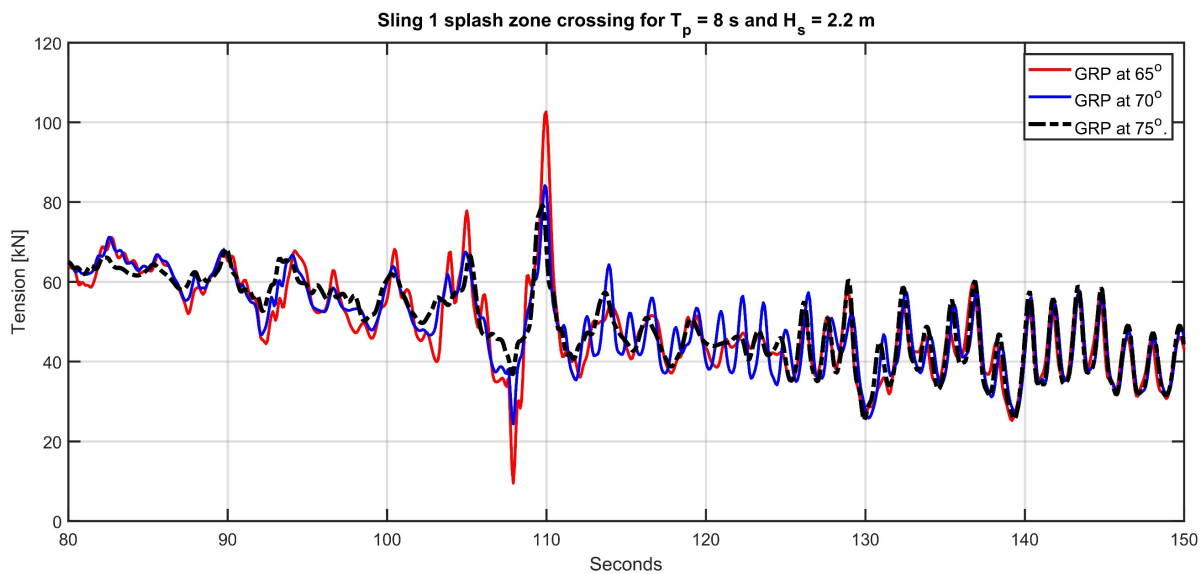


Figure 6 - 6 Example of tension in sling 1 for splash zone crossing at different lifting angles.

6.2.3 Discussion of Lifting Angles

When executing a splash zone crossing for an object with low weight and a large surface area, it is important to minimize the hydrodynamic forces on the object. This can be done as shown in this section by decreasing the waterplane area, yielding lower slamming forces. As expected, the lifting angle with the lowest waterplane area yielded the highest allowable sea states.

From the operational criteria, the only limiting factor observed was the minimum allowable tension for the sling. The correlation between slamming forces and slack defined the allowable sea states, even if the tension after slack never surpassed the working load limit. This is consistent with the observed results from Solaas et al. [10], where the occurrence of slack did not yield tension above the working load limits. However, there will always be a risk of damaging equipment/objects or injuries to personnel due to snap loads. The sudden burst of force experienced by the crane, wire, and lifted object will always induce risk, even if the sling tension never reaches the working load limit.

6.3 Assessment of Allowable Sea States

6.3.1 Operational Limit

From subchapter 6.2.1, the defining criteria for the allowable sea states were the minimum tension of the slings. From the observed results, this applies to this subchapter as well. The minimum clearance will always be above the operational limit of five meters, even when implementing a new wave direction with increased roll motion. For the maximum tension, as observed from the previous subchapters and Solaas et al. [10], the occurrence of slack does not yield forces above the working load limit. As stated earlier, the minimum tension gives the limits of what can be defined as the acceptable sea states. Figures 6 - 7 and 6 - 8 show examples of Gumbel probability plots for minimum tension to assess allowable sea states.

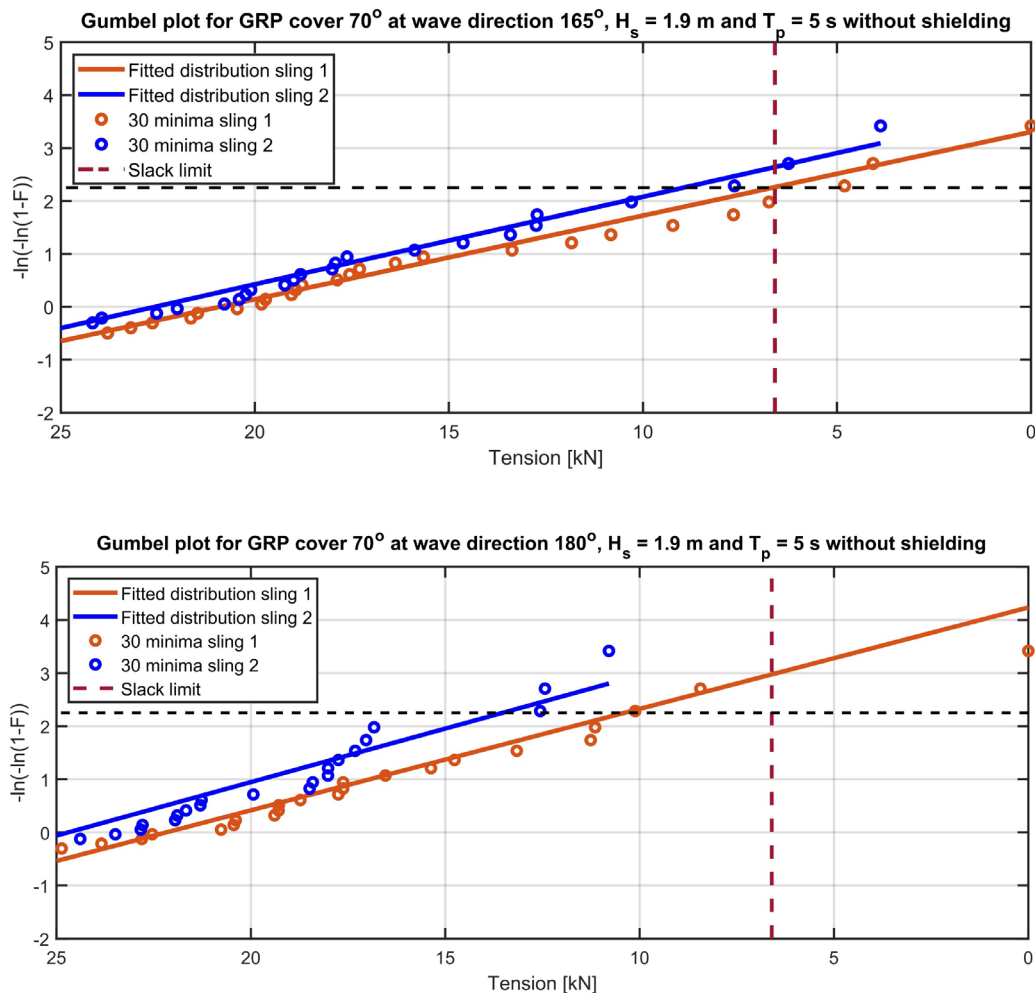


Figure 6 - 7 Gumbel plot for wave direction 165° and 180° for $T_p = 5$ s.

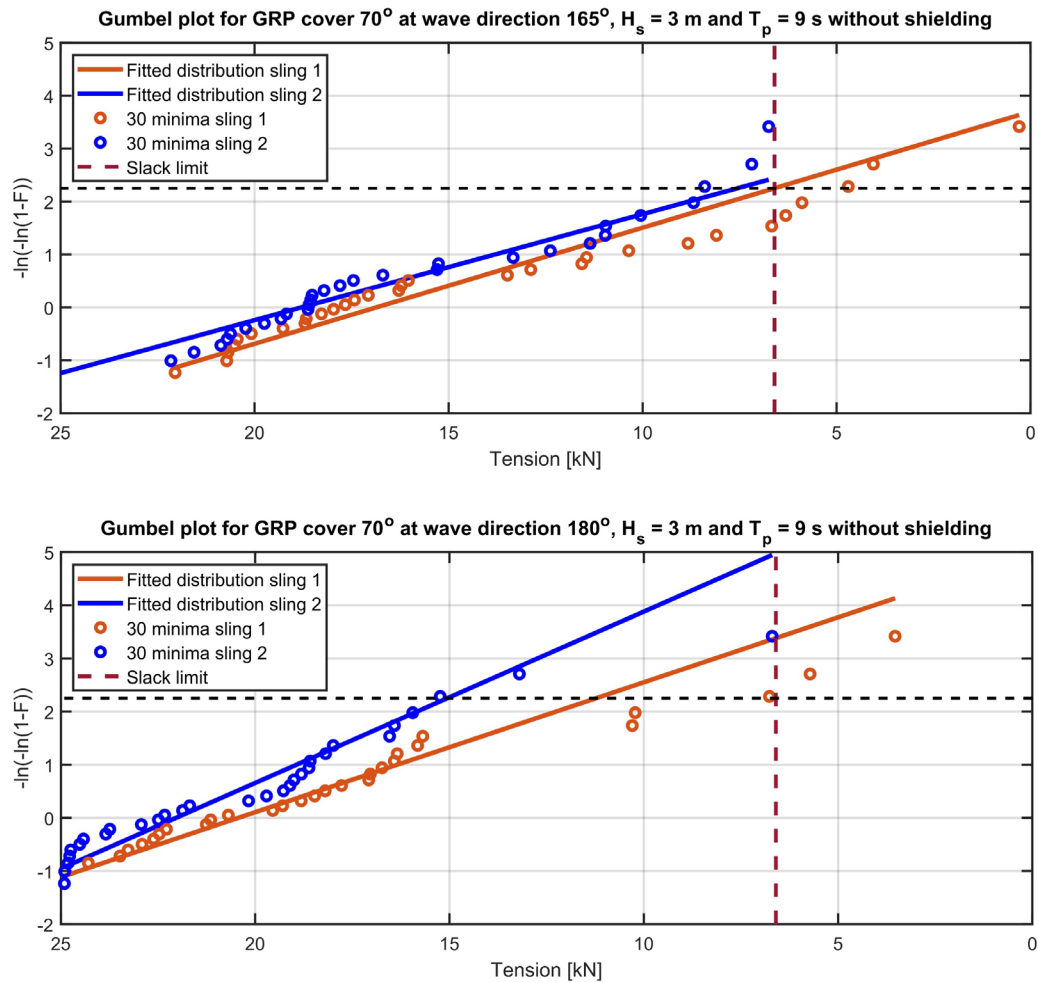


Figure 6 - 8 Gumbel plot for wave direction 165° and 180° for $T_p = 9$ s.

A common trend is observed for all the Gumbel probability plots for the different fitted wave directions of 165 and 180 degrees. For the same fitted Gumbel distribution, head waves will always yield better conditions for lowering through the splash zone compared to the wave direction at 165 degrees. This trend continues for all the applicable sea states, where the increase in roll motion for 165 degrees tends to lower the acceptable sea states. This can be seen in the examples given, where for the wave period at nine seconds and wave direction at 165 degrees, sling 1 is barely below the slack limit of 6.6 kN and, therefore, not acceptable.

6.3.2 Allowable Sea States

From the operational criteria and the fitted Gumbel distribution, the head waves for the vessel will always yield better condition for lowering through the splash zone. The roll motion that is applied in the wave direction at 165 degrees will increase the slamming loads on the cover. The increased slamming forces for wave direction at 165 will result in lower average minimum sling tensions for the uncoupled system. The increase of hydrodynamic forces on the cover due to roll motion is more related to longer wave periods, where the vessel tends to follow the wave.

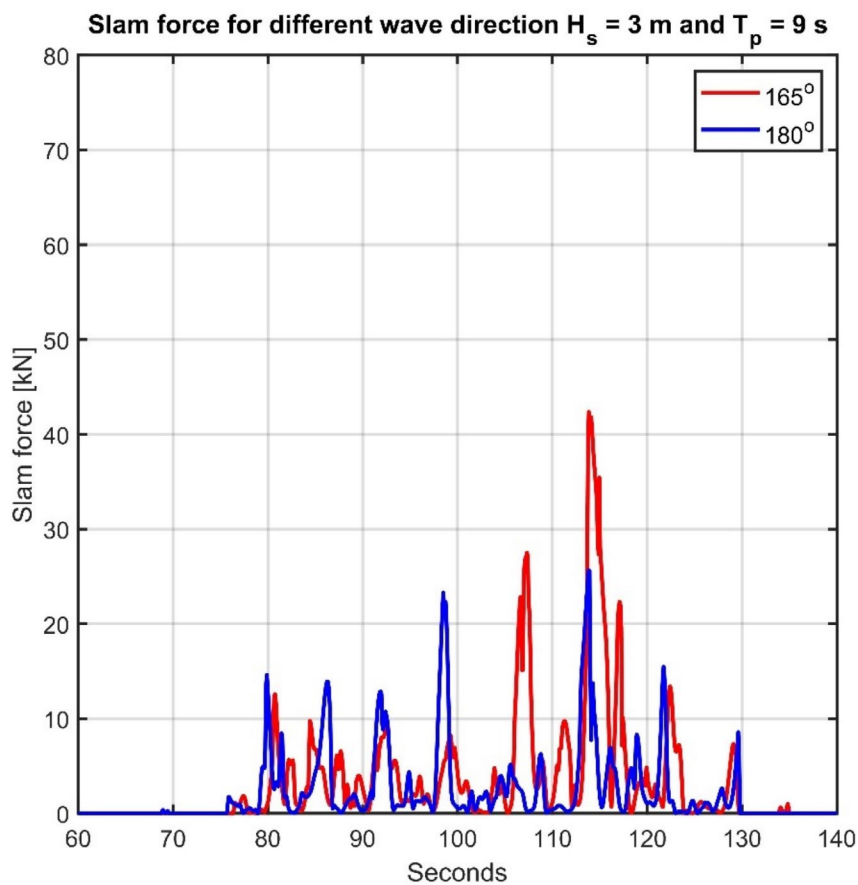


Figure 6 - 9 Example of slam forces for $T_p = 9$ s at different wave directions.

For longer wave periods, as shown in Figure 6 - 9, the slamming loads on the cover for wave direction at 165 degrees is almost double in magnitude compared to the head waves. These large slamming forces as stated previously directly translate to slack wires and snap loads. The correlation between the slamming force and tension can be seen in Figure 6 - 10.

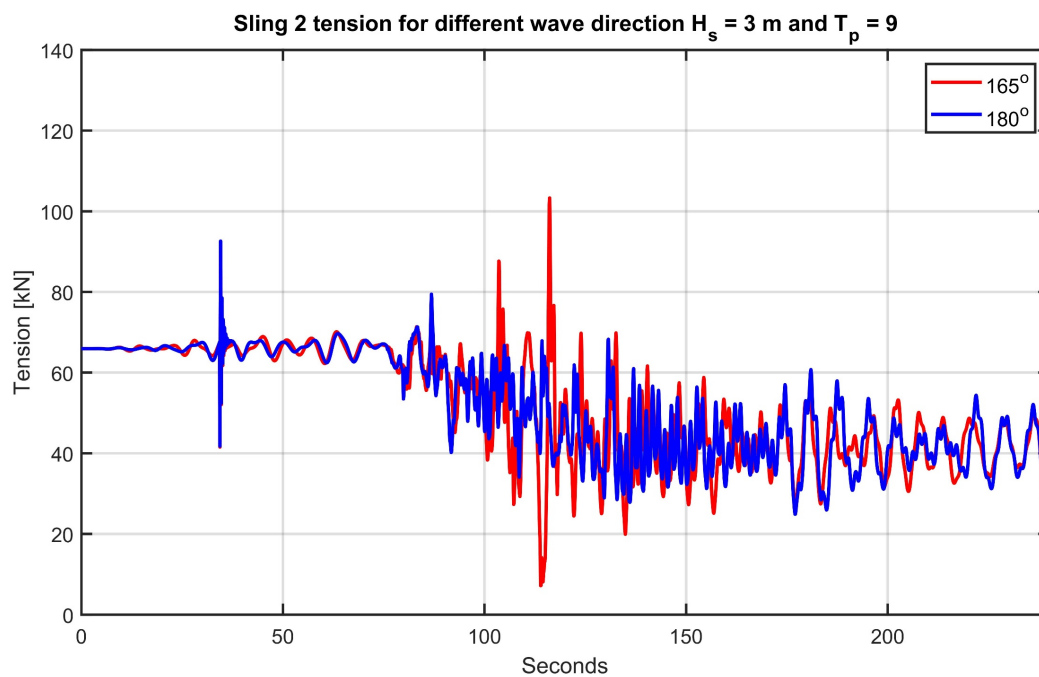
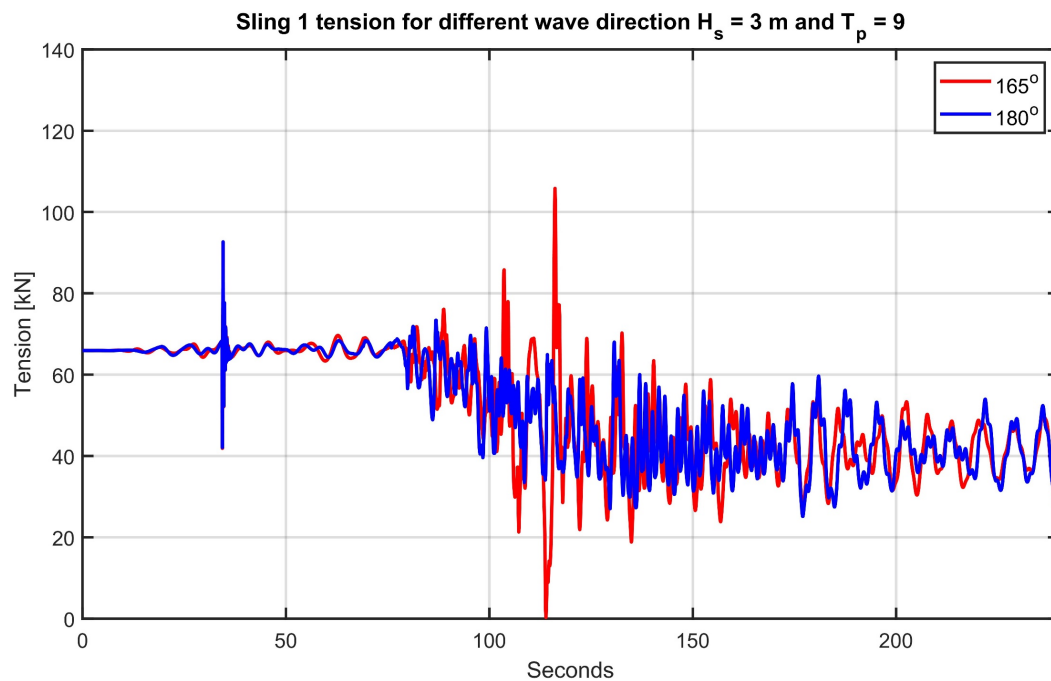


Figure 6 - 10 Example of sling tension for $T_p = 9$ s at different wave directions.

The hydrodynamic forces on the cover for the different wave directions tend to act similarly for shorter wave periods. However, the increased roll motion for waves at 165 degrees will still generate larger slamming forces on the cover, as seen in Figure 6 - 11.

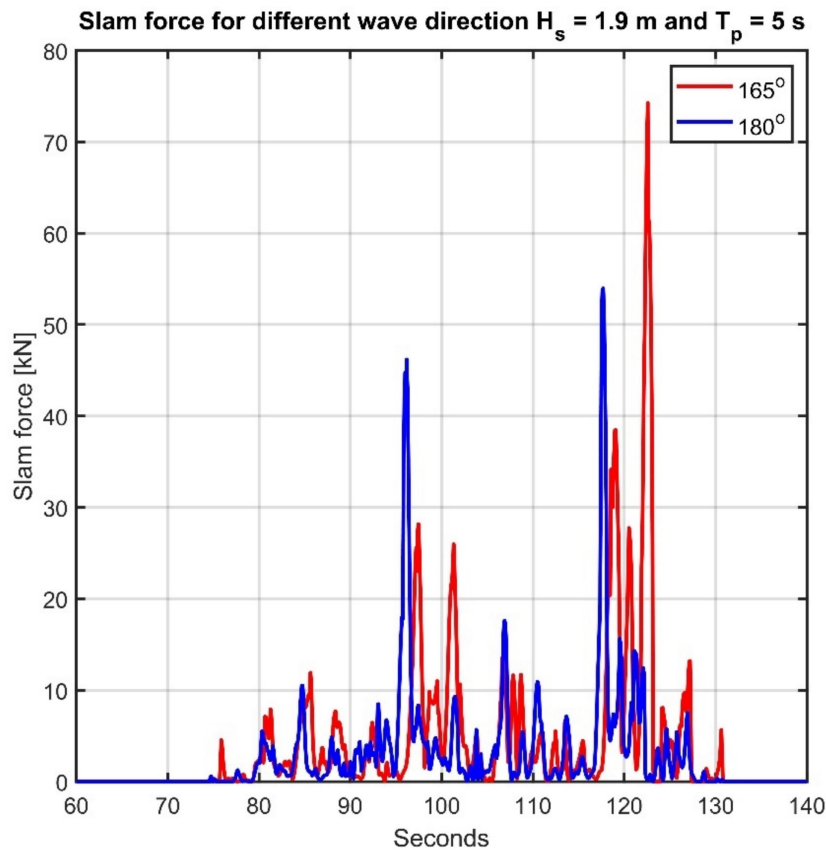


Figure 6 - 11 Example of slam forces for $T_p = 5$ s at different wave directions.

For the shortest wave period, the sling tension and the slamming force tend to be closer in magnitude, of which the sling respond similarly for the two given wave directions. There will still be a greater magnitude of force on the cover for the waves at 165 degrees. However, the wave direction contributes less to the allowable sea states at shorter wave periods than compared for longer. This can be seen in Figure 6 - 12, where the magnitude of tension is closely related for the individual wave directions. The allowable sea states for the different wave directions are given in Table 6 - 1 and Table 6 - 2, with head waves for the vessel yielding the best assessment for the sea states.

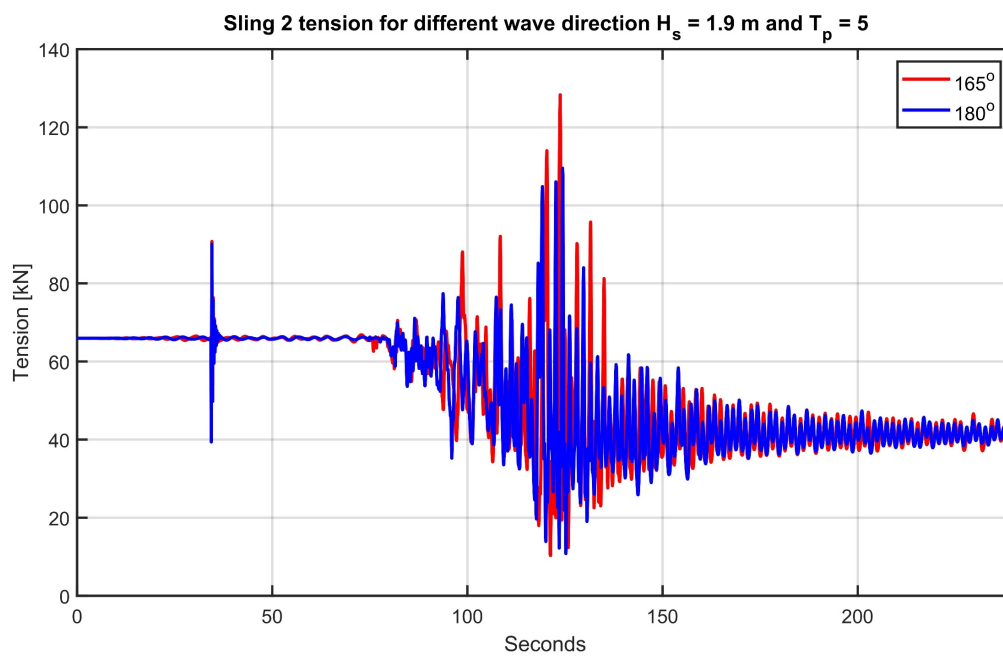
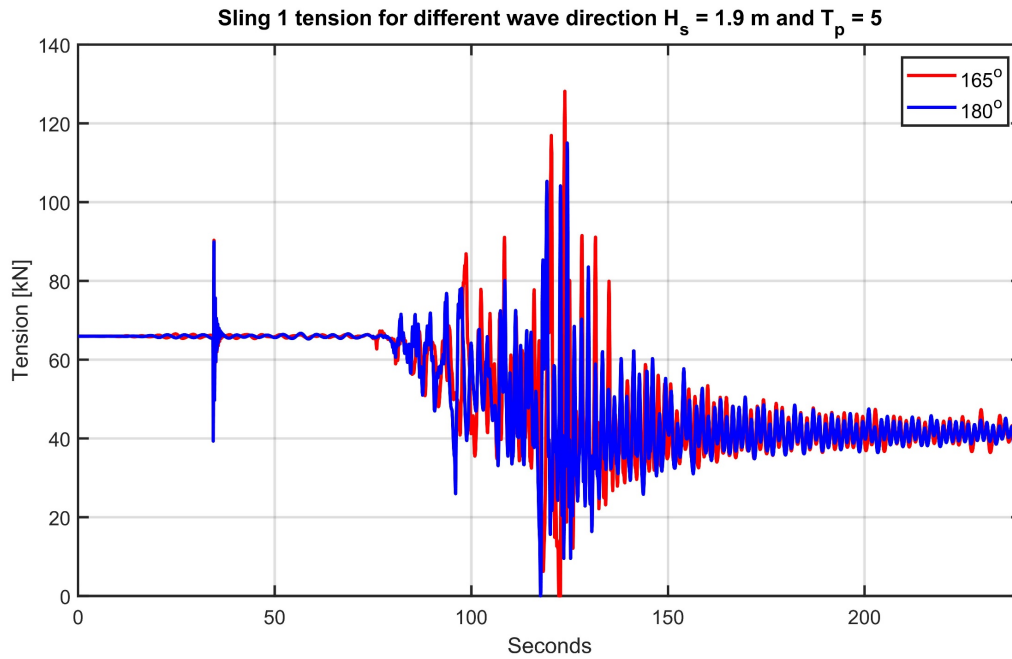


Figure 6 - 12 Example of sling tension for $T_p = 5$ s at different wave directions.

Table 6 - 1 Allowable sea states for wave direction 180°.

Allowable sea states for wave direction at 180°								
T_p \ H_s	5 s	6 s	7 s	8 s	9 s	10 s	11 s	12 s
1.8 m	Green	Green	Green	Green	Green	Green	Green	Green
1.9 m	Yellow	Green	Green	Green	Green	Green	Green	Green
2 m	Red	Green	Green	Green	Green	Green	Green	Green
2.1 m	Red	Green	Green	Green	Green	Green	Green	Green
2.2 m	Red	Green	Green	Green	Green	Green	Green	Green
2.3 m	Red	Green	Green	Green	Green	Green	Green	Green
2.4 m	Red	Green	Green	Green	Green	Green	Green	Green
2.5 m	Red	Yellow	Yellow	Green	Green	Green	Green	Green
2.6 m	Red	Red	Red	Yellow	Green	Green	Green	Green
2.7 m	Red	Red	Red	Red	Green	Green	Green	Green
2.8 m	Red	Red	Red	Red	Green	Green	Green	Green
2.9 m	Red	Red	Red	Red	Green	Green	Green	Green
3 m	Red	Red	Red	Red	Green	Green	Green	Green

- Operational criteria not met; snap loads will occur.
- Operational criteria met; slack may occur.
- Above operational criteria.

Table 6 - 2 Allowable sea states for wave direction 165°

Allowable sea states for wave direction at 165°								
T_p \ H_s	5 s	6 s	7 s	8 s	9 s	10 s	11 s	12 s
1.8 m	Green	Green	Green	Green	Green	Green	Green	Green
1.9 m	Yellow	Green	Green	Green	Green	Green	Green	Green
2 m	Red	Green	Green	Green	Green	Green	Green	Green
2.1 m	Red	Green	Green	Green	Green	Green	Green	Green
2.2 m	Red	Green	Green	Green	Green	Green	Green	Green
2.3 m	Red	Yellow	Green	Green	Green	Green	Green	Green
2.4 m	Red	Red	Green	Yellow	Green	Green	Green	Green
2.5 m	Red	Red	Yellow	Red	Green	Green	Green	Green
2.6 m	Red	Red	Red	Red	Green	Green	Green	Green
2.7 m	Red	Red	Red	Red	Green	Green	Green	Green
2.8 m	Red	Red	Red	Red	Green	Green	Green	Green
2.9 m	Red	Red	Red	Red	Yellow	Green	Green	Green
3 m	Red	Red	Red	Red	Red	Green	Green	Green

■ Operational criteria not met; snap loads will occur.

■ Operational criteria met; slack may occur.

■ Above operational criteria.

6.3.3 Shielding Effect on the Allowable Sea States

The shielding effect due to the vessel greatly improves the allowable sea states for the shorter wave periods tested. The allowable wave height for the shortest wave period increases by one meter in both directions. The common trend observed for shielding is an increase of magnitude for the average sling tension, which significantly reduces the risk of snap loads. This directly correlates with what was observed in subchapter 3.3.2, where the sea state RAO is greatly reduced for shorter wave periods, which lowers the hydrodynamic forces on the cover.

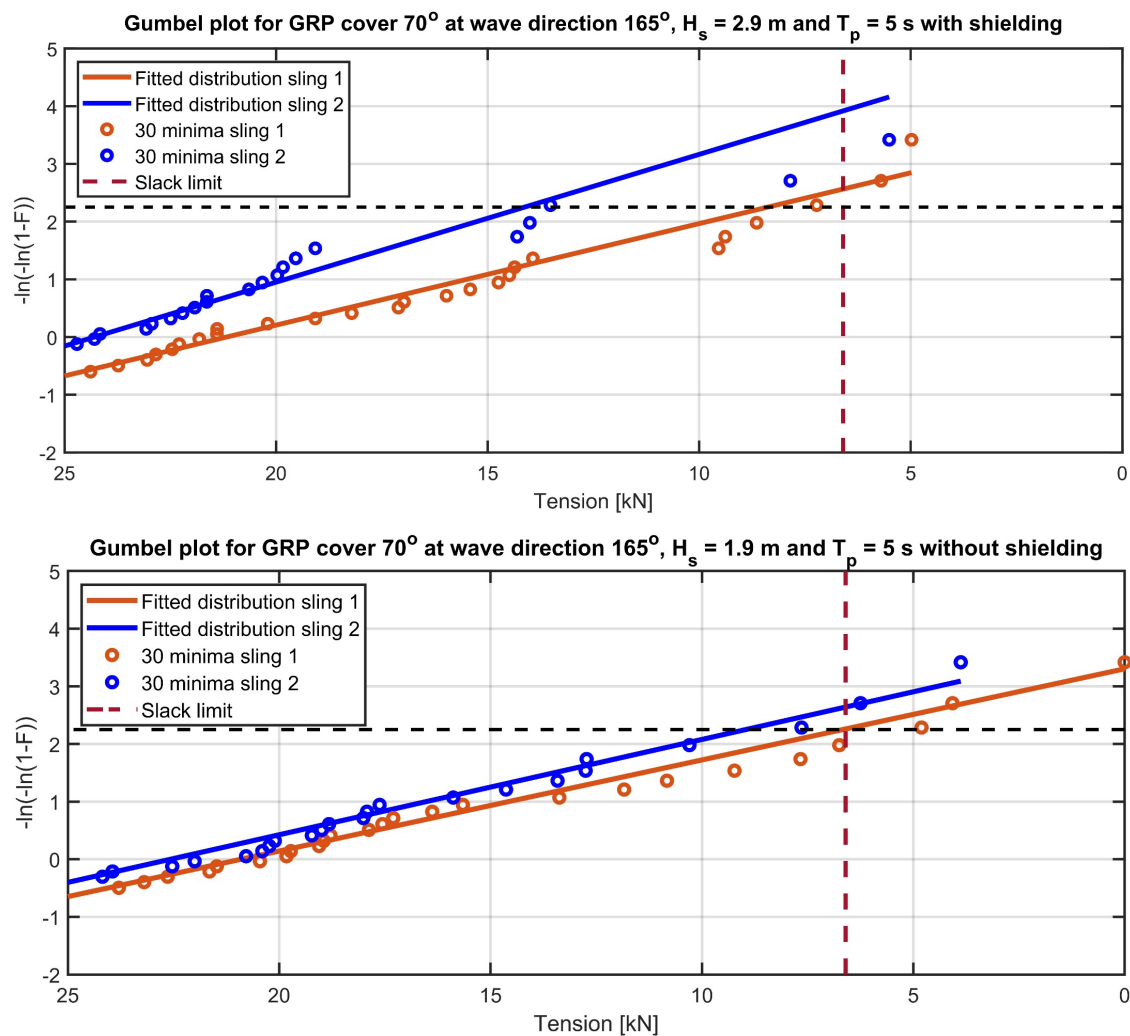


Figure 6 - 13 Gumbel plot for $T_p = 5$ s with and without shielding.

This can be seen in Figure 6 - 13 for the Gumbel distribution with and without shielding. The use of shielding has increased the allowable wave height by one meter, where the lowest observed seed for shielding is still greater in magnitude compared to the unshielded minimum value.

The reduction of hydrodynamic forces on the cover due to shielding can be seen from the decrease of slamming forces in Figure 6 - 14. As observed in the previous chapter, large slamming forces will yield slack and limit the allowable sea state. When the vessel disrupts incoming waves at shorter periods, the effect of slamming loads is reduced by more than half its magnitude. The observed decrease in slamming loads due to shielding will significantly improve the allowable sea states. The hydrodynamic force on the cover with shielding remains lower in magnitude compared to the acceptable sea states given in subchapter 6.3.2.

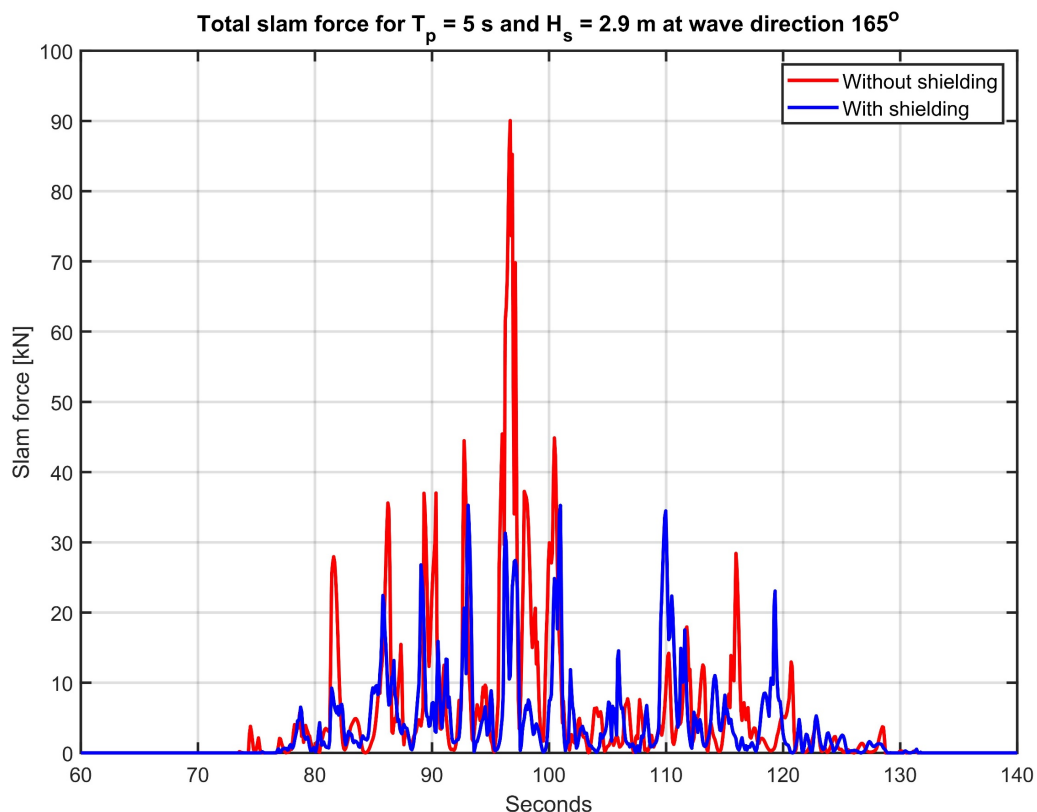


Figure 6 - 14 Example of slam with and without shielding.

The allowable sea states for the shielding effect are given in Table 6 - 3. From the allowable sea states, the use of the shielding effect greatly improves the operational conditions. The result makes it possible to lower the cover through the splash zone at a wave height of 2.9 meters for all given wave periods. This will significantly reduce the risk of unnecessary economic consequences from waiting on weather.

Table 6 - 3 Allowable sea states for different wave directions with shielding.

Allowable sea states for wave direction at 180° with shielding					Allowable sea states for wave direction at 165° with shielding				
T_p	5 s	6 s	7 s	8 s	T_p	5 s	6 s	7 s	8 s
H_s					H_s				
1.8 m					1.8 m				
1.9 m					1.9 m				
2 m					2 m				
2.1 m					2.1 m				
2.2 m					2.2 m				
2.3 m					2.3 m				
2.4 m					2.4 m				
2.5 m					2.5 m				
2.6 m					2.6 m				
2.7 m					2.7 m				
2.8 m					2.8 m				
2.9 m					2.9 m				
3 m					3 m				

- Operational criteria not met; snap loads will occur.
- Operational criteria met; slack may occur.
- Above operational criteria.

6.3.4 Discussion of Assessment of Allowable Sea States

The observed difference between the wave directions is greater for the longer wave periods than for shorter ones. However, using the wave direction that yields the lowest magnitude of hydrodynamic forces is always beneficial, which in return lowers the risk associated with the operation. Therefore, the vessel for this case should be positioned for head waves to get the best possible conditions for the operation.

For the allowable sea states given in Table 6 - 1 and Table 6 - 2, it is important to note that the acceptable sea states marked yellow will yield some seeds with slack. This is because these acceptable sea states are the predicted minimum, where it is possible to lower the cover through the splash zone. Therefore, operations conducted for the acceptable yellow sea states will imply that there will be a greater risk of snap loads. However, risk and hazards will always be involved when executing a marine operation, even when the operational criteria are met. Hence, the tables are made to give an insight into the level of risk associated with the individual sea states.

Shielding during the splash zone crossing significantly improves the allowable sea states. If the shielding effects were not accounted for, the predicted responses would be greatly overestimated. Thus, making the weather window more conservative leads to unnecessary economic consequences.

It is also important to note again that the allowable sea states for the different wave directions must not be mistaken as limits for the entire operation. The sea states may be lower for the operation than for the splash zone crossing. Marine operations are usually divided into multiple phases with separate allowable sea states. Other factors must also be accounted for, such as the duration of the entire operation, weather conditions at the site, possible weather windows, and use of α -factors from DNV-OS-H101 [31]. Lastly, the person executing the operation will always have the final say before the operation is conducted. The operation will not commence if the personnel deem the current conditions a risk to their safety and wellbeing.

Chapter 7

Conclusion and Future Work

7.1 Conclusion

This master thesis examines the allowable sea state and operability for lowering the GRP pipeline cover through the splash zone. First, the hydrodynamic properties used in this study were manually estimated using the DNV-RP-H103 simplified method [1], then implemented into each buoy. Next, Autodesk Inventor was used for modeling the lifted object based on the information extracted from Solaas et al. [10]. Lastly, all the results extracted from the numerical time-domain simulations were plotted in MATLAB [33].

In chapter 5, two sensitivity studies were conducted to establish the number of wave seeds and the vessel motion. From the number of seeds, the main conclusions are:

- The number of wave seeds used will yield slightly different sea state predictions.
- Thirty wave seeds were assumed to be acceptable given the extracted results.
- The Weibull probability paper yielded a poorer fit for the extreme values.

The results showed that 30 wave seeds were sufficient to achieve reliable estimations of extreme values for the time-domain model. However, it is important to note that with a different set of random wave seeds, it is a possibility that rather 50 or 100 seeds would achieve a better fit. The 30 extracted wave seeds were, of course, fixed for the rest of the simulation, with the foremost benefit of lower the extreme computational power needed to simulate the effect of shielding.

From the vessel motion, the main conclusions are:

- Coupled motion yielded slightly more conservative values.
- Large pendulum motions for the lifting wire occurred for both systems.
- More significant yaw rotations on the cover for the coupled system.

The vessel motion produced unexpected results according to DNV-RP-H103 subchapter 7.3.3.3 and Hauge et al [16], with the conservative motion being the coupled system. For the assessment of sea states, it was decided to use the uncoupled vessel motion. The primary reason for uncoupled vessel motion was the observed small difference between the sling tension. Secondly, for longer periods it was observed more extensive yaw rotations on the vessel for coupled motion (Appendix C). Therefore, the uncoupled motion was used to contain these significant rotations without needing to add artificial stiffness or extra mooring lines for the vessel. However, adding extra mooring lines and artificial constraints to the coupled system would yield a new model with different responses to the given sea state. The coupled motion would be more constricted even for roll motion, which would minimize the differences observed between the vessel motions.

The results for the splash zone crossing of the cover would also differ depending on the vessel motion. The coupled system yielded larger rotations on the cover, which could induce an unwanted position. Therefore, when performing installation, it is important to control the motions of the cover for the lift in air. Using uncoupled vessel motion lowered these yaw rotations on the cover and the likelihood of an unwanted position. These rotations were also experienced by Solaas et al. [10], where they used artificial stiffness and smaller simulation timestep to lower the cover. However, the difference in lifting setup and model properties will yield variation in the behavior of the cover between the studies.

The pendulum motions were also observed by Solaas et al. [10]. These pendulum motion occurred during submergence of the cover and was present for both the motions. After reaching the water, the cover's motion would calm down with the motions of the hook increasing with a pendulum motion. These observed pendulum motions contributed to large fluctuations of the sling tension. For the coupled system for seed 19, the large snap load was due to a combination of vessel roll, an undesired position on the cover, and pendulum motion for the hook.

The operational criteria were selected based on the sling working load, allowable snap load limit, and clearances between the object and vessel. From the observed results, the only limiting factor for the acceptable of sea states was the allowable snap loads. However, the structural

integrity of the cover was not implied in this thesis. Therefore, it will be uncertain for possible large point forces on the cover and the acceptable limits of deformation or damage.

Firstly, in the assessment of allowable sea states, three different lifting angles were tested to assess the importance of the waterplane area for the splash zone crossing. As expected, the lifting position with the lowest waterplane area yielded the best prediction for allowable sea states. In addition, the correlation between snap loads and slamming forces on the cover greatly visualizes the importance of the waterplane area. Therefore, the lifting angle with the lowest waterplane area should be used for an object with low weight and a large surface area to lower the risk of snap loads. For the different tested wave directions, head waves yielded the lowest risk of snap loads due to lower hydrodynamic forces on the cover.

Shielding during the splash zone crossing significantly improved the allowable sea states. When the vessel is used to disrupt the incoming waves, the sea state RAO will be significantly reduced for shorter wave periods, as seen in chapter 3. In addition, the shielding effect reduces the hydrodynamic forces such as slam, which lessens the risk of possible snap loads. The use of shielding will, for this study, increase the weather window and lower the economic risk of waiting on weather. This is the same conclusion Li et al. [11] had on the effect of shielding during the lowering of an offshore wind turbine monopile.

The tested sea states by Solaas et al. [10] were for one wave period of eight seconds, with the conclusion that the installation may be performed at wave heights between 2.5 to 3 meters. This corresponds to the observed result from this study, where a wave period of eight seconds yielded acceptable sea states for head waves between 2.6 to 3 meters, depending on whether shielding is considered.

Lastly, the sea state description used for these simulations was only JONSWAP. Li et al. [14] concluded that different descriptions for the sea states, such as Torsethaugen, yield significantly less values for the vessel compared to JONSWAP. It is important to note that different sea states

will yield different results, of which the only sea state description used in this study was JONSWAP for wind sea.

7.2 Recommendations for Future Work

To fully assess the allowable sea state of the installation for the GRP protection cover. It would be interesting to continue the work for the entire installation operation. Firstly, assessing the operability with the uncertainties surrounding the weather forecast with the implementation of α -factors [31]. Time-domain simulation for pre-lift and the over boarding phase to assess the allowable limits for the entire operation with the inclusion of structural integrity.

The hydrodynamic properties for the cover were based on the DNVs simplified method. This can be improved by conducting CFD analysis and model tests. It would be fascinating to see the difference in results between each method used and obtain more accurate values from the real-life model. The slamming coefficient used in this study is relatively conservative, where from the results obtained, the slam loads directly correlate with slack and snap loads. Conducting a model test on the slamming loads acting on the cover can potentially impact the minimum sling tension. It would also be interesting to validate the shielding results with real-life experiments.

It is also possible to conduct new sensitivity studies for the GRP protection cover. For example, an investigation of the pendulum motion and the cover rotations was also observed by Solaas et al. [10]. In addition, how the slings, lifting set-up, and equipment may influence the cover's position and pendulum motion. This can be conducted using tugger lines to restrict the motions, different slings arrangements, artificial constraints, and shackle types.

References

- [1] DNV, DNV-RP-H103: Modelling and Analysis of Marine Operations, Høvik: DNV, 2009.
- [2] W. Thomson, Volume IV. Hydrodynamics and general dynamics pp. 254-267, London: Cambridge University, 1910.
- [3] A. Gray, Lord Kelvin an account on his scientific life and work pp.207-213, London: J.M. Dent & CO, 1908.
- [4] Wikipedia, “Tide-predicting machine” [Online]. Available:
https://en.wikipedia.org/wiki/Tide-predicting_machine [Accessed 19 February 2022].
- [5] Wärtsilä, “Encyclopedia of Marine and Energy Technology,” Wärtsilä [Online]. Available:
<https://www.wartsila.com/encyclopedia/term/pipelaying-methods>. [Accessed 18 February 2021]
- [6] L. Li, Z. Gao and T. Moan, “Response analysis of a nonstationary lowering operation for an offshore wind turbine monopile substructure,” Journal of Offshore Mechanics and Arctic Engineering, vol. 137, no. 5, 2015.
- [7] Norsk Petroleum “Åsgard subsea compression template” [Online]. Available
https://www.norskpetroleum.no/framework/0087794-asgard-subsea-compression-template-photo-oyvind-hagen-statoil_605x314/ [Accessed 12 February 2022].
- [8] DNV, DNV-RP-C205: Environmental Conditions and Environmental Loads, Høvik: DNV, 2007.
- [9] Orcina, “OrcaFlex documentation,” [Online]. Available:
<https://www.orcina.com/webhelp/OrcaFlex/Default.htm>. [Accessed 04 November 2021].
- [10] F. Solaas, P. Sandvik C. Pákozdi, C. Kendon, T. Larsen, K. and Myhre, E. (2017). Limiting Sea States for installation of GRP Protection Covers. Technical Report OMAE2017-62499, MARINTEK.

- [11] L. Li, Z. Gao, T. Moan and H. Omberg, "Analysis of lifting operation of a monopile for an offshore wind turbine considering vessel shielding effects," *Marine Structures*, 2014.
- [12] L. Li, C. Parra, X. Zhu and M. C. Ong, "Splash zone lowering analysis of a large subsea spool piece," *Marine Structures*, vol. 70, no. 102664, pp. 1-17, 2020
- [13] W. Guachamin-Acero, L. Li, Z. Gao and T. Moan, "Methodology for assessment of the operational limits and operability," *Ocean Engineering*, vol. 125, pp. 308-327, 2016.
- [14] L. Li, S. Haver and N. Berlin, "Assessment of operational limits: Effects of uncertainties in sea state description," *Marine Structures*, vol. 77, 2021.
- [15] N. O. Hauge, "Numerical study on splash zone crossing with subsea template and ROV," Master thesis - UiS, Stavanger, 2021.
- [16] N.O Hauge and L. Li, "Numerical study on deployment of subsea template using coupled and uncoupled model," *IOP Conf. Ser.: Mater. Sci. Eng.* 1201, 2021.
- [17] J. Journée and W. Massie, *Offshore Hydromechanics*, Delft: TU Delft, 2001.
- [18] Y. A. Cengel, J. M. Cimbala, *Fluid Mechanics Fundamentals and Applications Fourth Edition in SI units*, McGraw-Hill Education, 2020.
- [19] O. T. Gudmestad, *Marine Technology and Operations: Theory & Practice*, Southampton: WIT Press, 2015.
- [20] S. Haver, *Metoocean Modelling and Prediction of Etxremes*, Stavanger: UiS, NTNU, 2018.
- [21] T. Moan, S. Haver, N. Spidsøe, *Stochastic Theory of Sealoads Probabilistic Modelling and Estimation*, Trondheim: NTNU, 2019.
- [22] E. J. Gumbel, "Statistical Theory of Extreme Values and Some Practical Applications," *National Technical Reports Library*, Washington D.C., 1954
- [23] Orcina, "OrcaWave documentation," [Online]. Available: <https://www.orcina.com/webhelp/OrcaWave/Default.htm>. [Accessed 03 March 2022].
- [24] WAMIT, "WAMIT V7," [Online]. Available: <https://www.wamit.com/> [Accessed 12 March 2022].

- [25] Autodesk, “Autodesk: Products: Inventor,” Autodesk, [Online]. Available: <https://www.autodesk.com/products/inventor/overview?plc=INVPROSA&term=1-YEAR&support=ADVANCED&quantity=1>. [Accessed 22 November 2021]
- [26] NORSOK, NORSOK R-002: Lifting Equipment, Stavanger: OD, 2017.
- [27] L. Li, Z. Gao and T. Moan “Numerical simulation for installation of offshore wind turbine monopiles using floating vessels,” OMAE 2013
- [28] Baarholm GS, Haver S, Økland OD. Combining contours of significant wave height and peak period with platform response distributions for predicting design response. Mar Struct 2010;23(2): 147–63.
- [29] A. Matland, “Simulation of marine lifting operation with focus on structural response control,” Master thesis – NTNU, Trondheim, 2014.
- [30] L. Li, A. M. Amer and X. Zhu “Numerical analysis of an over-boarding operation for a subsea template,” Ocean Engineering and Science vol.6, pp. 146-159, 2021
- [31] DNV, DNV-OS-H101: Marine Operations, General, Høvik: DNV, 2011.
- [32] Gunnebo Industries, “Wire Rope Sling 2-legged,” [Online]. Available: <https://www.gunneboindustries.com/no/Lifting/Produkter/Steel-wire-ropes/Wire-rope-slings/Wire-Rope-Sling-2-legged/> [Accessed 27 November 2021]
- [33] MathWorks, “MathWorks: Products: MATLAB,” MathWorks, [Online]. Available: https://se.mathworks.com/products/matlab.html?s_tid=hp_ff_p_matlab.

Appendix A

Python Simulation Code

```
import pandas as pd
import OrcFXAPI
import random
from multiprocessing import Pool, Manager
OUTPUT = "Result_HS.csv"
NUM_TRIALS = 50          # Numbers of simulations
SEED = 15                # Fixed random seeds

WaveHeight = [2.5]
WaveDirecetion = [180]
WavePeriod = [8]

runs = []

for wave in WaveHeight:
    for waveDir in WaveDirecetion:
        for WavePer in WavePeriod:
            data = {
                'waveHeight': wave,
                'WaveDirecetion': waveDir,
                'WavePeriod': WavePer
            }

            runs.append(data)

runIter = iter(runs)

def getNext():
    nextValues = next(runIter, None)
    return nextValues

random.seed(SEED)

def seed():
    seed = random.randint(int(1),int(9999999999))
    return seed
```

```
def runSimulation(args):

    global df
    result = []
    for trails in range(NUM_TRIALS):

        print(args)
        model = OrcFxAPI.Model()
        model.LoadData('C:/Users/Marius/OneDrive/Skrivebord/New Model.dat')

        env = model.environment
        env.WaveType = 'JONSWAP'
        env.WaveHs = args.get("waveHeight")
        env.WaveTp = args.get("WavePeriod")
        env.WaveDirection = args.get("WaveDirecetion")

        env.WaveSeed = seed() # Extracts value for the wave seed

        model.RunSimulation()

        Sling1 = model.objects[27]
        Sling2 = model.objects[26]
        Sideplate1 = model.objects[10]
        Sideplate5 = model.objects[14]

        Sling1_tension =
Sling1.TimeHistory('Tension',OrcFxAPI.SpecifiedPeriod(30.0,240.0))
        Sling2_tension =
Sling2.TimeHistory('Tension',OrcFxAPI.SpecifiedPeriod(30.0,240.0))
        SideplateY =
Sideplate1.TimeHistory('Y',OrcFxAPI.SpecifiedPeriod(0.0,80.0))
        SideplateY2 =
Sideplate5.TimeHistory('Y',OrcFxAPI.SpecifiedPeriod(0.0,80.0))




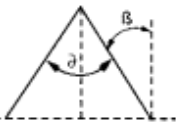
        maxSling2 = max(Sling2_tension) # Max sling 2 tension
        minSling2 = min(Sling2_tension) # Min sling 2 tension
        maxSling1 = max(Sling1_tension) # Max sling 1 tension
        minSling1 = min(Sling1_tension) # Min sling 1 tesnion
        maxSideplateY = max(SideplateY) # Max position for Y-direction
        minSideplateY = min(SideplateY) # Min position for Y-direction
        maxSideplateY2 = max(SideplateY2) # Max position for Y-direction
        minSideplateY2 = min(SideplateY2) # Min position for Y-direction

        data = [
            {
                'Sling 1 min': minSling1,
                'Sling 1 max': maxSling1,
```

```
        'Sling 2 min': minSling2,  
        'Sling 2 max': maxSling2,  
        'Sideplate1 Y min': minSideplateY,  
        'Sideplate1 Y max': maxSideplateY,  
        'Sideplate5 Y min': minSideplateY2,  
        'Sideplate5 Y max': maxSideplateY2,  
        'Seed': env.WaveSeed,  
        'WaveHs':env.WaveHs,  
        'WaveTp':env.WaveTp,  
        'WaveDirection': env.WaveDirection,  
    }  
]  
  
    result.append(data)    # extracts the results  
  
    return result  
if __name__ == '__main__':  
    dfs_list = Manager().list()  
    pool = Pool(processes=20) # start 20 worker processes  
    results = pool.map(runSimulation, runs) # do some work  
    #print("result", results, "\n")  
  
    for res in results:  
        for result in res:  
            dfs_list.append(pd.DataFrame(result[0], index=[0]))  
  
    pool.close()  
    pool.join() # block at this line until all processes are done  
  
    df = pd.concat(dfs_list, ignore_index=True) # the final result  
    print(df)  
  
    df.to_csv(OUTPUT, encoding= "utf-8") #Generates a datasheet with the  
results  
    print("Finished") # The simulations is finished
```


Appendix B

Sling Data

Working Load Limit					
Nom. diam. mm	1-leg			2-leg	
					
	Straight	Choke hitch	Basket hitch	$\alpha 0^{\circ}-90^{\circ}$ $\beta 0^{\circ}-45^{\circ}$	
3	0,09	0,07	0,18	0,12	
4	0,15	0,12	0,30	0,21	
5	0,25	0,20	0,50	0,35	
6	0,35	0,28	0,70	0,50	
7	0,50	0,40	1,00	0,70	
8	0,75	0,60	1,50	1,10	
9	0,90	0,80	1,80	1,26	
10	1,20	0,95	2,40	1,70	
11	1,40	1,10	2,80	2,00	
12	1,70	1,30	3,40	2,40	
13	2,00	1,60	4,00	2,80	
14	2,30	1,80	4,60	3,20	
16	3,00	2,40	6,00	4,20	
18	3,80	3,10	7,60	5,30	
20	4,70	3,80	9,40	6,60	
22	5,70	4,60	11,40	8,00	
24	6,80	5,40	13,60	9,50	
26	8,00	6,40	16,00	11,20	
28	9,30	7,40	18,60	13,00	
32	12,00	9,70	24,00	16,80	
36	15,00	12,00	30,00	21,00	
40	19,00	15,00	38,00	27,00	
44	23,00	18,00	46,00	32,00	
48	27,00	22,00	54,00	38,00	
52	32,00	26,00	64,00	45,00	
56	37,00	30,00	74,00	52,00	
60	43,00	34,00	86,00	60,00	

Appendix C

Vessel yaw motion

